NISSAN TECHNICAL REVIEW

2023
No.
89

"Tough Gear" and "High Quality" for New X-TRAIL／
Test Technologies Contributing to Electrification

NISSAN
MOTOR CORPORATION

NISSAN TECHNICAL REVIEW

2023 No.89

“NISSAN TECHNICAL REVIEW” WEBSITE

https://www.nissan-global.com/EN/TECHNICALREVIEW/

NISSAN TECHINICAL REVIEW 2023 No.89

Contents

Published in July, 2023

◆ Preface

◆ Special Feature 1 : "Tough Gear" and "High Quality" for New X-TRAIL

◆ Special Feature 2 : Test Technologies Contributing to Electrification

◆ Introduction of Technical Award Winners

Technologies and processes for establishing products from advanced technologies

Corporate Vice President **Mitsuro Antoku**

1. Introduction

With the spirit “Do what others won’t” in our DNA and as indicated by the vaunted name “Technology of Nissan,” Nissan has created values through technology and delivered them to our customers as products and services.

Any advanced technology is meaningless unless its resulting product can be used with pleasure by customers and unless it contributes to solving social issues such as global warming and traffic accidents. This preface describes how advanced technologies necessary for offering such value are born, nurtured, and applied to products.

2. Technology roadmap

At Nissan, the roadmap for developing technology required to realize future visions was created long ago. All research and advanced developments are conducted based on this technology roadmap.

The technology roadmap was created considering the following: “What values offered in our future products and services will our customers find attractive?” To answer this, the requirements and trends of society, as well as the issues that arise from them, are investigated. Technological developments necessary to realize a solution to such issues are incorporated into this roadmap.

In most cases, establishing a new technology requires a long time. Therefore, it is crucial to develop a roadmap, which is a long-term technological strategy. Further, it is important to update this technology roadmap considering changes in social trends, changes in customers’ values and activities, and the evolution and innovation of the technology. The technology roadmap for electrification and intelligence are shown as examples.

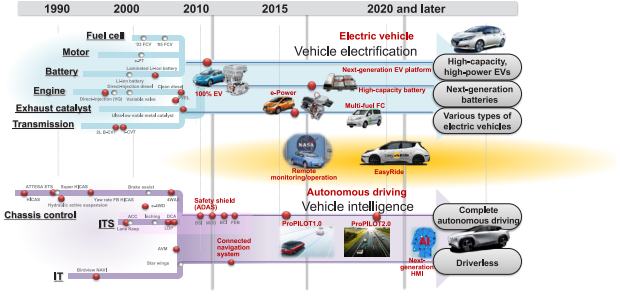

Progress of Nissan’s technological development

3. Research and development to advanced development

A new technology is established in a step-by-step manner from basic research and development (for creating the basis) to advanced development (for practical applications). After completing the research and advanced development of individual technologies, it is possible to combine them to create a new technology. However, sometimes, even after the advanced development process is completed, these technologies may not yet be ready for product application. In such cases, it is crucial to continue the development activities to achieve the original roadmap.

The research and development of motors and batteries, which Nissan had started prior to 1990, did not bear fruit until 20 years later in 2010 as the product Nissan Leaf, the world’s first mass-produced EV, and until 2017, as Nissan’s unique electrification system e-POWER, which offers new value to many of our customers. Another example is e-4ORCE technology, which originated from the 4WD control technology ATTESA ETS and chassis control technology HICAS, which were cutting-edge technologies in the 1990s. They have evolved over the years, integrated with electrification technology, and bore fruit as an integrated control technology e-4ORCE. The e-4ORCE technology performs minute integration control of the front/rear motor drive AWD and chassis system such that the ease of handling, ride comfort, and sense of security can be realized at a high level in any driving scenario.

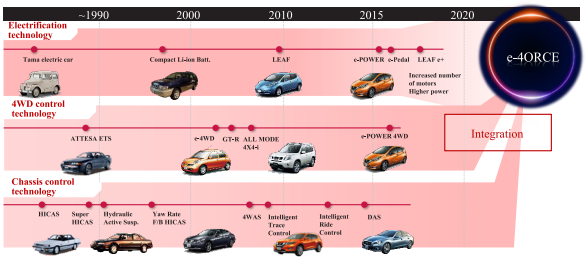

History of e-4ORCE

Nissan's VC-TURBO engine, which achieves both high power and low fuel consumption through its variable compression ratio mechanism, took 18 years to develop from its conception to realization. The impressive results achieved were the result of the dedication and hard work

of engineers who made steady progress through research and development, including the advancement of manufacturing technology.

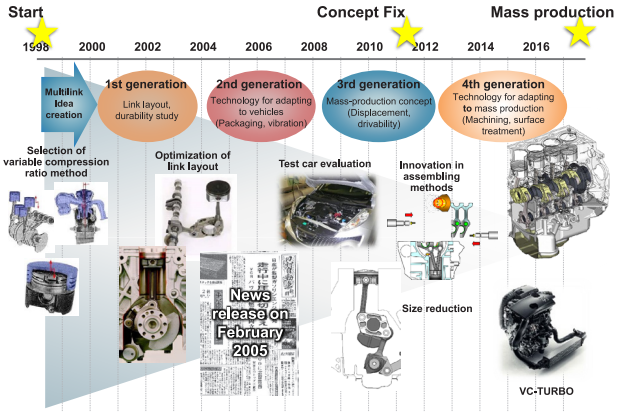

Development history of variable compression ratio

For the drive-assist technology ProPILOT, the development of its basic elemental technology began more than 20 years ago, and individual technologies (many of which were the world's first at the time) have been applied to products since then. These technologies have achieved results and gained market experience, and ProPILOT is a compilation of these technologies.

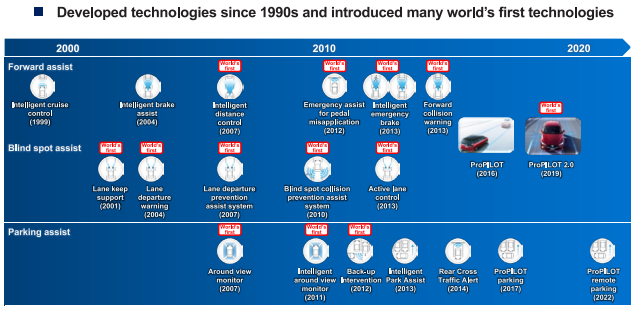

Evolution of drive-assist technology

4. Development for application to products

The development of a product starts by deciding what characteristics (concepts) to assign to the product. The product concept is determined after performing sufficient market research. Some factors to consider in the research include "Where does the target customers live, and what should the customers' social status be? What kind of value do customers desire?" In the meantime, existing technologies, as well as technologies that have undergone research and advanced development over the years, are combined to study whether it is possible to create new value for the target customers. Such values are coordinated as a whole to convert them to characteristics that are consistent as a product. Thus, value is elevated to an attractive product concept. Teams involved in development, planning, design, and marketing and sales performed these activities, and the characteristics of the products were determined during this process.

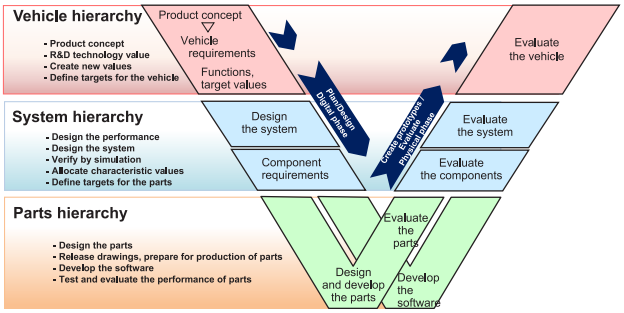

Flow of product development

The next step is to define functions and target performances for realizing the product concept and determine the technologies and their combinations that need to be applied. Advanced technologies are part of the technologies intended for application. To develop a technology for product application, its functionality and performance are enhanced to transform it into a new value. Multiple reviews are conducted to ensure that customers can comfortably and easily use the technology at all times and that the final product is easy to comprehend and operate. During this process, it is essential to investigate the required functionality and performance by considering the different ways in which the product will be used.

After the functionality and target performance of a vehicle are defined, the next step involves performing a detailed design of the systems and parts necessary to achieve the functionality and target performance. To achieve the targets of a vehicle in a complex system, it is necessary to allocate performance targets to the systems and parts and then verify the level of achievement of each target. This activity is the so-called performance-design process. This is an important product development process. Technologies for performing system-level and part-level tests and simulations play an important role in this process.

As featured in this technical review, improvements in testing and simulation technologies have enabled the evaluation of elements and systems in the design phase, contributing significantly to improving the level of design assurance. Nissan is also committed to analyses using digital technology, which reproduces actual vehicle-level events in cyberspace in real time.

Using virtual reality (VR) technology, events based on tests and measurements are reproduced and verified in advance during the development and design phases. Models with actual dimensions can be evaluated in cyberspace. For example, a VR experience that reproduces the visibility according to the driver's actions (e.g., driving) can be realized if not only the design information but also the environment outside the vehicle (e.g., the surrounding environment 360° around the vehicle and the surrounding environment for the travelling distance) are reproduced when evaluating drivability, such as

driving operation and visibility. This experience helps evaluate drivability during driving. Owing to this technology, the evaluation accuracy of the visual field of the mirror and ease of using/viewing the switches for driving operations have improved.

After the steps described above and the design of the system and parts were completed, the vehicle prototype is manufactured, and the testing and verification processes are started. This is the process of testing and verifying the assurance of functions and performance at each part, system, and vehicle level.

Owing to the recent improvements in testing and simulation technologies, it is now possible to enhance the efficiency of physical testing and verification. By integrating testing and simulation technologies, it is feasible to carry out accurate product development evaluations within a shorter timeframe. This approach has become indispensable, particularly in complex systems.

While performing efficient verification in the development phase, data are shared with the production engineering department, production plants, and suppliers. This helps ensure cooperation between the members of mass-production quality, production engineering, plant manufacturing, and suppliers to verify and confirm mass-production quality for ensuring build quality. An example of the application of advanced technology to the new X-TRAIL, which is covered in another feature of this technical review, is provided below.

When Nissan decided to use the VC-TURBO engine for e-POWER, they aimed to achieve not only high power and low fuel consumption but also a high level of quietness and a comfortable acceleration sound. Compared to conventional engines, the VC-TURBO engine could change the compression ratio in a flexible manner, which required the checking of 2.8 times more constants for conformity. The conformity check was based on various factors, including the ambient environment, driving situations, battery charging status, fuel consumption, emissions, heat management, engine sound, and quietness. Since there were many combinations of driving conditions to be checked, a model-based tool was developed, and simulations, bench tests, and actual vehicle tests were used together to efficiently determine the large number of constants that needed to be conformed to.

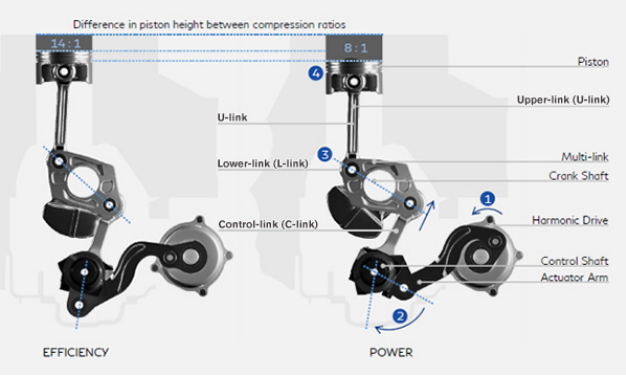

VC-TURBO engine

The "flat ride" concept, which is one of the values offered by e-4ORCE, was realized by fully utilizing the driving simulator. The targets for "flat ride" could not be set by comparing it with those of conventional vehicles. Therefore, Nissan fully utilized the driving simulator, and the targets were set by analyzing "how occupants feel" when a vehicle accelerates and decelerates as well as when pitching motion occurs. Before manufacturing the actual vehicle, a driving simulator was used to check whether it was possible to provide the intended feeling by the design in line with the targets.

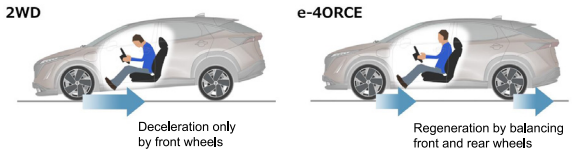

Flat ride provided by e-4ORCE

When launching ProPILOT as a product, it was necessary to consider various requirements, such as the environment of the roads to drive on, traffic situations, and driving conditions. In addition to performing evaluations of individual parts and systems, driving simulators, and actual vehicle tests on the test tracks, Nissan performed public road driving tests for over several tens of thousands of kilometers to ensure functionality and performance. Another important part of technological development before launching the product was the development of a fail-safe design that enables customers to safely use the product, even if a component fails or if the product becomes subject to an external environment exceeding the functional limit.

When Nissan decided to apply ProPILOT to the new X-TRAIL, they undertook developments to improve its display and operability. This was done with the aim of making it more understandable, secure, and safe for customers to use. When optimizing a human-machine interface (HMI), the driving simulator is an essential technology for evaluating the operability of people with different characteristics, such as body build, age group, and driving experience.

Technologies that have undergone research and advanced development undergo a development process for application to a product. After that, the technology is established as a product that will be used with pleasure and a sense of security by customers.

The process flow does not end even after a product is launched in the market. To further enhance customer satisfaction, our technologies undergo further development so that they will evolve further and be ready for the next generation.

5. Summary

Based on the technology roadmap, an advanced technology undergoes research and development, advanced development, and development for applying to a product before it is delivered to our customers as a

product. Simultaneously, established technologies are combined and improved further so that new and higher values can be created and established as products, making them more competitive.

The advanced technologies incorporated in the new X-TRAIL were developed and established as products as described in this preface. Testing technologies, which are the other topics featured in this technical review, play an important role in establishing a product such as the new X-TRAIL. These testing technologies are often used practically after research, development, and advanced developments.

Nissan has implemented a strategy to reduce the time required for applying advanced technologies to their products. We have started to conduct early assessments of potential concerns that may arise during the product development process and are proactively working on solutions during the advanced development stage. By doing so, Nissan can establish solutions for potential issues before they become major problems and accelerate the technology integration process.

Nissan is committed to continuing to develop and integrate their unique "Technology of Nissan" into their products.

1. Evolution of genuine SUVs: New X-TRAIL e-4ORCE

Tetsuya Yamamoto*

1 .Introduction

In 2021, the SUV segment sold 35 million units globally, becoming the top-selling vehicle type with a 45.9% market share (Fig. 1). Since then, vehicle manufacturers have successively launched new vehicle models, significantly intensifying the competition.

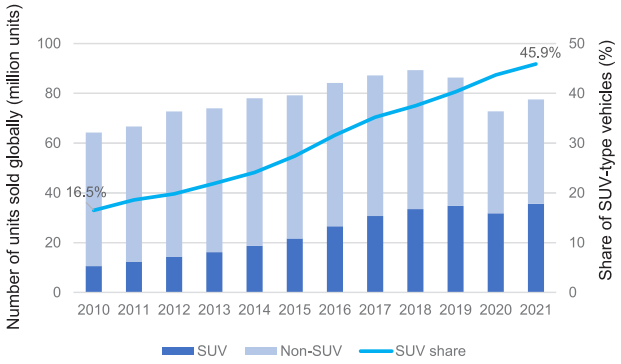

Fig. 1 Number of SUVs sold globally and share by vehicle type

Nissan has actively promoted electrification to achieve carbon neutrality and incorporated its unique e-POWER technology into the new X-TRAIL to develop convention-defying SUVs that offer and the pleasure and comfort of driving a 100% motor-driven SUV.

Fig. 2 New X-TRAIL e-4ORCE

2. Evolution of the new X-TRAIL

After Nissan pioneered the first-generation X-TRAIL in the middle-segment SUV market, subsequent models have inherited the powerful driving performance and highly convenient equipment that only genuine SUVs offer and have evolved by incorporating the cutting-edge technology of the time. X-TRAIL was selected by customers worldwide to travel in various environments with different road surface conditions and at different speed ranges.

The development goals for the fourth-generation X-TRAIL, which incorporate the evolved second-generation "e-POWER" × "VC-TURBO" and the electric drive four-wheel control technology "e-4ORCE," were to evolve the rough-road drivability inherited as "Tough Gear" from the first-generation model, and realize a level of quietness and ride comfort that provide a "high quality" feeling during on-road driving, which is not possible with conventional SUVs.

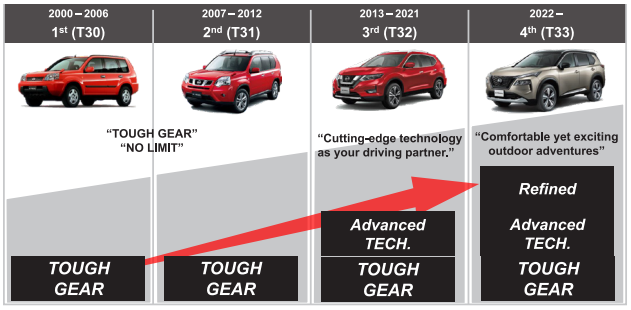

Fig. 3 Heritage and evolution of X-TRAIL

The capability to drive off-road and on snowy road surfaces provides drivers with a sense of power and security. For example, when starting from a stationary position and climbing a dirt hill with a 20% gradient (as shown in Fig. 4), a high torque is applied instantaneously to the rear tires without causing them to spin idly. This enables the vehicle to climb the hill with a speed acceleration performance 1.7 times higher than that of conventional models.

*Product Development Department No.2

Further, driving and regenerative braking forces were controlled in units of 1/10,000 s while calculating the grip limit of each wheel. This allows the driver to operate the accelerator pedal without feeling insecure even when driving on slippery, downhill, and snowy road surfaces.

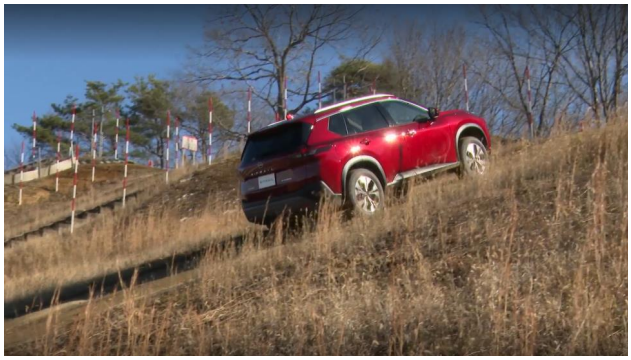

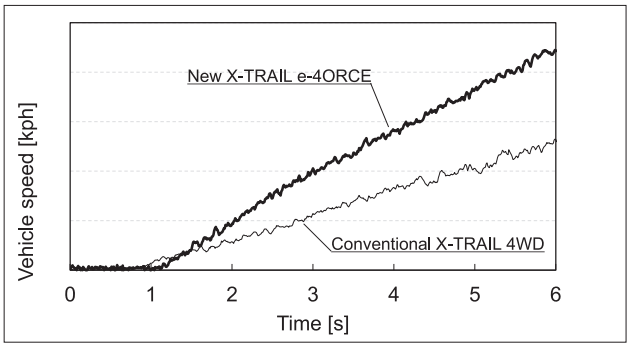

Fig. 4 Hill-start performance when climbing a dirt hill with a 20% gradient

In addition, the level of quietness and ride comfort is improved significantly, thus providing a "high quality" driving experience. The new X-TRAIL operates like an EV when driving at low speeds (e.g., in urban areas). Even when the engine generates electricity, the level of realized quietness does not allow the occupants to notice that the engine is running (Fig. 5).

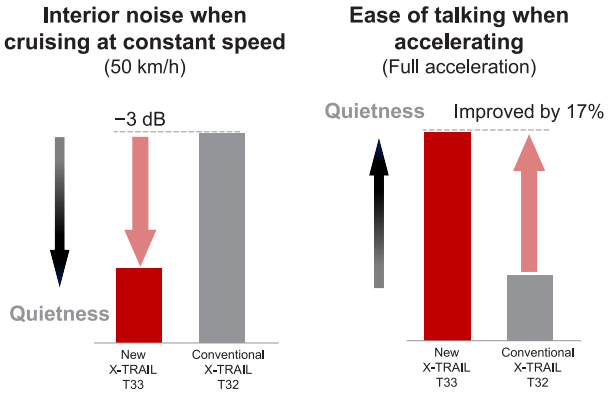

Fig. 5 Level of quietness

The sinking behavior and body motion of the vehicle during deceleration are suppressed by reforming the suspension and using the pitching control of e-4ORCE. Thus, the occupants are less likely to feel the bodymotion in the front-rear direction when the vehicle is repeatedly started and stopped (e.g., driving in urban areas and in congested traffic). This helps realize a comfortable and high quality riding experience not only for the driver but also for the occupants in the passenger seat and rear seats.

The technological innovations that enabled the "Tough Gear" × "High Quality" concept of the new X-TRAIL are summarized in the following sections.

3. Power and high level of quietness: "e-POWER" × "VC-TURBO"

The new X-TRAIL is mounted with high-power motors at the front and rear. The variable compression ratio engine "VC-TURBO" (Fig. 6), mass-produced for the first time in the world by Nissan, is adopted as the power generation engine. This engine provides benefits such as powerful acceleration performance, low fuel consumption, and significantly improved level of quietness.

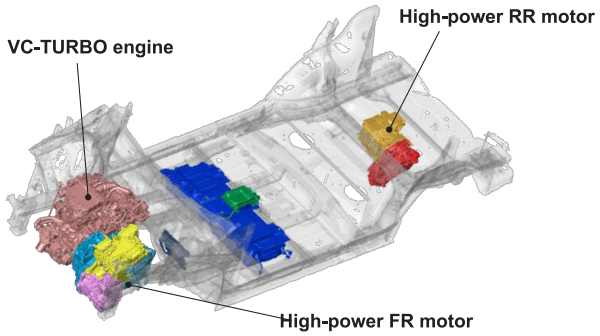

Fig. 6 Second-generation e-POWER × VC-TURBO

3.1 Second-generation e-POWER

The second-generation e-POWER system incorporated in the new X-TRAIL includes high-power/high-torque front (150 kW/330 N·m) and rear motors (100 kW/195 N·m), which enable quick response and powerful acceleration performance on high-speed roads and off-road tracks. During normal cruising, low fuel consumption is achieved by optimizing the energy efficiency based on the area of frequent engine usage in the e-POWER system.

Energy management is performed by minimizing the engine starting frequency when driving at low speeds (e.g., in urban areas) and by generating electricity at low engine speeds efficiently, even when the engine needs to be started. Furthermore, the adopted control technology detects road surface conditions and starts the engine when the road noise is high, which leads to a level of quietness that can be compared to that of EVs during normal driving.

3.2 VC-TURBO engine for e-POWER

In the conventional e-POWER system, a high engine speed is required to obtain high power from the engine. Compared with the conventional system, the VC-TURBO engine lowers the engine speed while significantly increasing torque and power. In scenarios where low fuel consumption is required, the compression ratio is increased to generate electricity with high efficiency. In scenarios where high power is required, the compression ratio is lowered and the boost pressure is raised during electricity generation (Fig. 7). Consequently, low fuel consumption, high power, and a high level of quietness are achieved at a high level, thereby allowing a buffer when supplying electricity to the high-power motor.

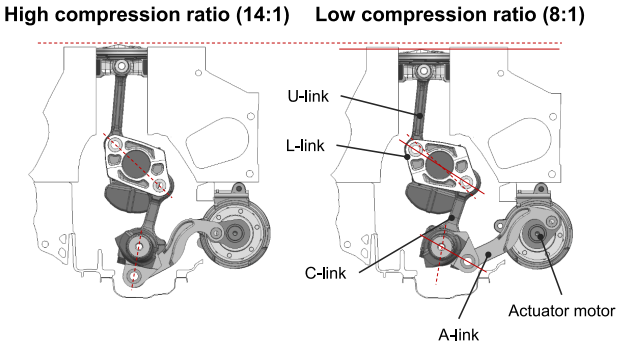

Fig. 7 VC-TURBO engine for e-POWER

3.3 Evolution of e-Pedal Step

The e-Pedal Step, which enables the driver to control the vehicle speed using only the accelerator pedal, employs regenerative brake/hydraulic brake integrated control for the first time in an e-POWER-incorporated vehicle to realize a stable deceleration of up to 0.2 G. The hydraulic brake is activated automatically depending on the scenario, thus enabling the driver to drive the vehicle with a sense of security and comfort in various scenarios such as urban areas (where acceleration and deceleration are repeated), long downhill roads, and snowy road surfaces.

4. "e-4ORCE": Changing the concept of 4WD

The electric drive four-wheel control technology "e-4ORCE" that integrates Nissan's electrification technology, 4WD control technology, and chassis control technology was mounted as a new feature. The driving force of each wheel is optimized by performing integrated control of the high-power motors (one each mounted at the front and rear) and left/right brakes. This optimization provides an exciting driving experience and a comfortable riding experience to all vehicle occupants when the vehicle is driven in various scenarios and under different road surface conditions (e.g., exerting drivability on snowy road surfaces and mountain roads and driving the vehicle for daily use in urban areas).

<Value provided by e-4ORCE>

・Easy path following as per driver's expectations: Cornering, as intended by the driver, is realized with the minimum number of steering operations by judging the road surface and vehicle conditions instantaneously and by fully utilizing the friction force of the tires by controlling the brakes and driving force of the front/rear motors precisely.

・Confidence anywhere: Smooth starting and driving experiences are realized by avoiding slipping and stuck tires and by helping to secure optimal traction, even in off-road situations and on snowy road surfaces.

・Comfortable ride for all: The oscillation of the occupant's head in the front-rear direction is mitigated when decelerating while driving in an urban area by stabilizing the vehicle body behavior via adjustments to the amount of regenerative braking applied by the front and rear motors.

・Powerful and smooth driving: A feeling of strong, sustained acceleration is realized by having high-power motors respond quickly when the driver steps on the accelerator pedal. This feature enables smooth merging with expressway traffic.

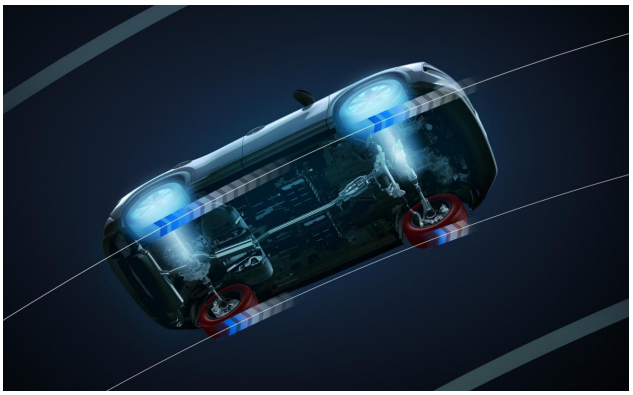

Fig. 8 e-4ORCE

5. High-stiffness body/chassis that supports the powerful driving performance

In the new X-TRAIL, the platform is modified completely to achieve a high level of handling stability, ride comfort, and quietness.

For the body, the usage ratio of high-tensile-strength steel sheet is increased to 42%, and a cross-frame structure that has no center tunnel or splitting portion (Fig. 9) is adopted, which increases the body torsional stiffness by 44% while suppressing the increase in mass. These new measures significantly improve the safety and dynamic performances (e.g., handling stability, ride comfort, and quietness) of the X-TRAIL.

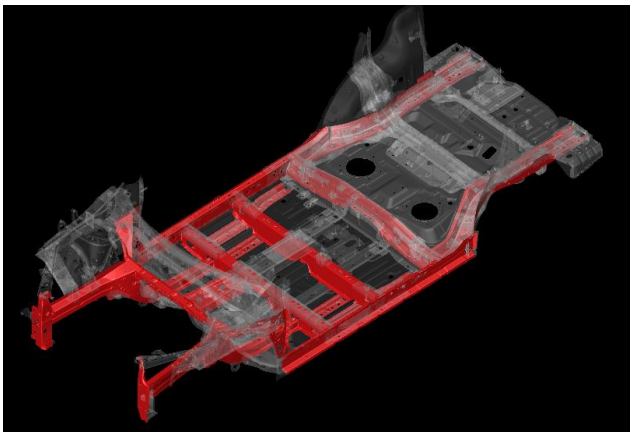

Fig. 9 Platform body

The newly designed multilink suspension, which utilizes the technology developed for the higher segment, is adopted for the rear suspension to improve stability and ride comfort (improvement in ride comfort is achieved by a 30% reduction in impact shock, which is difficult to achieve simultaneously with stability improvement). By combining these structures with a high-stiffness, quick-ratio, rack-type electric power steering system, a highly responsive handling performance requiring minimal corrective steering is realized. We hope that the drivers experience pleasurable, exhilarating, and confident driving pursued by Nissan.

6. Advanced and high quality interior space

The interior design of the new X-TRAIL aims to provide both toughness and high quality ride comfort (Fig. 10). The center console, designed as a bridge structure floated in the air, is provided with cup holders for large cups. Facial tissue boxes and lap blankets can be stored below the console. The console lid, which also functions as an armrest, has a double-door structure to allow stored goods to be removed from the rear seat.

Fig. 10 Cockpit

The newly developed seat material "TailorFit™" (Fig. 11) improves the smoothness because the gap between the crests of the fabric pattern are made similar to those between the crests of a fingerprint. A stable friction force and smooth touch are realized by adding particles to the top coating. Therefore, a texure comparable to that of soft leather is realized.

Fig. 11 New seat material "TailorFit™"

For the meter, a 12.3-inch advanced drive-assist display capable of selecting between two types of display modes is adopted. Further, a 10.8-inch head-up display is mounted so that the information can be displayed in an easy-to-understand manner that requires little eye movement (Fig. 12). The 12.3-inch Nissan Connect navigation system, adopted for the center display, is equipped with voice assistance and Amazon Alexa to allow occupants to perform operations using plain language. Thus, an HMI that provides various types of services while maintaining safety and convenience is realized.

Fig. 12 Head-up display

In terms of luggage space, the opening and luggage space width are widened to realize best-in-class roominess and make loading and unloading easier. A 100 VAC power supply (1500 W) outlet is provided in the luggage space. The power supply outlet can be used during outdoor activities and as an emergency power source during natural disasters. (Fig. 13).

Fig. 13 Luggage space and 100 VAC power supply

7. Summary

The new X-TRAIL has become a convention-defying middle-class SUV that achieves power, smoothness, and an EV-like level of quietness because of its innovative powertrain and vehicle body technology; further, it features an excellent driving performance owing to e-4ORCE. In urban areas and on winding roads, drivers can drive as comfortably as intended. On rough roads such as snowy road surfaces and off-road conditions, the drivers can drive easily with ease and a sense of security.

Nissan hopes that our customers will drive and experience our new X-TRAIL, which realizes both the “Tough Gear” × “High Quality” concept. We wish that our passion will resonate with our customers.

Authors

Tetsuya Yamamoto

2. "VC-TURBO" and "e-POWER" System

Naohiro Yoshida* Jun Hasegawa* Masaki Takaoka*

1. Introduction

A new e-POWER system was developed and installed in the X-TRAIL for the first time to satisfy the development concepts of "Tough Gear" and "High Quality." The purpose, outline, and system design of the e-POWER system are described in this chapter.

2. Overview and lineup of the e-POWER system

Fig. 1 shows the powertrain system of the e-POWER system, wherein 100% of the electric power is generated by the engine and 100% of the driving force is provided by the motor.

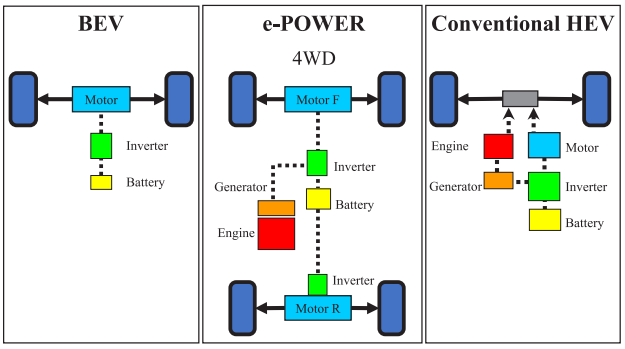

Fig. 1 e-POWER system configuration

The e-POWER system utilizes the characteristics of a 100% motor drive that generates the maximum torque at low revolutions and does not utilize a transmission mechanism. In addition, Nissan's unique motor control technology, which is created through the development of Leaf, is used to respond quickly to the accelerator pedal to ensure smooth acceleration. This is the primary feature of the e-POWER system. Further, the engine can be controlled independently of the drive system of the wheel shaft, which allows the start/stop time to be set independently of the vehicle driving pattern. Based on fixed-point engine operation, high fuel consumption efficiency can be achieved by improving the energy efficiency once the engine is started.

In 2016, the 1st-generation e-POWER system was installed in a compact car for the Japanese domestic market for the first time. Later, in 2018, the range of models equipped with the system was expanded to include mini-vans and small Sports Utility Vehicles (SUVs) for the domestic market.

In 2020, the 2nd-generation e-POWER system was installed in a new compact car, and its most significant features—strength, smoothness, and quietness—were evolved further to create a more electric vehicle (EV)-like feeling. To this end, the motor, inverter, battery, and engine that constitute the system were improved for increasing not only the output and the torque, but also fuel efficiency. Fig. 2 shows the e-POWER lineup.

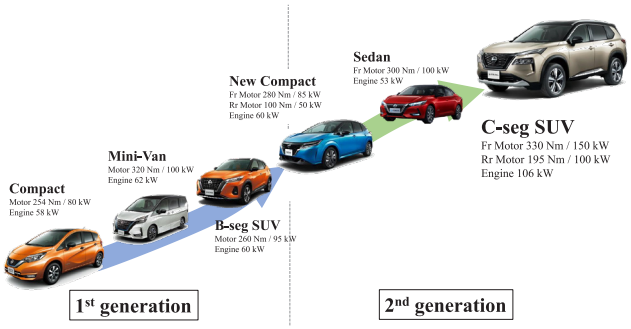

Fig. 2 Line-up of e-POWER installed vehicles

3. Aim of the X-TRAIL-dedicated e-POWER system

The new e-POWER system is developed as a powertrain for C-segment SUVs. It will be launched globally for the first time, with improved quietness, smoother acceleration, and increased fuel efficiency.

In recent years, the demand for C-segment SUVs has increased rapidly in the automobile market given the increase in customer requirements. To this end, the top-class levels of quietness and acceleration performance related to "EV-ness" and sufficient fuel efficiency performance need to be achieved for satisfying the

*Powertrain and EV Engineering Division Powertrain and EV Project Management Department

high-performance requirements. Along with global expansion, the need to respond to towing requirements and high-speed driving requirements were also added.

Fig. 3 illustrates the newly developed e-POWER system and Table 1 summarizes its main specifications. Compared to the existing 2nd-generation e-POWER system, the drive motor is enlarged, the displacement of the power generation engine is increased from 1.2 L to 1.5 L with a supercharger, and the VC-TURBO engine is equipped with a variable compression ratio mechanism. Further, the 4WD model is added to the lineup.

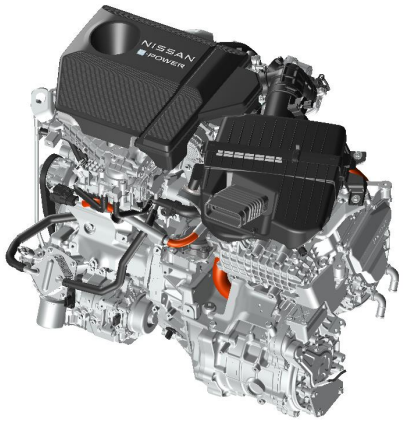

Fig. 3 New e-POWER system

Table 1 Specifications of the new e-POWER system

		Compact(2nd gen.)	C-seg SUV
Drive system	Fr Motor power	100 kW	150 kW
	Rr Motor power	50 kW	100 kW
Generating system	Generator Power	60 kW	116 kW
	Engine type	Gasoline L3 NA	Gasoline L3 Turbo
	Engine displacement	1.2L	1.5 L
Battery	Type	Li-ion	Li-ion

4. Overview of X-TRAIL-dedicated e-POWER system

The existing e-POWER system is based on fixed-point engine operation, and therefore, the fuel consumption rate during the fixed-point operation considerably affects the fuel efficiency of the vehicle. This trade-off between the fuel efficiency and the output performance needs to be eliminated to increase the engine output while maintaining fuel efficiency during fixed-point operation. To this end, the new e-POWER system employs a VC-TURBO engine to achieve high output with the compression ratio set to low at the output point, while maintaining high fuel efficiency by setting a high compression ratio during fixed-point operation. Fig. 4 shows the compression ratio map and engine operating point frequency of the VC-TURBO engine.

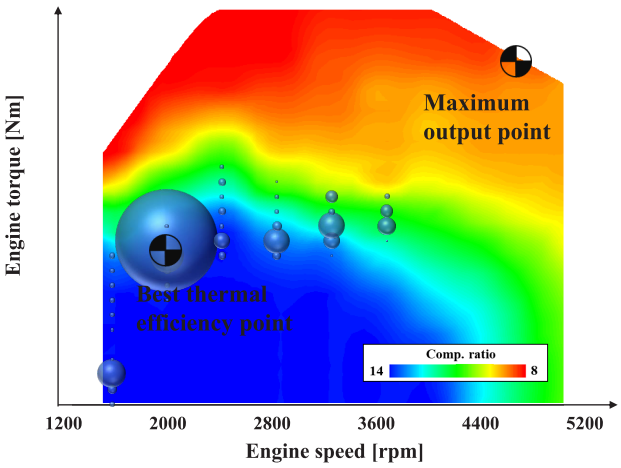

Fig. 4 VC-TURBO compression map

A special exhaust system is specifically developed for the engine operating point unique to the e-POWER system, which does not utilize engine speeds below 1500 rpm. The exhaust system reciprocates the tube in the rear muffler to reduce resonance and exhaust noise. In addition, an optimal bypass route is set to generate low exhaust pressure for ensuring sufficient engine output.

For the brake system, an electric control brake unit was incorporated in the e-POWER system for the first time; this resulted in improved quietness through collaborative control with the e-POWER system. In the previous e-POWER system, there was a need to start the engine to generate negative pressure when braking. However, the use of an electric brake eliminates this need, which reduces the frequency of starting the engine. Further, the previous e-POWER system generated a deceleration G through a regeneration system when driving downhill; however, after the vehicle is fully charged, it was necessary to maintain the deceleration G while rotating the engine at high speed and discharging the regenerative energy. The new X-TRAIL is equipped with an electric controlled brake unit that stops regeneration after a full charge and activates the electric brake to ensure deceleration G, which helps suppress an increase in engine speed and improves quietness.

5. Overwhelmingly superior performance

The overwhelmingly superior quietness, acceleration performance, drivability, fuel economy, and exhaust performance provided by the X-TRAIL e-POWER system are described below.

5.1 Quietness

5.1.1 Engine operating frequency

The C-segment SUVs are heavier than compact cars, and therefore, the former requires more energy when starting and accelerating compared to that for the latter. Thus, the engine operating range expands if conventional energy management system is used, which can lead to an increase in the engine start frequency and a loss of

"EV-ness."

The new e-POWER system defines the area where the driver senses the engine noise, and it is designed to prevent the engine from starting in this area to realize a quieter driving experience wherein the driver does not sense the engine starting noise.

Fig. 5 presents the above-mentioned engine operating range. The noise level inside the vehicle is evaluated. The engine startup frequency is reduced in the low speed range where the engine noise is greater than the road noise generated outside the vehicle; the frequency is increased in the high speed range where the engine noise is lower than the background noise.

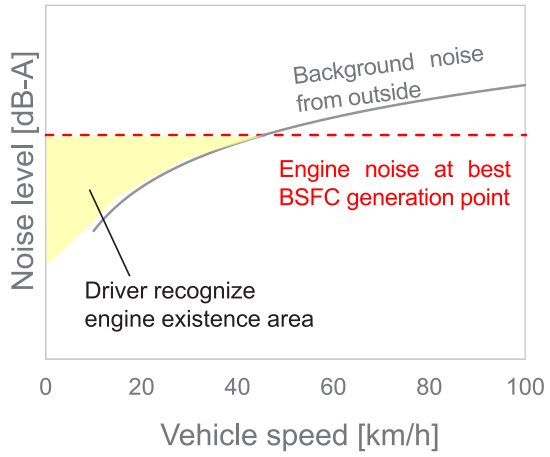

Fig. 5 Relationship between background noise and engine noise

Fig. 6 shows the frequency of engine startups at each vehicle speed in a practical driving pattern. Compared to the 2nd-generation compact car, which reduced the number of engine startups for all vehicle speed ranges, startups for the new vehicle is reduced to the 20–40 km/h range, while it is increased in the 40–60 km/h range. Therefore, it is now possible to improve quietness while increasing power generation energy.

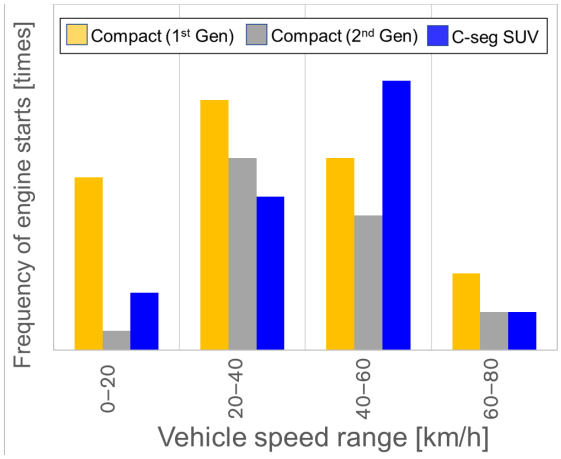

Fig. 6 Comparison of engine startup frequency

The engine is started and stopped depending on various conditions such as vehicle speed, State of Charge (SOC) of battery, and required driving force. The frequency of engine startups during one run is significantly reduced by increasing the amount of charging energy per power generation cycle at the start. Fig. 7 shows the engine operating time in the Worldwide-harmonized Light vehicle Test Cycle (WLTC) mode. The frequency of the engine startups can be considerably reduced, which helps improve quietness and fuel efficiency.

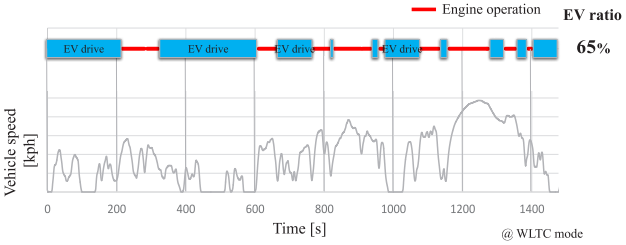

Fig. 7 Engine operation time

5.1.2 Lowering engine speed

Combined with the newly developed e-POWER system, the VC-TURBO engine can generate higher torque at lower revolutions than that with conventional naturally aspirated engines. This characteristic allows generating equal output at a lower engine speed compared to that with naturally aspirated engines and helps reduce the engine speed during fixed-point engine operation. Fig. 8 shows the engine speed during fixed-point operation at each vehicle speed. Compared to that for the 2nd-generation compact car, it is possible to lower the engine speed over a wide range: from low vehicle speeds with low background noise to high vehicle speeds. This facilitates reducing the engine noise level even when the engine is in operation.

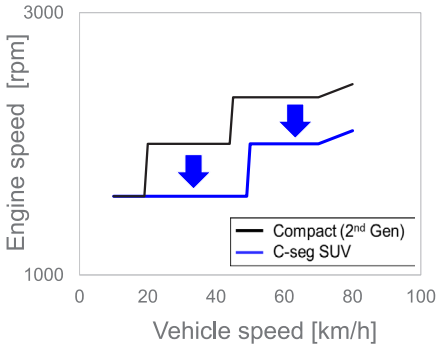

Fig. 8 Engine speed of fixed-point operation

5.2 Acceleration performance and drivability

5.2.1 Acceleration performance

The high driving power provided by the new motor of the newly developed e-POWER system and the high-output power generated by the VC-TURBO engine enable the car to achieve the top-level acceleration performance in its class.

Fig. 9 shows a comparison of acceleration G and vehicle speed profiles during the start acceleration with the conventional HEV system. The acceleration G is quickly launched immediately after starting acceleration by exploiting the 100% motor drive characteristics, which helps realize the high response. In addition, the high G is maintained to produce a feeling of acceleration growth even after the rise in acceleration G.

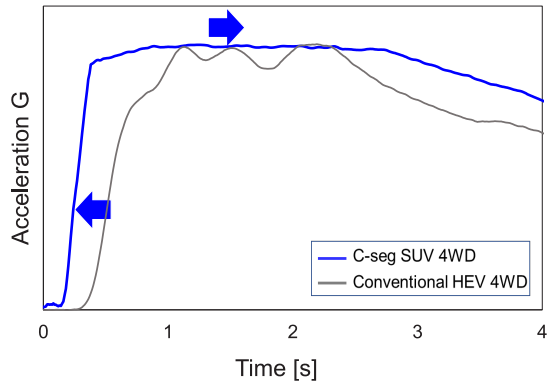

Fig. 9 Acceleration G at standing start

5.2.2 Drive torque control matched to supercharged engine characteristics

A supercharged engine is accompanied by a delay in the supercharging response when the torque increases compared to that for the naturally aspirated engine. Given this characteristic, the newly developed e-POWER system incorporates a new technology that controls the drive torque to ensure smooth acceleration while generating supercharging pressure.

Fig. 10 shows the relationship between the supplied energy and the generated drive torque during acceleration. The battery energy is used immediately after acceleration to generate driving torque with a good response. Meanwhile, the engine is started, and then, the energy generated by the engine is added to the energy of the battery to increase the driving torque.

The supply of the energy generated by the engine at this time is delayed because of the delay in the supercharging response. However, the drive torque is controlled to ensure a smooth increase without temporary drops attributed to this delay (a). The driving force is changed based on the acceleration request of the driver because it is possible to supply the generated energy after the engine is supercharged (b). Thus, a large acceleration is achieved compared to that of a naturally aspirated engine, whereas a smooth and boosted supercharging pressure is generated without the uncomfortable feeling produced when the accelerator is operated.

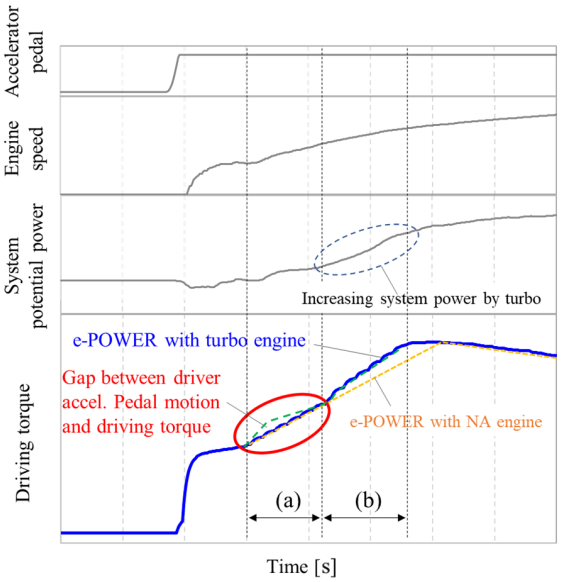

Fig. 10 Time chart of driving torque

5.2.3 Improved feeling of acceleration due to engine sound

We developed a technology that provides a pleasant feeling of acceleration from the sound of the engine during power generation to allow the driver to feel the acceleration not only from the acceleration G but also from the sound of the engine.

The e-POWER system can control the engine and wheel axle drive systems independently, which allows the engine speed during acceleration to be set freely. In addition, the VC-TURBO engine can generate sufficient engine torque even in the low revolution range. Utilizing these two features, the e-POWER system enables the engine speed to not only increase immediately, but also to increase in conjunction with the vehicle speed even if the driver strongly requests acceleration (when the accelerator pedal is depressed considerably).

The relationship between the engine sound (rpm) and the driver's acceleration request is defined to set the engine speed linked to the vehicle speed for the following two zones through sensory evaluation.

Zone 1, where the engine sound (rpm) is high relative to the vehicle speed.

Zone 2, where the vehicle speed and engine sound (rpm) are synchronized.

Fig. 11 shows both zones 1 and 2. In Zone 1, the engine sound (rpm) rises before the vehicle speed, which creates a sense of discomfort during acceleration. In Zone 2, the vehicle speed and engine sound (rpm) rise in tandem, which generate a comfortable feeling of acceleration that matches the acceleration request. If the driver's request for acceleration is stronger, Zone 2 can be used.

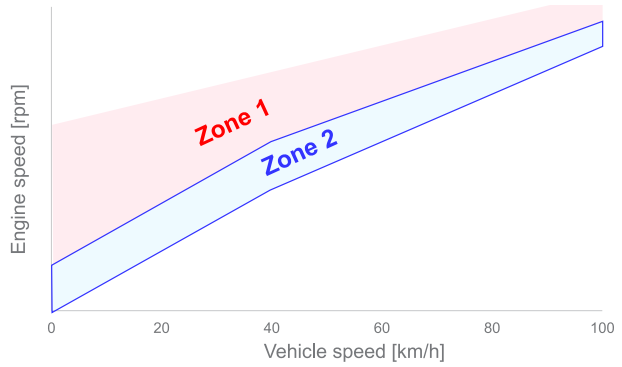

Fig. 11 Zone definition of engine sound

5.3 Fuel consumption and exhaust performance

The engine and drive shaft are not mechanically connected in the e-POWER system, and therefore, the engine start time and the operation point after startup can be selected freely. Fuel efficiency and exhaust performance are greatly improved by exploiting this feature.

In addition to the improvement of the frequency of engine operation described in 5.1.1, the best fuel economy point of the engine is improved with the use of the VC-TURBO engine (BSFC 217 g/kWh @ 2000 rpm), which results in the top-level fuel efficiency in its class (18.4 km/L for 4WD and 19.7 km/L for 2WD in the WLTC mode). In terms of exhaust performance, a 75% reduction in emissions from the 2018 standard is also achieved.

6. Summary

The following technologies were developed through the development of the e-POWER system for the new X-TRAIL.

Quietness)
Optimal control of the engine operating frequency and timing while lowering the engine speed during power generation by utilizing the characteristics of the VC-TURBO engine.

Acceleration performance)
Drive control utilizing the newly developed motor for generating high torque and high output to allow for quick response and constant high G.

Acceleration feeling)
Engine speed control to create an engine sound based on the driver's acceleration request and vehicle speed.

Fuel efficiency and exhaust performance)
Optimum control of power generation at the best engine fuel efficiency point while optimizing the engine operation frequency.

Through these technologies, best in class levels of quietness, driving power, drivability, fuel efficiency, and exhaust performances in the C-segment SUVs were achieved.

References

(1) Akihiro Shibuya, Naoki Nakada, Makoto Kimura: Development of a Brand New Hybrid Powertrain for Compact Car Market (2016)
(2) 渋谷 彰弘 ほか:電気駆動の魅力の拡散　日産技報 No.87 (2021)
(3) 仲田 直樹:システムの特徴と今後の発展　日産技報 No.87 (2021)

Authors


Naohiro Yoshida


Jun Hasegawa


Masaki Takaoka

3. Engine Evolution of e-POWER

Kazuhiro Ogino* Yorihisa Tsuchiya* Hideaki Mizuno**
Yuuki Sakai** Yasuhide Abe***

1. Introduction

A 1.5 L turbo engine is developed for the new X-TRAIL to further enhance the powerful acceleration, quietness, and fuel efficiency performance features of the e-POWER system. This engine combines the world's first variable compression ratio (VCR) mechanism adopted in a mass-produced engine by Nissan in 2018 and a new low-pressure-cooled EGR (LP-EGR). The outline and features of the new KR15DDT engine installed in the new X-TRAIL are described in this chapter.

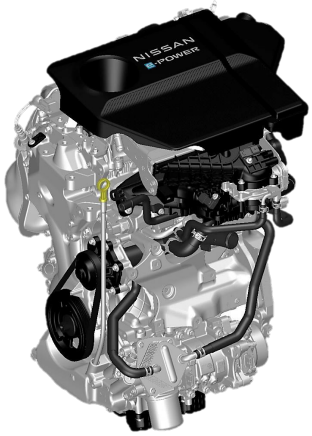

Fig. 1 New KR15DDT engine

2.1 Aim of engine development

The 1.2-L 3-cylinder naturally aspirated engine installed in the previous e-POWER system was improved to considerably increase the power output, quietness, and efficiency for improving the power generation energy to realize the concept of the new X-TRAIL ("Tough Gear" and "High Quality"). A 100% motor drive is attractive to achieve the high levels of quietness and smooth acceleration performance (EV-ness). To further upgrade these features, the engine was developed with the following aims.

[1] High thermal efficiency at a fixed-point operation
[2] High power at the maximum output point
[3] High level of quietness
[4] Compact engine

Fig. 2 shows the engine operating range and key performance concepts in the e-POWER system. Nissan has already succeeded in mass-producing the VCR system, and thus, it is possible to switch to a high compression ratio at [1] and to a low compression ratio at [2] using that mechanism. Moreover, it is possible to achieve both high efficiency and high output if the VCR mechanism is combined with LP-EGR.(1)

The multilink system that comprises the VCR mechanism can reduce the friction of the piston in the thrust direction. Therefore, the engine speed at the optimum fuel efficiency point can be lowered if it is combined with the improved thermal efficiency achieved by setting a high compression ratio. Further, it is possible to lower the rpm at the maximum output point by setting a low compression ratio, which helps satisfy the quietness requirement [3].

For compactness [4], the variable timing control system(VTC) is simplified for further downsizing and a 3-cylinder engine is selected. In conventional hybrid electric vehicle (HEV) engines, the compression reaction force of the engine is reduced as a vibration damping measure at engine startup. However, it is now possible to reduce the compression reaction force without the intake VTC and satisfy the relevant performance by utilizing the VCR mechanism. In addition to narrowing down the engine operating range specific to the e-POWER system, the performance-based design of variable compression and LP-EGR can achieve high efficiency, high output, and excellent exhaust performance without relying on the VTC.

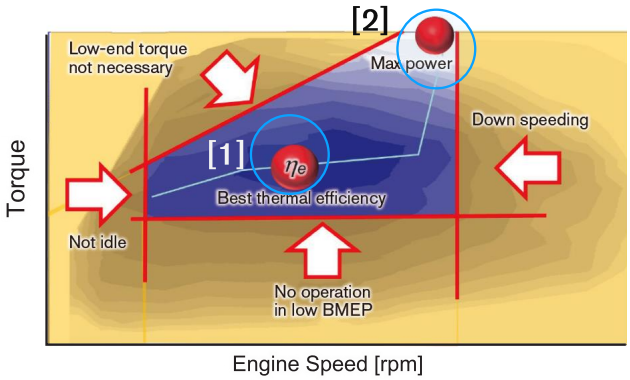

Fig. 2 Engine operating range for e-POWER system

*Powertrain and EV Engineering Division Powertrain and EV Project Management Department
**Powertrain and EV Engineering Division Powertrain and EV Mechanical system Technology Department
***Powertrain and EV Engineering Division Powertrain and EV Performance Calibration Engineering Department

2.2 Working principle of variable compression ratio engine

Fig. 3 shows the configuration of the multilink system in the VCR mechanism. When the rotational posture of the control shaft changes clockwise with respect to the engine block and the eccentric axis, i.e., when the swing point of the C-link moves downward, the L-link rotates clockwise around the crankpin to enlarge the angle between the U link and L link at the top dead center; further, the U-link and piston move upward, which increases the mechanical compression ratio of the engine[1]. Conversely, changing the rotational attitude of the control shaft to counterclockwise can reduce the mechanical compression ratio. For an in-line multicylinder engine, the control shaft is shared by each cylinder, and thus, by changing the rotational posture of one control shaft relative to the cylinder block, the mechanical compression ratios of all cylinders can be switched simultaneously.

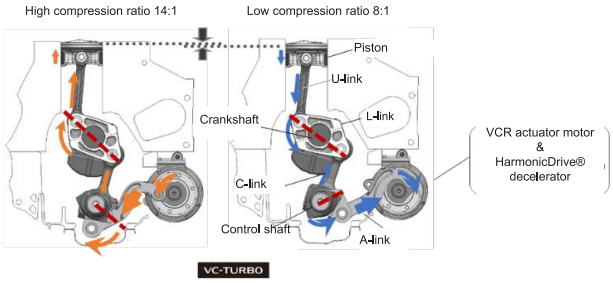

Fig. 3. Configuration of Multilink mechanism

3. Achieved performance

The adoption of the VC-TURBO engine greatly improved the engine torque compared to that with HR12DE engine (Fig. 4). This increases the flexibility of the engine operating point required for power generation and energy management, which in turn improves both the fixed-point operating points and quietness. Further, the generated engine noise is greatly reduced by lowering the engine speed at the maximum output point, even when the engine is under heavy load.

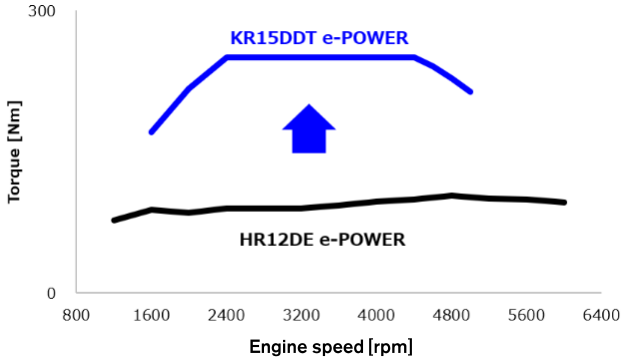

Fig. 4 Torque curve of the new engine

3.1 Fixed-point operation, best fuel efficiency, and quietness

Compared to the previous e-POWER HR12DE engine, the EGR rate and compression ratio (C/R) for the new e-POWER system are controlled throughout the low-load and high-load fuel consumption ranges, respectively, to improve both fuel efficiency and quietness. A transition from the quick engine start to a fixed-point operation was implemented, and performance-based design was conducted with the best thermal efficiency point at 2000 rpm (minimum brake specific fuel consumption: 217 g/kWh) as the steady-state operation point (Figs. 5 and 6).

a) A negative-pressure-control butterfly valve was added to the EGR inlet to expand the EGR range and improve thermal efficiency by suppressing knocking under supercharging and high compression ratios.
b) A flat piston and high tumble-intake port strengthen the gas flow in the cylinder and ensure combustion stability in the high EGR range.
c) The multilink mechanism reduces piston thrust force, which leads to low friction.

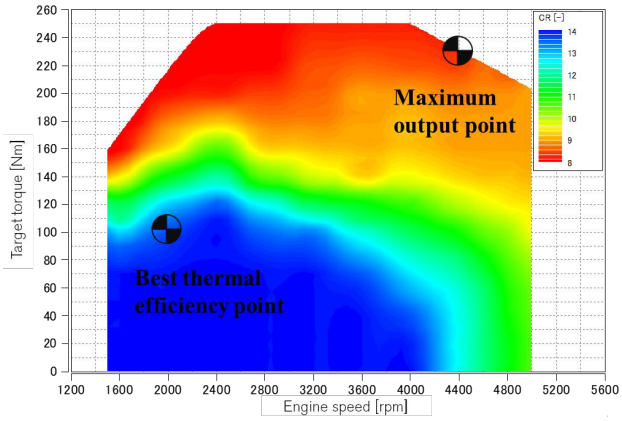

Fig. 5 Compression ratio map

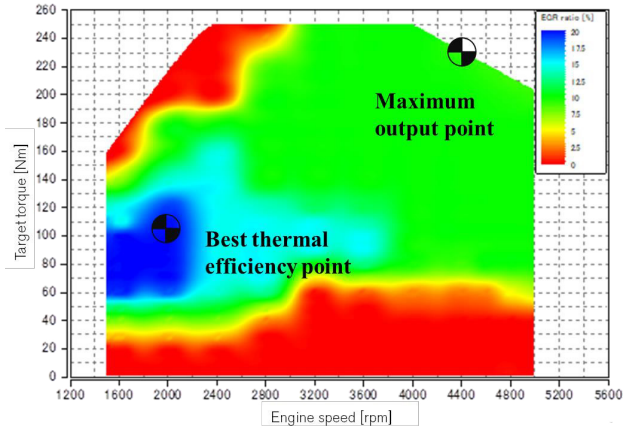

Fig. 6 EGR rate map

Conventionally, the fixed-point operation of the e-POWER system is set at around 2350 rpm to balance energy management. However, it is now possible to perform energy management at the best fuel-consumption point of engine operation through the increased options for the engine operating point attributed to the large increase in torque.

Changing the engine speed of this fixed-point operation (2350 → 2000 rpm) improves quietness considerably, which reduces engine noise by about 2 dBA. This helps eliminate the annoying engine noise while driving, which makes it possible to provide customers with the EV-ness feeling.

Now, more than 80% of the operating time can be provided in "WLTC + Extra High" mode at the best fuel efficiency point by achieving high efficiency and quietness while satisfying energy management requirements (Fig. 7).

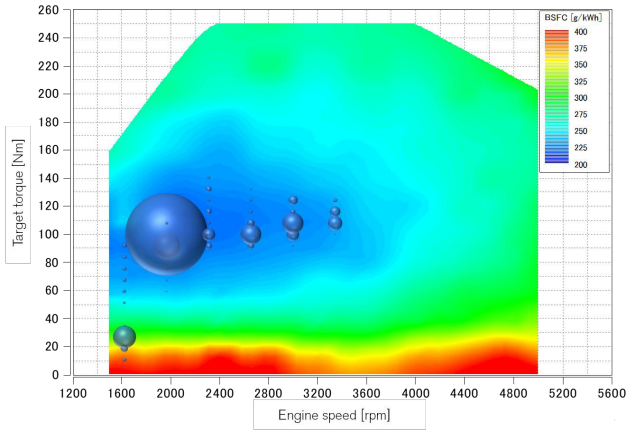

Fig. 7 Engine fuel efficiency and engine operating frequency

3.2 Maximum output point and quietness

The C/R of a general engine requires a design that considers the balance between fuel economy demand and output requirements. The VCR mechanism allows the C/R to be selected freely (ranging from 8.0 to 14.0) because of the VC-TURBO engine, which allows for performance-based design exclusively for the maximum output point; therefore, "C/R = 8.0" is selected. The maximum output of 106 kW is achieved at 4400 rpm (for domestic market).

This C/R setting and engine sound are compared with those of a general engine; the comparative engine setting is assumed to be C/R = 10.5. At this C/R, the maximum output point needs to be set at 5600 rpm to avoid knocking (abnormal combustion), whereas the VC-TURBO engine allows the maximum output point to be set at 4400 rpm. The engine speed can be set lower by 1200 rpm, and therefore, the engine noise is reduced by approximately 3.5 dBA under high-load conditions such as during continuous high-speed driving.

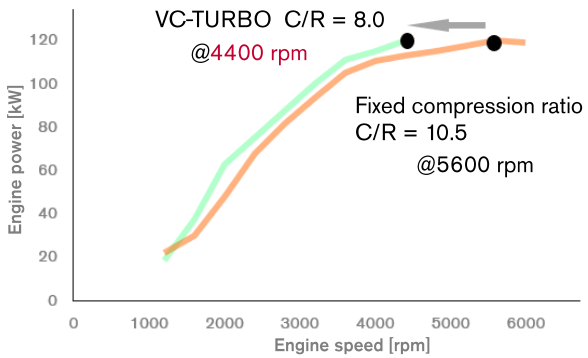

Fig. 8 Maximum output speeds at different compression ratios

3.3 Sound quality of 3-cylinder VC-TURBO engine

The sound pressure level of the engine at the maximum output point can be reduced considerably; however, it is not possible to completely block the engine noise from the driver. Thus, the VC-TURBO engine is designed to create a pleasant sound unlike that generated by a conventional 3-cylinder engine[3].

In a conventional 3-cylinder engine, the main component of engine speed is the 1.5th order attributed to torque fluctuations, and therefore, the tone of the engine sound is full of low frequencies.

In contrast, the VC-TURBO engine has a high-order component in the vertical inertial excitation force of the piston because the piston motion (Fig. 9) has different ascending and descending strokes unique to the multilink mechanism.

Fig. 9 shows the waveforms of the piston's vertical inertia force of each cylinder and the graph of the resultant force at each crank angle.

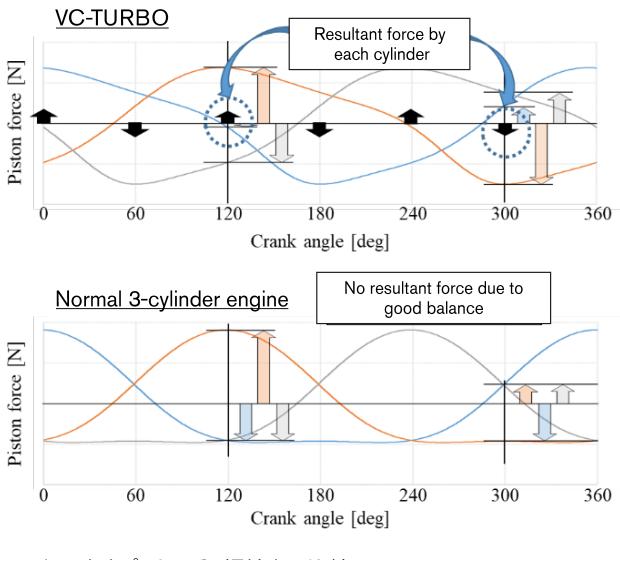

Fig. 9 Comparison of vertical piston system and piston force

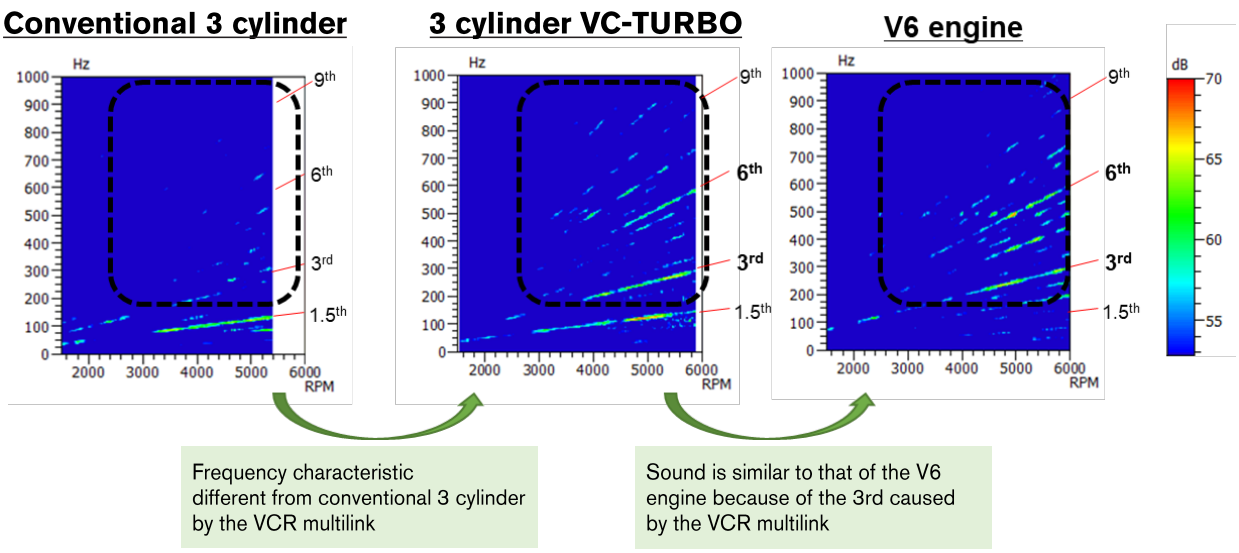

Fig. 10 Interior engine sound and frequency analysis

In a conventional 3-cylinder engine, there is no resultant force because each cylinder is balanced; in contrast, the VC-TURBO engine can generate vertical inertia force in a 120° cycle (3 cycles per engine speed). Thus, the sound heard inside the vehicle is a light sound (Fig. 10) based on the 3n-order engine speed.

4. Summary

The new 3-cylinder VC-TURBO engine achieves a low rpm at the fixed-point operation and with low fuel consumption, which enables a maximum output of 106 kW at as low as 4400 rpm.

These technologies contributed greatly to achieving the goals of the new X-TRAIL performance by supporting precise power generation and energy management to realize EV-ness and quietness beyond the conventional limits.

References

(1) Kiga shinichi et al.:The world's first Production VariableCompression Ratio engine -The new Nissan VC-T (Variable Compression-Turbo) engine, 38th International Vienna Motor Symposium, 2017
(2) 松岡一哉 他: 新型 高効率1.5L 3気筒 可変圧縮比エンジン開発 自動車技術会 2021年度 秋季自動車技術会
(3) Tsuchiya Yorihisa et al.:Development of the Second-Generation VC-TURBO, KR15DDT Engine, 30th Aachen Colloquium Sustainable Mobility, 2021

Authors


Kazuhiro Ogino


Yorihisa Tsuchiya


Hideaki Mizuno


Yuuki Sakai


Yasuhide Abe

4. Application of e-4ORCE to Full-Scale SUVs

Takeji Katakura* Ryota Suzuki*

1. Introduction

Nissan Motor plans to combine the electric powertrain system "e-POWER," which enables 100% power generation with the engine and 100% motor-based drive, and the electric all-wheel drive (AWD) system, which incorporates two motors in the front and rear wheels, in a full-fledged SUV, New X-TRAIL (Fig. 1). The new electric AWD control technology "e-4ORCE" unveiled at the 2019 Tokyo Motor Show "ARIYA Concept" will also be applied in combination.

Fig. 1 New X-TRAIL

This chapter describes the e-4ORCE technology and AWD performance for the New X-TRAIL, which is Nissan's first full-fledged SUV equipped with an electric powertrain.

2. Overview of e-4ORCE

The AWD system equipped with an internal combustion engine powertrain installed in the previous X-TRAIL model was designed to mechanically distribute the power generated by the internal combustion engine to the front and rear wheels through a coupled propeller shaft (Fig. 2, left). This causes a mechanical delay in the power transmission and introduces a mechanical limit to the resolution of the distribution. Further, unlike an electric motor, the internal combustion engine has difficulty controlling the output with a high response, and it cannot control the total driving force on the order of 0.1 s.

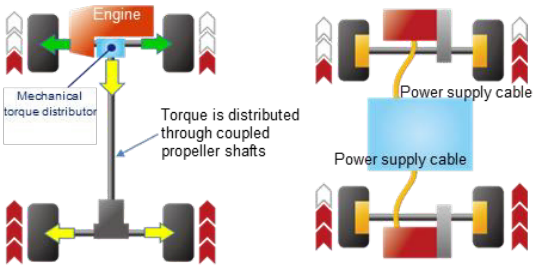

Fig. 2 Comparison of powertrain system configuration

The basic configuration of the electric powertrain "e-4ORCE" equipped with independent front and rear electric motors is shown in Fig. 2 (right). e-4ORCE enables the accurate distribution of the front and rear driving forces with high responsiveness.

One of the "e-4ORCE" control concepts is to extract 100% of the driving force of the four tires and transmit it to the road surface to stabilize the movement of the vehicle under any driving scenario. The vehicle body is supported by all four wheels, and the load applied to each wheel changes constantly depending on the road surface and vehicle conditions. Although the limit of each tire's ability to transmit the driving force to the road surface (tire grip force) (Fig. 3) changes based on the wheel load, a stable driving performance can be achieved by controlling all tires in a well-balanced manner such that they are within their limits. The new X-TRAIL e-4ORCE control function distributes the driving forces to the front and rear wheels to optimize the gripping ability of each tire based on the changes in wheel load caused by the road surface and driving conditions. Moreover, this control function controls the left and right brakes according to the driving scenario, and the braking forces are combined to improve the driving performance, except when decelerating.

*Powertrain and EV Performance Engineering Department

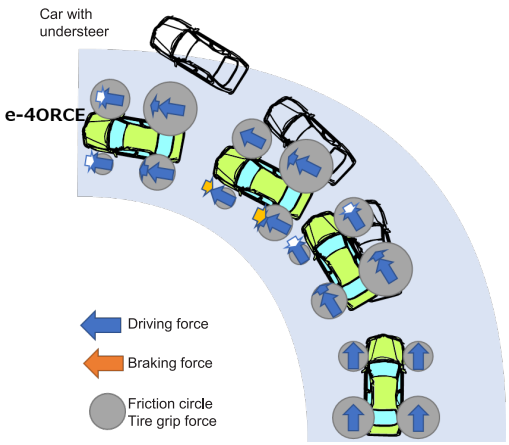

Fig. 3 Gripping ability and driving force distribution of the tire during turning

Another feature of the "e-4ORCE" control concept is vehicle pitching control, which considers the difference in the front and rear driving forces. Fig. 4 shows that the movement around the center of gravity of the vehicle shown in Equation (1) is generated according to the driving forces Ff and Fr of the front and rear tires, respectively, and the squat and dive angles (θ_f and θ_r) of the front and rear suspensions, respectively. Pitching control is based on the suspension strokes generated at the front and rear tires.

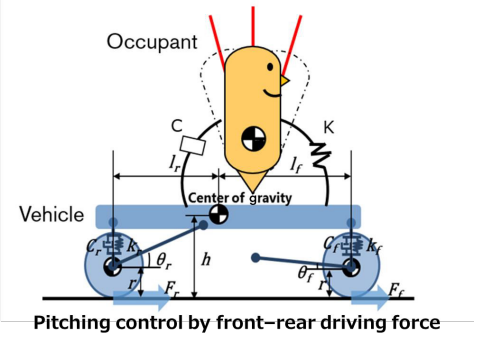

Pitching control by front–rear driving force

$$My = lfFf\tan\theta f + lrFr\tan\theta r - (Ff+Fr)(h-r) - Tdf - Tdr \quad (1)$$

Fig. 4 Pitching control by front and rear driving forces

The e-4ORCE controls the difference in the regenerative braking force between the front and rear motors for suppressing changes in the vehicle attitude during regenerative deceleration (Fig. 5). Thus, the pitch behavior of the vehicle body can be optimally suppressed, and a smooth and comfortable ride can be provided not only for the driver, but also for the front and rear seat passengers. (Adopted from Note: e-Power 4WD)

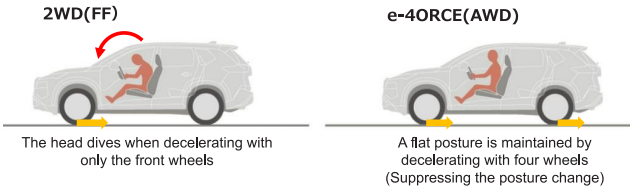

Fig. 5 Differences in car body posture attributed to pitching control

3. Values provided by e-4ORCE

Fig. 6 Values provided by e-4ORCE

The values provided by e-4ORCE are shown in Fig. 6 and listed below:

1) Easy to follow the path as per the driver's expectation
2) Comfortable ride for all passengers
3) Confidence to drive anywhere

Descriptions for 1) "Easy to follow the path as per the driver's expectation" and 2) "Comfortable ride for all passengers" have already been described in section 2. This chapter describes the key value in applying e-4ORCE to the new X-TRAIL, designed as a full-fledged SUV, that is, 3) "Confidence to drive anywhere," and it is explained from the perspective of the driver's driving operation and how the car moves in response to the driving operation using the following two characteristic driving scenes as examples.

Scene 1: Deep snow start

Fig. 7 Deep snow start

As shown in Fig. 7, a routine problem encountered in parking lots in snowy areas is to start a car in deep snow after a snowfall. The characteristics of this scene are that the tires are buried in the snow and create a large amount

of resistance against the direction in which the car is moving; therefore, a large driving force (torque) is required to overcome this resistance. The frictional resistance between the snow ground surface and tire is approximately 30% less than that of a typical dry asphalt road surface, which makes the tires slip easily. Under such conditions, precise motor torque control is required to prevent the tires from slipping while providing a driving force that overcomes the running resistance. e-4ORCE can ensure a stable start with a simple accelerator operation through the coordination of optimum front and rear motor torque control and brake control based on the vertical load on the tires.

Fig. 8 compares the deep-snow starting data between the previous X-TRAIL (with ICE and mechanical AWD) and the new X-TRAIL (with e-POWER and e-4ORCE).

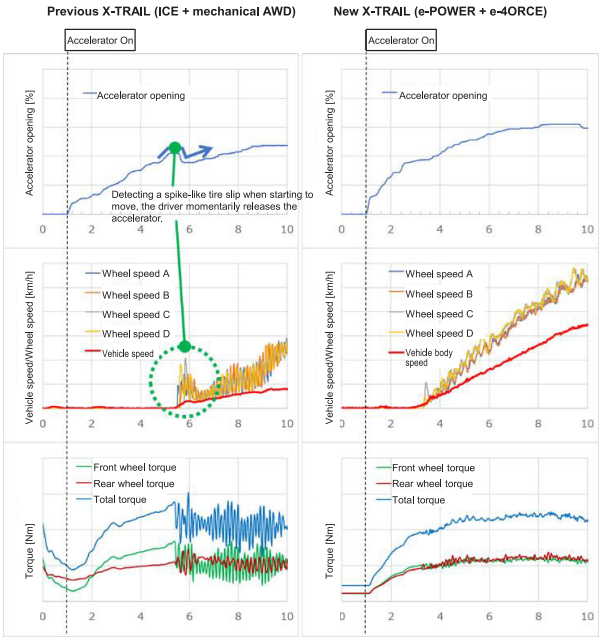

Fig. 8 Comparison of the performance when starting in deep snow

The top-row graphs show the accelerator pedal stroke, and the middle-row graphs present the correlated tire slip. In the previous model, excessive tire slip occurred as soon as the vehicle started to move and the accelerator was released. In the new e-4ORCE, which controls the amount of slip to the optimum level proportional to the increase in vehicle speed, the driver can step on the accelerator without worrying about complicated accelerator operations. For the front and rear torque comparison shown in the bottom graph, the e-4ORCE of the new model allows the front and rear torques to increase smoothly through a high torque response and through the precise control of the motor although the FF-based mechanism. The AWD of the previous model causes torque hunting because the front wheels slip.

Scene 2: Driving on mogul roads (rough surface, uneven roads)

Fig. 9 Driving on a bumpy road

Although it is unusual for a vehicle to encounter uneven terrain (bumpy roads) as shown in Fig. 9, a vehicle may encounter it at campsites, leisure facilities, off-road after bad weather, and in the event of a disaster. The characteristics of this scenario are that a large driving force is required to overcome the unevenness of the road surface, and that the running resistance of each tire changes because the vertical load condition of each tire varies depending on the unevenness of the road surface. Further, tires that have lost contact with the ground spin idly. Conventional vehicles require complicated pedal operations, such as stepping on the accelerator to apply traction each time to overcome a bump, and stepping on the brake to stop rushing after passing it. The e-4ORCE control makes use of the individual regenerative braking functions of the front and rear motor, which makes it possible to smoothly overcome the ups and downs during driving, while maintaining a constant speed simply by operating the accelerator pedal. Moreover, it allows for further reduction in the need to switch pedals because of the coordination with the brake control system that instantly suppresses the tires that have lost contact with the ground from spinning.

Fig. 10 shows a comparison of the bumpy road driving performance of the previous X-TRAIL (with ICE and mechanical AWD) and the new X-TRAIL (with e-POWER and e-4ORCE).

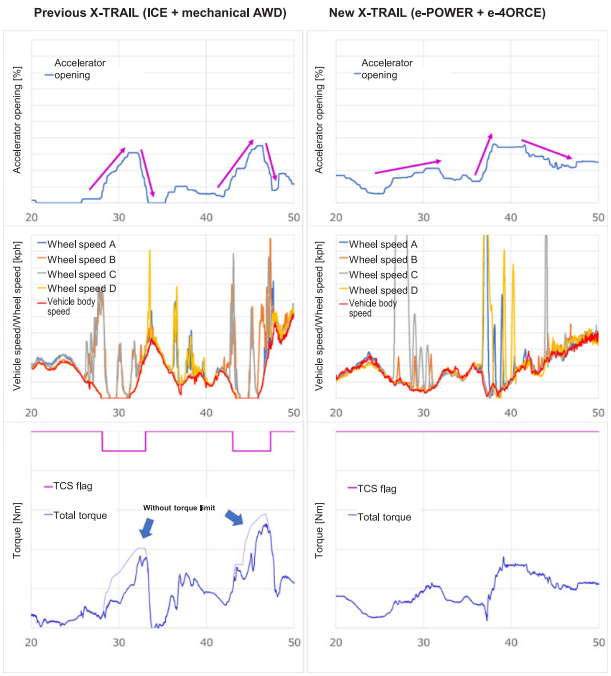

Fig. 10 Comparison of mogul road driving performance

The top-row graphs show the accelerator pedal strokes. In the previous X-TRAIL model, the accelerator pedal was turned on/off each time the car ran over uneven road surfaces. The new X-TRAIL model allows running by simply changing the amount of depression of the accelerator pedal. The bottom graphs show the tire-slip and traction control states. In the previous model (ICE + mechanical AWD), TCS (traction control) intervenes every time the tire spins to limit the engine torque; however, in the new model (e-POWER + e-4ORCE), the tire spin is appropriately controlled so that there is no need for traction control intervention. This enables continuous, powerful driving without unintended drive-force limitations.

4. Conclusion

The 100% electrically driven e-POWER system and the front/rear motor AWD control system e-4ORCE installed in the new X-TRAIL achieved a high level of ease of driving operation, comfort, and sense of security in each driving scene, which is expected for SUV applications. The responsive driving, comfortable ride, and sense of security, regardless of the road surface described in this study can be experienced in a wide range of situations, from everyday use to leisure, regardless of weather, climate, and other conditions.

We hope that more customers will enjoy the new electric AWD-equipped full-scale SUV provided by Nissan.

References

(1) 平工 良三、ほか：特集2-成長するe-POWER_6. 価値を高める電動AWD技術、日産技報No.87（2021）
(2) 富樫 寛之、ほか：特集2-次世代のフラッグシップARIYA_7. 日産が考える電動AWDの進化「e-4ORCE」、日産技報No.88（2022）
(3) 町田 直也、ほか：ドライビングシミュレータとCAEを用いた電動AWD車加減速挙動設計手法の開発、自動車技術会2022春季大会

Authors


Takeji Katakura

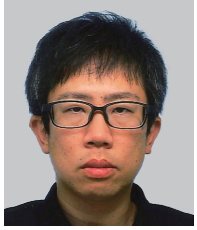
Ryota Suzuki

"Tough Gear" and "High Quality" for New X-TRAIL

5. NV Technology to Achieve EV-Level Quietness

Mengze Li* Shinichi Suganuma* Toshihisa Kuwata* Nobunari Funatsu**
Hiroaki Fukuoka** Takefumi Mitani** Kazushige Maeda**
Yasutsune Terashima*** Yuichi Igarashi*** Kazuhisa Okada*

1. Introduction

In Nissan's electrification strategy, the e-POWER system works as a sustainable technology that satisfies both environmental and driving requirements and is an important solution in addition to battery electric vehicles (BEV). Although this system has an internal combustion engine (ICE), it uses 100% electric power to drive a vehicle (Fig. 1) and can maintain the acceleration performance and quietness, which are the advantages of BEVs, while offering the convenience of not requiring charging; therefore, it is widely used.

Unlike conventional ICE-equipped vehicles, the e-POWER system switches the engine on and off without synchronizing with the driving operation of the driver; therefore, it is important to reduce the difference in noise level when the engine is switched on and off.

This section describes the evolution of quietness realization technology that enables the e-POWER system, which has been developed for compact cars, to be applied to C-segment SUVs.

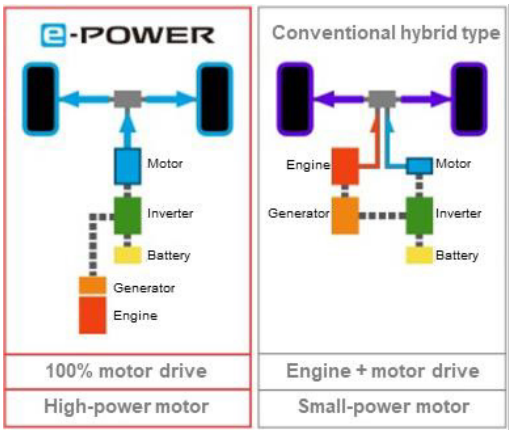

Fig. 1 Differences between e-POWER and conventional HEV systems

2. Challenge to higher quietness

The concepts of the new X-TRAIL include "Tough Gear" and "High Quality." To realize quietness, which is an important factor of "high quality," performance development is conducted to achieve the following three points:

(1) Reduce the frequency of engine operations (Section 3).
(2) Quiet the engine noise (Section 4)
(3) Match the engine sound to the driver's intention to accelerate (Section 5).

The engine used for power generation is changed to a high-output 3-cylinder downsized turbo engine to match the vehicle class of the C-segment SUV. Further, the entire vehicle, including the engine mounts, exhaust systems, active noise control, and vehicle bodies, is optimized to overcome NV-related issues such as low-frequency booming noise and vehicle body vibration.

Furthermore, the overall vehicle balance and noise insulation performance are significantly improved to ensure that customers can feel the overwhelming quietness the moment they enter or start the car. The quietness technology of the vehicles is described in Section 6.

3. Reducing the frequency of engine operation

Engine noise tends to stand out when background noise is low, such as when driving at low speeds. Thus, under such conditions, it is important to not operate the engine as far as possible. To this end, energy management control is implemented for actively generating power and storing it in driving scenes with high background noise. When driving at high speeds, the level of wind noise is high, which masks the engine noise and makes it less noticeable; therefore, power is actively generated. Conversely, when the vehicle speed is low (the background noise is also low), the engine is controlled so that it operates as little as possible based on the state of charge (SOC).

A road surface detection control system is adopted to control the engine start based on the road noise level to make the engine noise as inconspicuous as possible even under continuous low-speed driving conditions and to mask the engine noise with road noise.

Previous e-POWER-equipped vehicles needed to satisfy certain conditions to start the engine regardless of

*Customer Performance & Vehicle Test Department **Chassis Engineering Department ***Body Engineering Department

the SOC; therefore, some measures have been added to avoid engine startup requirements. There are scenarios in which the engine starts to supply negative pressure to the conventional brake system (Fig. 2); however, new brake system, electric control brake unit*, can avoid engine operation to create negative pressure for braking.

* Mainly adopted for Advanced driver-assistance system (ADAS) and collision safety performance, but it is also used for quietness improvement.

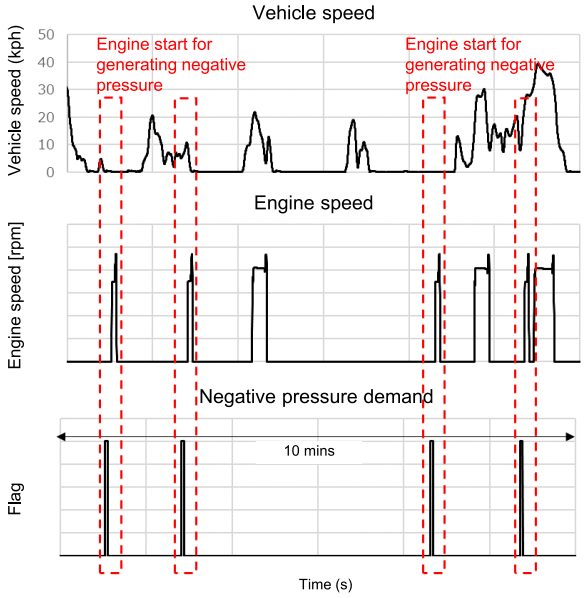

Fig. 2 Frequency of engine start for previous e-POWER system to generate negative pressure when driving in urban areas

4. Quieting engine noise

If the engine starts because of a decrease in SOC in a low-load and low-vehicle-speed scenario, the engine speed is lowered compared to that of the previous e-POWER system to ensure quietness. 1.5 L VC-TURBO engine, that was already adopted with CVT, was optimized for e-POWER system. It enables operation with higher torque and efficiency at a lower speed than the 1.2 L NA engine conventionally installed in compact cars. This allowed low-noise operation while securing sufficient power generation, which helped achieve both engine noise reduction and improved fuel efficiency.

5. Matching the engine sound to the driver's request for acceleration

High power must be supplied by the engine when strong acceleration is requested by the driver. However, the engine sound level needs to match the driver's request for acceleration to avoid discomfort during acceleration.

The engine sound level is highly sensitive to the rotational speed relative to the torque sensitivity (Figs. 3 and 4), and therefore, the engine speed increases linearly with the accelerator opening (acceleration G) and vehicle speed (Fig. 5).

In addition, the electric power required for driving* can be obtained through the characteristics of the variable compression (VC) engine by suppressing engine rotation and prioritizing torque so that the increase in rotation is considerably suppressed to provide a comfortable engine sound. For more details on 3, 4, and 5 in this chapter, refer to article 1-2. "VC-TURBO" and "e-POWER" System.

*Power generated by the engine = torque × RPM

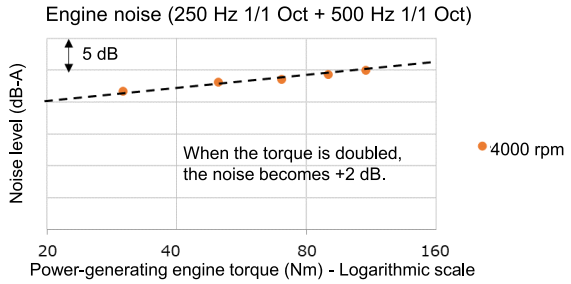

Fig. 3 Sensitivity of engine speed to engine noise

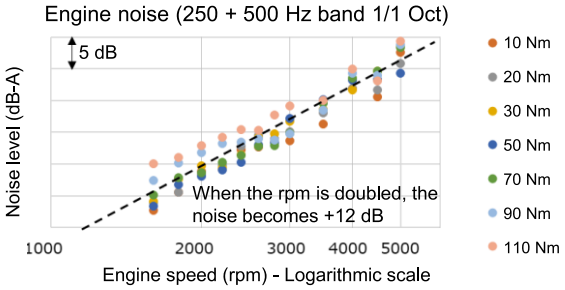

Fig. 4 Sensitivity of engine torque to engine noise

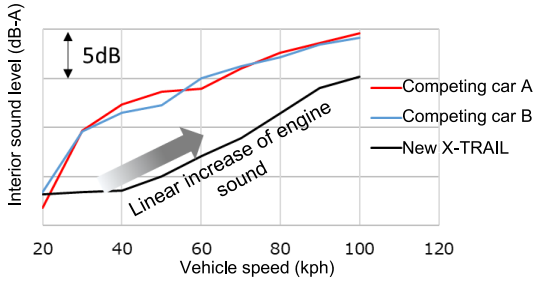

Fig. 5 Difference in engine noise at 0.2G acceleration between the new X-TRAIL e-POWER and competing cars

6. Vehicle technology that supports quietness

The use of a high-torque 3-cylinder engine is advantageous for reducing engine noise caused by low rotation; however, it is disadvantageous for low-frequency phenomena such as booming noise and vehicle body vibration. Therefore, the engine mount, exhaust, active noise control, and body are improved to reduce the low-frequency sensitivity.

Moreover, high-efficiency sound insulation technology is introduced to block high-frequency engine radiation noise sufficiently to realize overwhelming quietness.

6.1 Engine mount

The engine mount requires component technology to achieve EV-level quietness, not to bother drivers even when the engine is running. This chapter well describe a low-stiffness pendulum mount system dedicated design for the 3-cylinder high-torque e-POWER system. Mount system is develop to ensure a small change in stiffness, up to full-throttle acceleration, and maintain a balance between an optimal mount arrangement that considers the 3-cylinder vibration mode and the engine room layout for the new X-TRAIL.

6.1.1 Configuration of the mounting system

The conventional pendulum mount system is commonly used to support a lightweight, low-torque 3-cylinder engine. When the pendulum mount system handles a high-torque engine, an upper torque rod is added above the right mount to support reaction force, which will reduce input load to each mount.

For the new X-TRAIL e-POWER-dedicated mount system, the lower torque rod layout was accomplished to fit within the size of a current size torque rod by, reducing the input load and dividing the lower torque rod into a main rod and support rod. The two torque rods are placed across the nodes of the 3-cylinder engine 1st order vibration (rotational couple around the X and Z-axis of the vehicle) combined with an appropriate stiffness balance with the right-side and left-side mount. This will cancel phase of the 3-cylinder engine 1st order vibration and achieve an optimal anti-vibration engine mount design (Fig. 6).

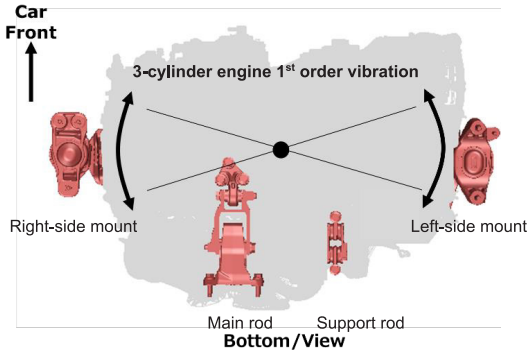

Fig. 6 Diagram of engine-mounting system

6.1.2 Effect of using two lower torque rods

The use of two lower torque rods contributes not only to compatibility with the layout and 3-cylinder engine 1st order vibration but also to quietness, because it ensures low-stiffness with small change up to full-throttle acceleration.

The support rod does not have a stopper structure and rubber shape is designed to be used in a shear direction to prevent stiffness increase when load is applied. Combining this rod to the main rod, it allows reduced input load (Fig. 7) and stiffness increase, even use of a current rod structure with a stopper function.

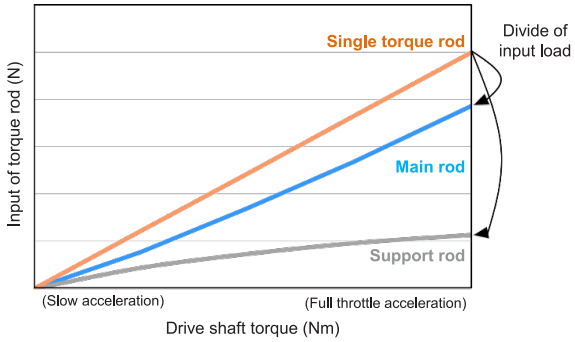

Fig. 7 Input load dividing by dual torque rods

Thus, the torque rod, which contributes to booming noise, is divided into two rods to achieve lower spring rates even at full-throttle acceleration. Low-stiffness torque rods that exhibit little change in rigidity over the entire range are used (Fig. 8).

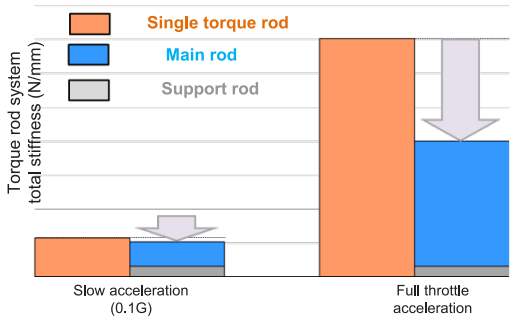

Fig. 8 Comparison of the torque rod system stiffness

6.2 Exhaust

In the new X-TRAIL e-POWER, the following is done to ensure vehicle quietness, especially in urban driving scenes,

・Low engine speed operation

・Engine running at high torque for power generation.

Both lower engine speed operation and higher torque increase exhaust noise. To achieve a high level of vehicle quietness during engine operation, exhaust noise reduction is required. To this end, we have developed long-flow exhaust technology that lowers the full-length resonance of the exhaust system.

6.2.1 Exhaust noise reduction concept using e-POWER features

To reduce exhaust noise when the 3-cylinder high-torque engine is in operation, a large-capacity muffler is required in the center and rear of the vehicle. However,

the e-POWER is equipped with a large Battery, DC-DC converter, Fuel Tank, Rear Suspension, and Rear Bumper. So, it is difficult to install a high-capacity muffler that achieves a high level of vehicle quietness due to packaging restrictions (Fig. 9).

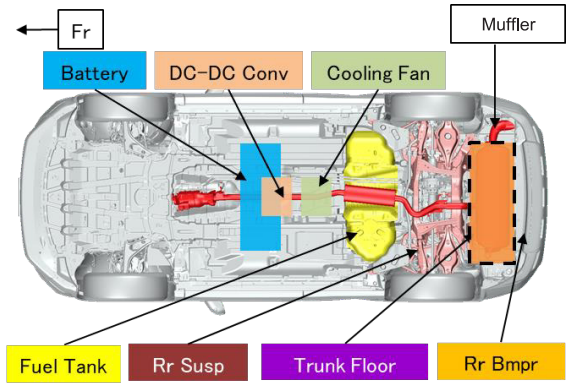

Fig. 9 Peripheral component layout

Therefore, we focused on the fact that the e-POWER does not use the idle engine speed range which is used by the ICE. The concept was to move the exhaust system full-length resonance to the idle engine speed range of the ICE. This reduces exhaust noise in the speed range which is used by the e-POWER (Fig. 10).

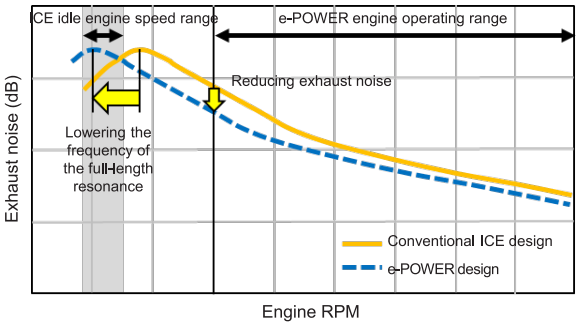

Fig. 10 Noise reduction concept of the muffler specially designed for e- POWER

6.2.2 Noise reduction by long flow exhaust system

To lower the frequency of full-length resonance, the exhaust gas flow path of the exhaust system was lengthened by 1.3 m compared to the conventional design of the ICE. It is most effective to lengthen the tail tube to bring the rear muffler closer to the antinode of the sound pressure in case of ensuring high silencing efficiency by extending the flow path. However, it is difficult to extend the flow path behind the rear muffler due to packaging restrictions. As a way to achieve both silencing efficiency and packaging, a long-flow exhaust system was created by reciprocating the tubes inside the rear muffler.

On the other hand, to realize a long flow system in a rear muffler, it is necessary to avoid the influence on exhaust noise caused by new resonance of the long tube. In addition, low exhaust pressure is required to realize high torque engine. Therefore, the optimum bypass path for the e-POWER was designed to control the long tube resonance and gas flow in a rear muffler.

To this end, a long-flow exhaust system specially designed for the e-POWER that can be installed in a C-segment package that simultaneously satisfies low exhaust noise and low exhaust pressure was developed (Figs. 11 and 12).

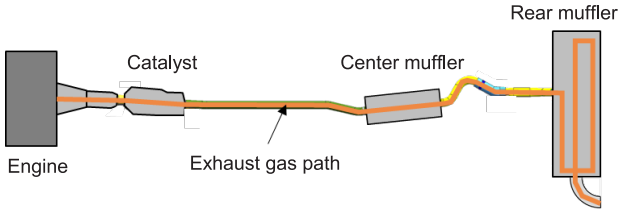

Fig. 11 Long flow exhaust system

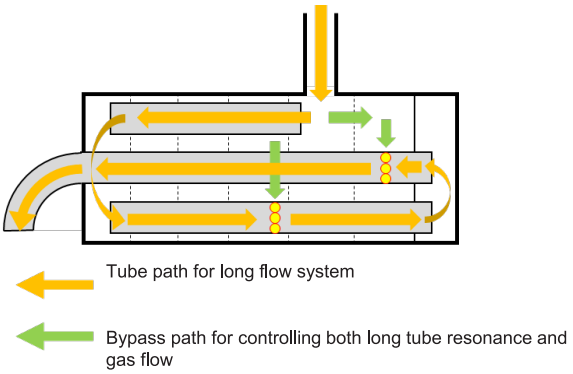

Fig. 12 Internal structure of muffler to realize long flow path

6.3 Active noise control

In low-load and low-vehicle speed scenes, noise reduction is achieved using the long flow exhaust path to lower the engine speed and ensure quietness. However, the necessary power generation amount needs to be secured through high-torque operation. Therefore, it is necessary to respond to the low-frequency excitation force of a 3-cylinder engine. To this end, active noise control (ANC), which is optimally suited for the VC-TURBO engine and e-POWER system, is also adopted to muffle the sound inside the car in addition to the newly developed engine mount and exhaust system.

Fig. 13 shows the booming noise reduction effect of the ANC.

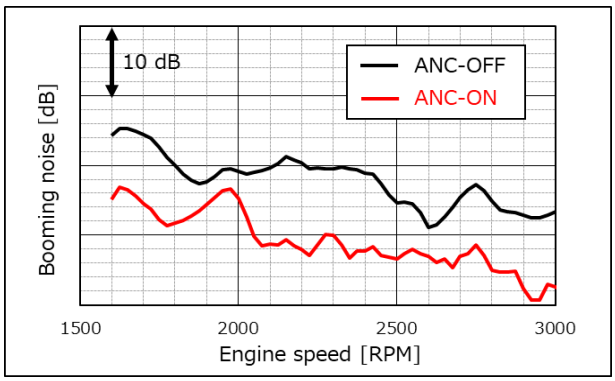

Fig. 13 Booming noise reduction effect of ANC on 1.5th order (rpm) under 0.1G acceleration

6.4 Low-sensitivity car body

For the new X-TRAIL, a high-rigidity, low-sensitivity body was developed to cope with the increase in the vibration level caused by the high-output 3-cylinder engine and to further improve NVH performance. A body that does not transmit noise or vibration to the users was realized by (1) reducing the eigenvalues (modes) of the body frame in the low-frequency range and (2) making the mode less likely to generate noise.

6.4.1 Reduction of frame eigenvalue density

The eigenvalue of the body frame is the unique vibration mode of the body frame, such as twist and bending, and it is considered the main factor that constitutes the sound sensitivity level because it amplifies the volume change in the cabin caused by the input of the engine, suspension, etc. The car body is likely to be excited in various modes in response to various inputs (i.e., easily generating sound) if many frame eigenvalues exist in the low-frequency range (high density). Compared with the previous X-TRAIL, the new one adopts a high-output 3-cylinder engine that tends to increase the engine vibration level. Therefore, it is necessary to reduce the eigenvalue density to improve the sound sensitivity of the car body (Fig. 14).

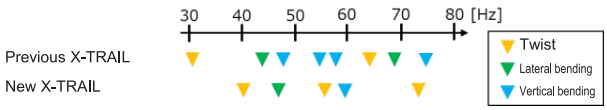

Fig. 14 Car body frame eigenvalue array table

6.4.2 Improving eigenvalues (modes)

Specific measures to improve the eigenvalues (modes) and reduce the sensitivity are shown in Fig. 15. The conventional C-pillar structure uses a cross section on the outer side as a countermeasure against twist resonance, which is the first eigenvalue. The new X-TRAIL employs a circular structure (1) with a cross section on the inner side (compression side), which contributes significantly to the rigidity and improves the eigenvalue of the frame from 30 to 40 Hz. For the lateral bending resonance of the engine compartment, which is the second eigenvalue, both the lateral rigidity and eigenvalue were improved by installing frame (2), which connects the tip of the hood ridge and the front side member. For the bending resonance in the longitudinal direction of the vehicle body, which is the third eigenvalue, the previously mentioned C-pillar inner circular structure suppresses the deformation mode in the vertical direction of the vehicle body at the rear part. Further, another circular structure (3) is provided in front of the floor tunnel to suppress the tunnel-opening mode and further increase the eigenvalue. The eigenvalue density in the low-frequency range is reduced and the sound sensitivity is significantly improved by applying these structures.

Moreover, the noise radiating panels are identified and stiffened to suppress noise radiation at eigenmode (reduce the vibration gain). For longitudinal direction dash panel vibration modes, which is one of the sounding parts, the dashed upper cross section is added to form a closed cross section (4) in the right and left directions above the dash. Further, the 7th cross member (5) is installed to connect the mounting points of the rear suspension members, which suppresses the vertical mode of the rear side members and the rear floor panel vibration mode and thus reduces the noise from the respective parts.

For other frameworks, the amount of offset from the center of the centroid is reduced, whereas the bending points of the ridgeline are minimized considering packaging restrictions. Thus, the local rigidity is improved by minimizing the seating surface of each mounting part and by increasing the rigidity efficiency. Consequently, the thickness and weight of the main frame are reduced compared to those of the previous X-TRAIL, whereas the torsional rigidity and vertical bending rigidity are increased by 44% and 40%, respectively. In this manner, a high-rigidity, low-sensitivity body that supports the high-output 3-cylinder engine of the new X-TRAIL is realized.

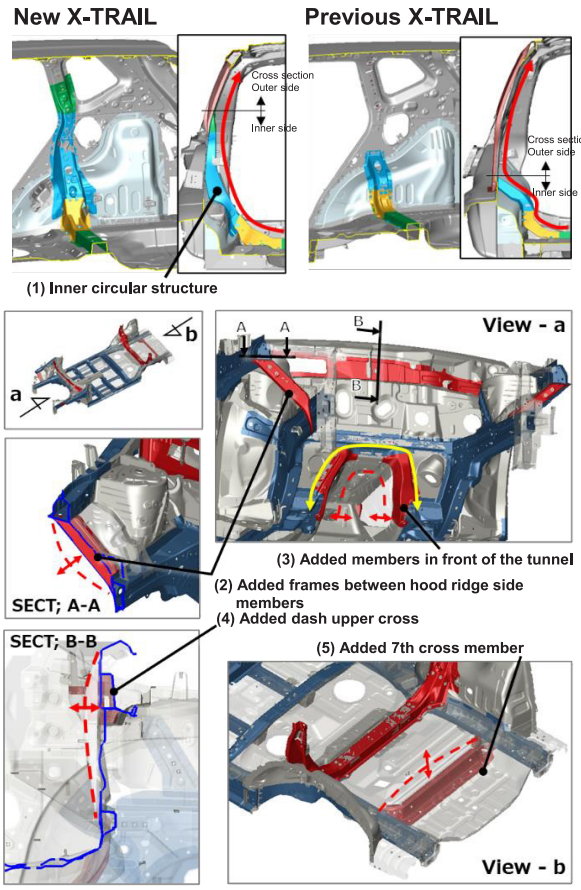

Fig. 15 Car body frame structure

The suspension is renewed (Fig. 16), and the front suspension member, which is a soft-mounted type on the previous X-TRAIL, is now a rigid type; this contributes to the high rigidity of the vehicle body. The sound sensitivity of the suspension mounting points is improved by increasing the body rigidity to maintain a low road noise level. In addition, the road noise level is improved by 1.5 dB compared to that of the previous X-TRAIL by applying softer front suspension bush and changing rear suspension member from rigid type to soft-mounted type (Fig. 17).

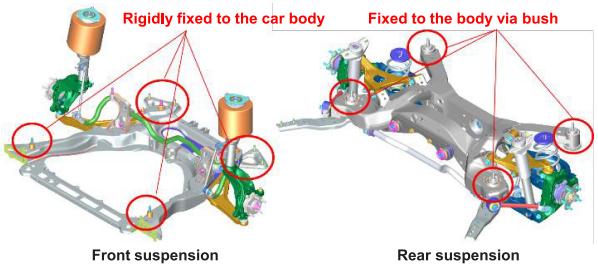

Fig. 16 Suspension structure

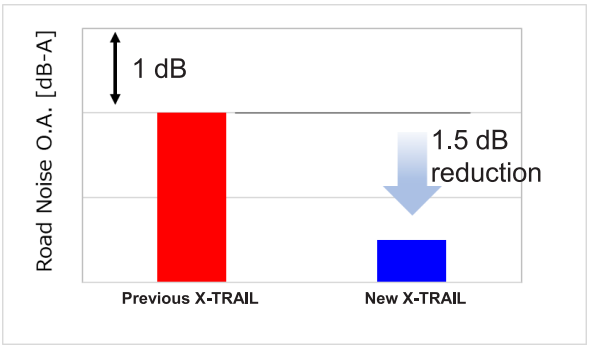

Fig. 17 Road noise level at a constant speed of 50 km/h on the rough surface road

6.5 Sound insulation technology

For efficiently improving the sound insulation performance, local sound leaks in the sound propagation path need to be prevented and sound insulation materials that have a double wall structure with a large distance between walls need to be used to improve the performance of individual components.

Weak points are identified on the body panel throughout the transmission path from the powertrain to the interior components, where the input contribution is high, and countermeasures based on our design policy of efficiently applying the double-wall structure are implemented.

An analysis of the existing vehicles reveals that the dash penetration and toe board contributed approximately 50% (Fig. 18). For the dash penetration part, a contribution level equal to that of the other portions is achieved by thoroughly reducing holes and gaps. For the toe board, the double-wall structure consisting of the dash panel and insulator is inherited from the existing model, and the performance is improved by 5 dB by making the insulator 157% thicker than the existing model (Fig. 19) and without adding parts or increasing the mass (B → A in Fig. 20). This contributes to a weight reduction of approximately 10 kg compared with the case where mass measures are considered instead of structural measures (C in Fig. 20).

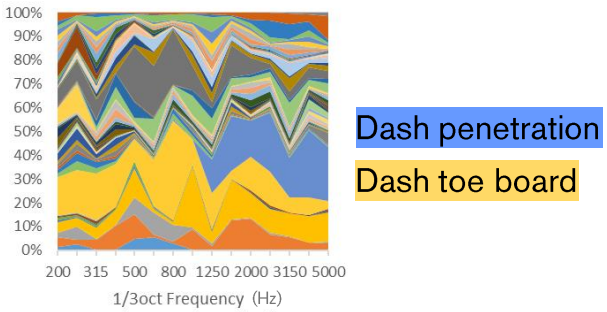

Fig. 18 Input contribution in existing vehicles

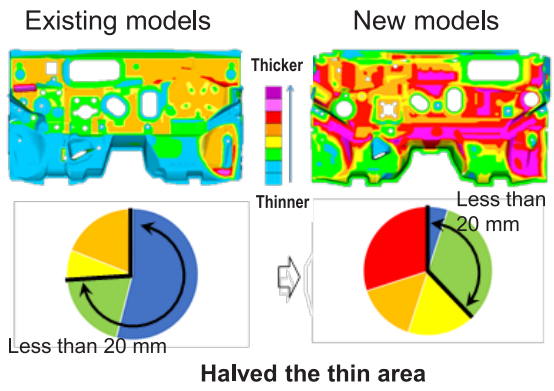

Fig. 19 Dash and insulator thickness distribution

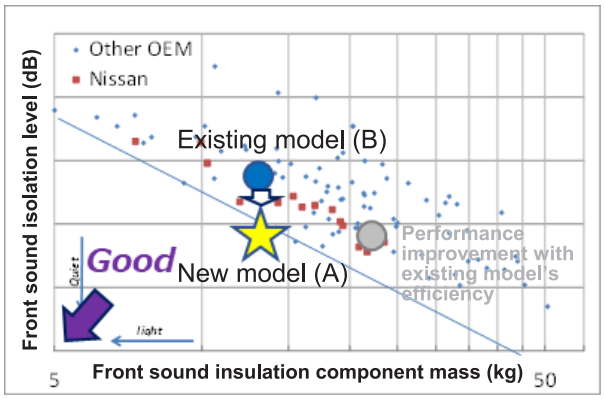

Fig. 20 Mass efficiency of front sound insulation

7. Summary

Nissan's original e-POWER system, which has been used mainly for small cars, has evolved with the technologies described above, and it can now support C-segment SUVs and realize powerful acceleration performance, excellent fuel efficiency, and overwhelming quietness at a high level.

We hope to continue to evolve the quietness improvement technology and contribute to society by providing more attractive electric vehicles (e-POWER, EV) to our customers.

Authors


Mengze Li


Shinichi Suganuma


Toshihisa Kuwata


Nobunari Funatsu


Hiroaki Fukuoka


Takefumi Mitani


Kazushige Maeda


Yasutsune Terashima

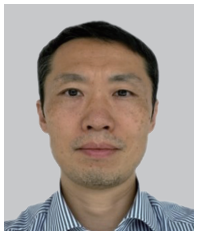
Yuichi Igarashi


Kazuhisa Okada

Test Technologies Contributing to Electrification

1. Test technologies that support the competitiveness of electric vehicles

Kohichiro Tanaka*

1. Introduction

The role of the Test Department in Nissan Motor Company's R&D division is to set performance targets for vehicles and systems that meet customer expectations and market requirements worldwide. It involves evaluating the achievement of performance targets through physical assessment after the design and prototyping phase. The engineers in the Test Department determine the type of tests necessary to fulfill this role. They are responsible for introducing the required equipment and measuring instruments for conducting tests, as well as developing evaluation and measurement technologies.

In this feature, we will introduce Nissan Motor Company's test technology, particularly the test technologies contributing to the electrification of vehicles as one of the responses to the current issue of global warming.

Fig 1 represents a simplified and conceptualized depiction of the automotive development process. It illustrates the vehicle hierarchy from the top (vehicle level) to the bottom (parts level). The development of a new car starts from the top-left and progresses towards the top-right, development completion and start of sales.

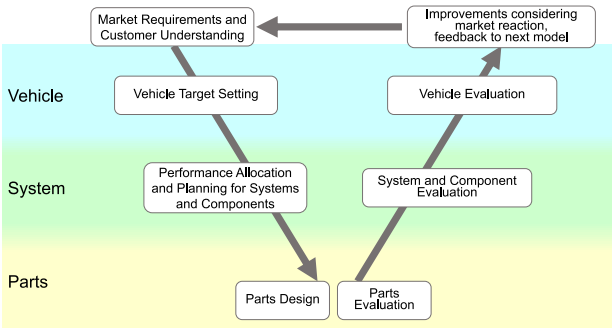

Fig. 1 Schematic of the development process of automobiles (V-process)

The role of the Test Department starts from the upper left section of the V-Model, from "Market Requirements and Customer Understanding" to "Vehicle Target Setting". Depending on the performance domain, the Test Department may also be involved in activities such as "Performance Allocation and Planning for Systems and Components". Afterward, the responsibilities shift to the design department and parts suppliers for "Parts Design" and "Parts Evaluation", followed by the Test Department's involvement in "System and Component Evaluation" and "Vehicle Evaluation" once again.

2. Various test technologies

2.1 Test technologies to understand market requirements and customers

To establish performance targets, it is necessary to understand how customers worldwide use and drive their cars, their expectations at that time, and the usage environment. Each country or region may have unique usage patterns, and customer expectations vary from person to person. The usage environment encompasses not only road conditions and traffic environments but also various climate conditions such as temperature, humidity, solar radiation, as well as altitude (air density), radio wave environment, and more, which form a vast combination.

To set targets for individual performance, components, and systems among these infinite combinations, it is essential to create a market model and extract scenes that represent the real world. Market research is a classic method used to understand real-world market requirements. This involves observing and interviewing customers, measuring data related to vehicles and the surrounding environment, analyzing the collected data. It requires specific technical expertise and know-how. In recent years, the analysis of big data using statistical methods has also become possible, enabling the understanding of market requirements through the collection and analysis of large amounts of data. These technologies are also essential test technologies.

2.2 Vehicle test technologies

To establish performance targets through vehicle-based tests and evaluate the achievement of vehicle performance, it is necessary to compare and evaluate the

*Customer Performance and Vehicle Test Engineering Department No.2

current models and competing vehicles, measuring surrogate characteristics that indicate the quality of each performance aspect. While it is sometimes evaluated through comparative test drives on public roads, ensuring reproducibility in real-world conditions is challenging due to the uncontrollable traffic environment. Therefore, closed test courses called "Proving Grounds (PG)" are constructed to run the vehicles. When establishing an in-house PG, the Test Department's engineers are involved in considering and planning the concept of the PG, working collaboratively with specialized design and construction companies to create the PG. This is an integral part of the responsibilities of the Test Department's engineers.

To efficiently and effectively evaluate and measure various performance aspects, it is necessary to design courses that encompass a wide range of combinations of flatness, elevation, and road surfaces. Often, real-world roads and surfaces are replicated. These may include famous roads with poor ride quality, roads that challenge road noise and “squeak & rattles”, and roads that allow assessment of handling performance, among others. Determining which types of roads should be replicated in the Proving Ground (PG) is also part of test expertise.

For example, Nissan Motor Hokkaido Rikubetsu Proving Ground in Japan is designed to replicate German autobahns and country roads. During winter, it becomes the coldest test facility in Japan, where surfaces such as compacted snow and ice are reproduced for test purposes.

Fig. 2 PG of Nissan's Rikubetsu Proving Ground (Hokkaido)

2.3 Bench test technologies of systems/components

By testing in PG, we can freely control and replicate the driving conditions. However, it is not so straightforward when it comes to climate and weather conditions. Furthermore, it is difficult to isolate and accurately measure various phenomena occurring in a moving vehicle and analyze them in detail. Therefore, it is necessary to establish bench test technologies that replace or supplement on-road tests, tailored to the performance, functionality, and system being evaluated. On the left side of the V-process, the phenomenon mechanisms are analyzed for each performance, and performance allocation to each component is conducted. On the right side of the V-process, evaluation and achievement confirmation are carried out for the system and performance. An important aspect here is determining what and to what extent should be replicated, depending on the objective, which showcases the skill of the bench test engineers.

For example, to evaluate the durability of the vehicle body and chassis, a road simulator is used to replicate inputs from road surfaces during driving and inputs from driving and braking forces. It reproduces forces acting on the four wheels in the front, rear, left, right, up, and down directions, as well as rotational moments around the X, Y, and Z axes. Rather than replicating the input waveforms exactly as they occur during actual driving, the waveforms are manipulated to accelerate the tests, allowing for durability evaluations in a shorter time frame. The fatigue damage is reproduced to be equivalent to the market model. However, the replication of temperature and lighting conditions is excluded since the evaluation mainly targets the fatigue strength of structures made of metallic materials.

Fig. 3 Photograph of the road simulator (as an example of bench test equipment)

In addition to on-road tests using actual vehicles or bench tests using the entire vehicle body, it is possible to extract specific components or systems and subject them to loads equivalent to those experienced in actual vehicles. This enables the elucidation of phenomena mechanisms that are difficult to observe and measure in vehicle conditions. Moreover, due to the smaller scale of tests, it becomes easier to compare and evaluate a larger number of specifications and increase the sample size for assessing variations. When constructing such bench tests for system-level evaluations, it is essential to determine how to replicate the vehicle conditions.

By breaking down the performance requirements from the vehicle level to the system level and further to the parts level, it becomes possible to align vehicle performance targets with the required specifications of parts. In the confirmation stage of target achievement, the evaluation is conducted in the following order: first, evaluating whether individual parts meet the

specifications (usually done by parts suppliers), then system-level evaluation, and finally, vehicle-level evaluation. This allows for easy identification of causes and implementation of countermeasures in case the target is not achieved, ensuring the progress of development reliably.

2.4 Test technologies for the digital phase

In the V-process diagram described above, it is depicted that progress should proceed smoothly along the V-shape without any backtracking. However, in actual development, if the evaluation results on the right side of the V-shape do not achieve the intended targets, iterations and backtracking occur. This means going through a feedback cycle of design -> prototype -> evaluation -> redesign -> prototype iteration -> evaluation iteration, which requires a corresponding amount of time and cost. Consequently, there is a need to perform preliminary assessments of the achievement level before creating actual physical prototypes. The phase before arranging the formal prototype vehicles is referred to as the digital phase, while the phase after the arrangement is called the physical phase. It is important during the digital phase to determine how to assess the performance achievement level of the prototype vehicles, as this helps reduce the need for design, prototyping, and evaluation iterations during the physical phase. So, how do we evaluate the performance when we don't have actual physical prototypes? This can be done by utilizing computer simulations or creating mock-ups that replicate certain parts of the vehicle. The technical challenge in the digital phase lies in deciding what and how to replicate based on the performance or system being evaluated.

For instance, a traditional method for evaluating aerodynamic performance involves creating clay models that accurately replicate the vehicle's shape, allowing convenient shape modifications and trial and error evaluations. In recent years, there has been a trend towards faithfully reproducing structures within the engine compartment and under floor. However, these models only replicate the shape and do not have functioning engines or the ability to drive. The decision on what and to what extent to replicate is made by the test engineer.

Lately, there has been an increase in partial prototyping using 3D printers. This is particularly useful for pre-evaluating components with new structures or features that lack prior performance records. Although these prototypes may have lower strength, durability, or different surface finishes compared to actual parts, they provide the advantage of being physically evaluated for usability and other factors. Furthermore, there is a growing trend of combining virtual evaluation environments and test pieces created through computer simulations with realistic mock-ups or advanced prototypes.

Fig 4 illustrates an example of Hardware in the Loop Simulation (HILS) previously introduced in Nissan Technical Bulletin (No. 71, 2012). In this example, the entire brake hydraulic circuit, from the brake master cylinder to the VDC unit (ECU and actuator integrated), brake tubes/hoses, and brake unit, is reproduced in the real domain (actual device), while the remaining vehicle model is reproduced virtually (CAE) and combined.

Determining what to replicate virtually and what to replicate in the real domain and how to combine them for evaluation is a crucial consideration.

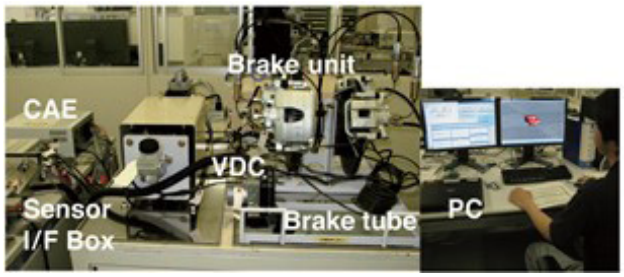

Fig. 4 VDC HILS (Source: NISSAN TECHNICAL REVIEW No. 71)

2.5 Measuring technologies

In discussing test technologies, another important element is measurement technology. To objectively and quantitatively capture vehicle performance, measurement is essential. Whether it is to reproduce and maintain the PG road surface, replicate the market environment on test benches, or recreate prototype vehicles based on design data, accurate measurement is necessary. To understand the mechanisms of phenomena and measure what needs to be known, the development of new measurement technologies is required. Additionally, in order to ensure the accuracy of test results, measurement accuracy assurance technology is crucial. This includes the establishment, implementation, and maintenance of facilities such as the Measurement Standard Center and the calibration equipment used within it. These responsibilities are also undertaken by engineers in the test department.

3. New Test Technologies Contributing to Electric Vehicle Development

In recent years, electric vehicle development has been progressing as a response to environmental issues such as global warming.

When it comes to developing new vehicles using matured technological areas, development can proceed relatively smoothly along the V-process using standardized know-how. However, when adopting new technologies, it is necessary to perform hypothesis verification through testing during the target setting and performance planning phases on the left side of the V-process. This allows for maximizing the value of the new technology and assessing the feasibility of its performance at an early stage to minimize backtrackings. This enables the development of high-value and competitive products for customers.

The first and most significant change in vehicle electrification is the replacement of the power source from an Internal Combustion Engine (ICE) to an electric motor. Electric motors generally offer superior responsiveness and finer control compared to ICE, thereby enhancing vehicle performance.

In Battery Electric Vehicles (BEVs), the vehicle is powered by rotating the driving motor using the stored electrical energy in the battery.

In Nissan's unique electric technology, e-POWER, a dedicated ICE drives the power generation motor to generate electricity, which in turn rotates the driving motor to move the vehicle.

Both in BEVs and e-POWER, the range of performance control through electronic control is expanded, providing greater flexibility. With increased flexibility, there is a need to test with a greater variety of specifications in order to find optimal solutions. Attempting to accomplish this solely through physical tests using prototype vehicles would require significant time, effort, and cost for vehicle prototyping, modification (specification changes), and test evaluations. Therefore, applying virtual test technologies, as mentioned earlier, becomes essential.

The following chapters will introduce driving simulator test technologies and e-POWER powertrain bench test technologies, which have been developed against this backdrop.

Fig. 5 Driving simulator

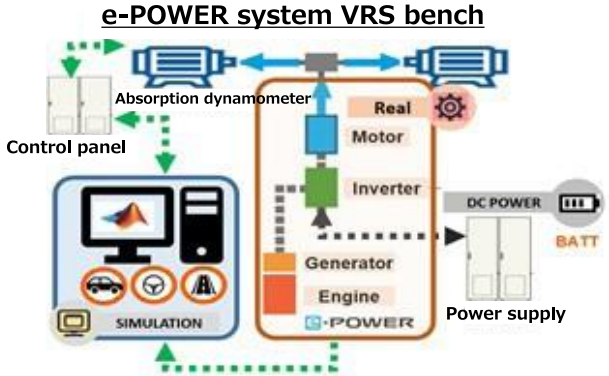

Fig. 6 e-POWER powertrain bench test technology

Compared to Internal Combustion Engine (ICE) vehicles, customers place a higher emphasis on the driving range when it comes to Battery Electric Vehicles (BEVs). The driving range of a BEV is determined by battery capacity and energy efficiency. Among the factors affecting energy efficiency, aerodynamic resistance has the most significant impact. As a means of reducing aerodynamic resistance, the adoption of electrically retractable door handles is becoming more prevalent. Even with the movement of such electric components, setting appropriate targets allows us to provide customers with emotional values such as a sense of luxury and advancement. In this regard, utilizing virtual technology is more efficient and effective than repeating trial and error with various prototype specifications. This is exemplified in Chapter 4, which introduces virtual reality test technologies.

With electrification, new challenges arise regarding heat balance. BEVs have high efficiency as they lack the waste heat energy generated by ICE, but this also means that interior heating utilizing waste heat is no longer possible. Furthermore, cooling is required during high-load driving and quick charging to maintain the battery and motor at optimal temperatures, and this cooling system is shared with the interior air conditioning system. Achieving an efficient thermal management system necessitates a vast number of test evaluations based on different combinations of driving, charging scenarios, and ambient temperatures, given the increasing complexity of the system.

To address this, Chapter 5 presents the thermal management system test technologies that have been developed.

Fig. 7 Heat management system test

The last technology to be introduced is X-ray CT non-destructive measurement technology. The demand for non-destructive measurement is increasing in areas such as the development of electric vehicle-specific components and systems like batteries and motors, as well as the adoption of new materials and methods for vehicle lightweighting. By having this technology in-house, Nissan is able to respond quickly to these needs.

What all these technologies have in common is that

they are not simply purchasing off-the-shelf products and using them as is. Instead, they are developed internally. Of course, in addition to in-house development, there are also cases where commercially available products are purchased or equipment and measurement instrument manufacturers are contracted to create specific items. However, it is the engineers in the test department who are responsible for determining what type of equipment to introduce, what specifications of measurement instruments are needed, and how to combine and operate them. As the individuals conducting vehicle evaluations, they have the ability to discern what is necessary.

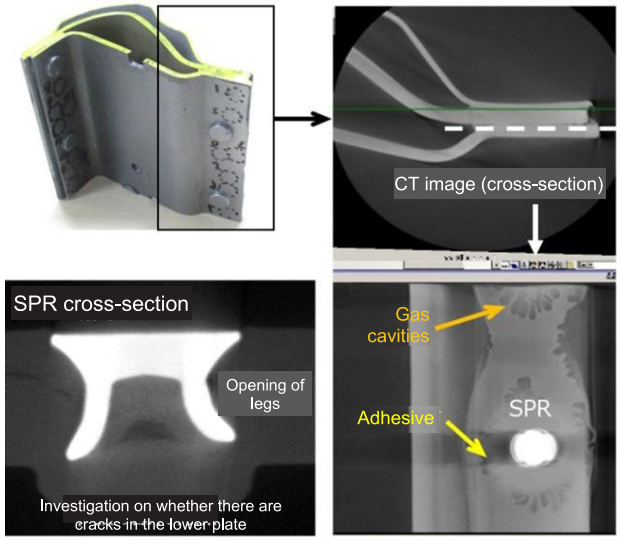

Fig. 8 Example of an X-ray CT

4. Summary

No matter how innovative a technology may be, without proper performance target setting and analysis of phenomena mechanisms backed by testing, it cannot be leveraged to create new value.

Through new test technologies, performance can be improved, development efficiency can be enhanced, and development timelines can be shortened, enabling the delivery of attractive new vehicles to customers.

Unlike technologies incorporated into vehicles, test technologies themselves are not directly delivered to customers. However, the performance and quality generated by test technologies deliver value to customers. Furthermore, while technologies incorporated into vehicles can be relatively easily known to competing companies through reverse engineering, it is difficult to obtain knowledge of test technology know-how from the outside.

Nissan will continue to refine its unique test technologies and contribute to the creation of highly competitive and appealing vehicles.

References

(1) 日産自動車ホームページ　もうひとつの品質物語
https://www.nissan-global.com/EN/SUSTAINABILITY/SOCIAL/QUALITY/STORY/THENEVERENDINGROAD/
(2) 日産技報　2015年 NO.77 実験・計測技術
(3) 日産技報　2012年 NO.71魅力ある新技術の創出と高い品質の実現を支える実験・計測技術

Authors

Kohichiro Tanaka

2. Driving Simulator Test Technologies for Establishing Unique Performances of Electric Vehicles

Hiromi Fujita* Youichi Isono* Masayuki Imamura*
Naoya Machida* Yutaka Hayashi*

1. Introduction

Considering the increasing electrification of vehicles, a novel driving experience can be induced by finely controlling the highly responsive driving force. The flexibility of compliance can also be enhanced by increasing the number of control parameters and range of adjustment, which requires considerable effort and a longer compliance period when using an actual vehicle.

Nissan Motors started the full-scale implementation of a driving simulator (DS, see Fig. 1) in 2019 and has since then employed it to test the safety of ProPILOT 2.0 (in the overriding mode) and the steering performance depending on the tire characteristics and vehicle specifications (e.g., height of the center of gravity and weight distribution). DS can evaluate the driving operation of general as well as highly skilled drivers, and therefore, it has recently been used to set new targets for driving experiences and complying with achievement levels based on the way people feel.

To this end, reproducing the driving feeling more accurately is essential, and therefore, the DS motion system is being improved, and cueing control and other technologies are being developed to pursue more accurate reproductions. The details of the development of the DS technology and examples of applications that utilize its results are presented in this article.

Fig. 1 View of DS

2. New DS technology development

2.1 Motion system improvements

Nissan Motors' DS includes long and short parallel rails, a hexapod, and a turntable to simulate real-time vehicle motion with one-to-one correspondence with a real vehicle (Fig. 2).

The Y-parallel rails can generate a maximum acceleration of 12 m/s^2 with an effective stroke of only ± 11 m before they are upgraded to ensure a safe stop at the maximum acceleration. However, in some cases, the DS system halted suddenly because of a shortage of effective strokes when performing various evaluations, such as acceleration sensation and control by electrification. In these cases, the feeling of acceleration was reduced by decreasing the gain in motion cueing or reducing the sensory time by using a filter. Some evaluation drivers commented that they felt a delay in motion in the DS evaluation compared to when using an actual vehicle, which implies that the system did not provide sufficient performance.

As a measure of improvement, the control method of the Y-parallel rails was revised to increase the effective stroke from ± 11 m to ± 14 m, which extends the effective distance by 6 m; further, the servo characteristics were changed to improve the response of the XY-parallel unit, hexapod, and turn table. These revisions improve the response by up to 344% compared with the conventional time constant for the Y-parallel rails.

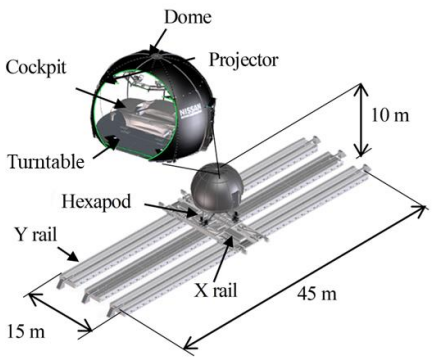

Fig. 2 DS system configuration

*Customer Performance and Test Engineering Methodology Innovation Department

The pure delay, time constant, and frequency characteristics of each step response are measured following the change in motion system control. The configuration of the DS control system is illustrated in Fig. 3. Signals are transmitted to the motion system within 1 ms using a real-time simulator. The characteristics are measured after the signals are sent from the PC in the real-time simulator until the acceleration is transmitted to the cockpit floor in the hexapod.

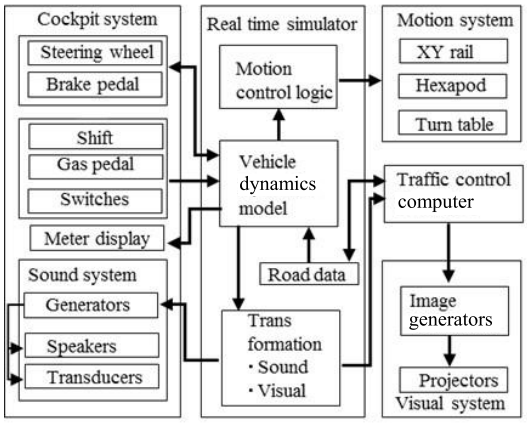

Fig. 3 Control system configuration

The pure delay from the start of the motion system until it is transmitted to the cockpit floor is listed in Table 1. The largest pure delay is for the turntable, which is a delay of 22 ms more than that for the parallel rails. Each transmission characteristic at 0.3 Hz is listed in Table 2. The transmission characteristics of the hexapods are worse than those of the others because the dome is structurally supported by six cylinders, which makes the inertial load less advantageous. These results, which indicate that only roll and pitch are delayed when signals are input simultaneously, suggest that parameters to match the area to be evaluated on the motion system cueing side must be set.

Table 1: Pure delay

		Pure delay [ms]
Rail	X	33
	Y	33
Hexapod	Z	37
	Roll	45
	Pitch	48
Turntable	Yaw	55

Table 2 Transmission characteristics

0.3 Hz		Gain [db]	Phase [deg]
Rail	X	-0.1	-4.1
	Y	0.2	-4.5
Hexapod	Z	0.1	-4.5
	Roll	0.3	-12.5
	Pitch	0.7	-12.9
Turntable	Yaw	-0.1	-3

2.2 Motion cueing development

Significant discomfort can be caused by a small change in the DS when driving experience is prioritized. Motion cueing is developed using the measured results of the transmission characteristics of the system to improve the sensory motion experienced by people. Developments in two aspects—the acceleration characteristics in the fine steering range and the roll motion of the upper structure—observed in the comments of evaluation drivers are discussed below.

The response in the DS vehicle motion simulation may be better than when driving an actual vehicle because of the absence of vehicle stiffness or mechanical delay caused by backlash, which can lead to discomfort in some cases. In an actual vehicle, the steering angle is derived from the operating force of the steering wheel based on the action and reaction forces. However, in the DS, the steering angle is used for the simulation instead of the operating force. The response delay is expected to be small because the steering angle is forcibly generated regardless of the balance of forces. Although a solution can be provided by an analysis that simulates the relationship between the steering force and steering angle, it is difficult to calculate it in real time with the current technology. Thus, a pseudo-rising delay is added to motion cueing to improve sensory motion. An example of such a control is presented in Fig. 4. The rise is moderately delayed with respect to the input, and the output is constant when the change is constant. Given this approach, control is changed for each signal sent to each of the devices and complied with such that the timing of the acceleration felt by people is consistent.

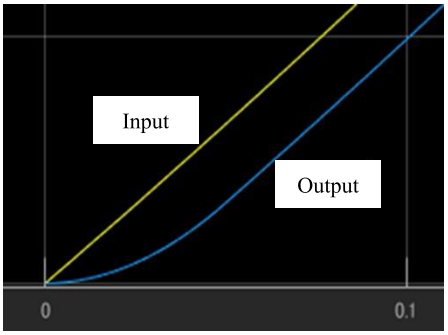

Fig. 4 Signal control

The center of rotation of the vehicle and that of the yaw are different in this system because the seat position of the driver is centered between the hexapod and yaw table in the DS (Fig. 5). Thus, the coordinates of the feeling of acceleration are transformed by the amount based on the difference between the positions of the center of rotation and center of gravity of the vehicle. DSs, which are referred to as racing simulators, often have a system where the seat of the driver is tilted or the center of rotation is set near the abdominal area. In this DS, the roll and pitch are controlled with the rotation center positioned near the abdomen of the driver.

However, the feeling is different from the actual sensation for motion of the upper structure because this method makes it difficult to feel the diagonal roll pitch sensation and vertical motion. Thus, the upper structure is designed to move along the roll axis for comparison. The center of rotation of the hexapod is transformed using a three-dimensional rotation matrix.

$$Roll' = \begin{pmatrix} 1 & 0 & 0 \\ 0 & \cos(Roll) & -\sin(Roll) \\ 0 & \sin(Roll) & \cos(Roll) \end{pmatrix}$$

$$Pitch' = \begin{pmatrix} \cos(Pitch) & 0 & \sin(Pitch) \\ 0 & 1 & 0 \\ -\sin(Pitch) & 0 & \cos(Pitch) \end{pmatrix}$$

$$Yaw\_hex = \begin{pmatrix} \cos 0 & -\sin 0 & 0 \\ \sin 0 & \cos 0 & 0 \\ 0 & 0 & 1 \end{pmatrix}$$

$$Yaw\_Tbl = \begin{pmatrix} \cos(Yaw) & -\sin(Yaw) & 0 \\ \sin(Yaw) & \cos(Yaw) & 0 \\ 0 & 0 & 1 \end{pmatrix}$$

$$S = \begin{pmatrix} X \\ Y \\ Z \end{pmatrix}$$

S: Seat position and rotation center vector

$$A = S \times Yaw\_Tbl$$

$$Ar = Roll' \times Pitch' \times Yaw\_Hex$$

$$S' = \begin{pmatrix} Surge \\ Sway \\ Heave \end{pmatrix} = A - Ar$$

S': Correction amount for the center of rotation for the hexapod

The center of rotation is changed based on the above to conduct a comparative evaluation. Some evaluators commented that they could feel the roll better than before, but not to the level of being able to fully reproduce the diagonal motion. This can be attributed to the motion in the pitch direction. The center of rotation of the pitch is expected to change dynamically depending on the situation; however, there is room for improvement in this regard.

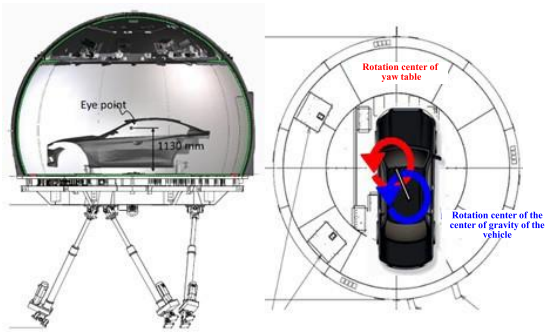

Fig. 5 Driver seating position

2.3 Evaluation results of the effectiveness of new DS technology development

The motion system improvements and developed motion cueing discussed in this chapter are incorporated and evaluated in comparison with previous specifications. This evaluation is performed by setting up the items necessary for vehicle motion evaluation and assigning a score on a scale of one to five to evaluate the drivers. A score of three is the minimum level at which an evaluation can be made in the DS.

Fig. 6 presents the evaluation results, which demonstrate that the overall evaluation is improved because of the DS technology developed in this study, which enabled the system to reproduce motions that are more consistent with those of an actual vehicle. By developing technologies to utilize DS, the evaluation area will be further expanded to include driving environments with disturbances such as uneven road surfaces and crosswinds, as well as special conditions such as snowy roads and race circuits.

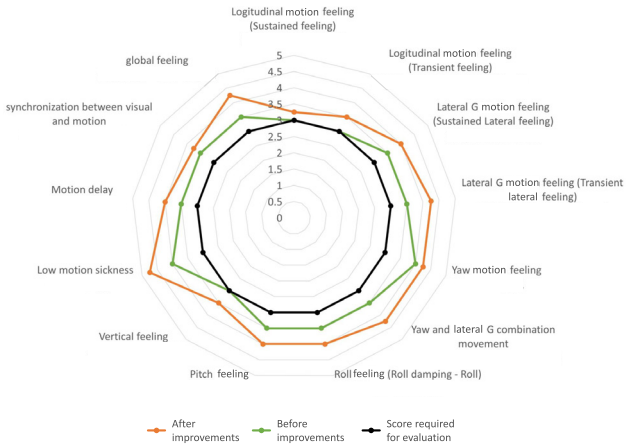

Fig. 6 DS evaluation results

3. Examples of development applications

3.1 Reproduction of growing acceleration feeling of AURA NISMO

AURA NISMO fine-tunes the sensation of acceleration. The driving force changes in response to the accelerator operation to provide the expected NISMO acceleration feeling. Currently, control parameters comply with each model in the development of NISMO, and the number of test patterns to evaluate various modes has increased in recent years. This has made it difficult to comprehensively find an optimal solution. Therefore, the DS is employed to achieve the feeling of acceleration emphasized by AURA NISMO by focusing on the human senses and analyzing each element of the feeling of acceleration.

Parameter studies were performed on the driving force and feeling of acceleration in response to the accelerator stroke with respect to three elements, “height,” “response,” and “growth” (Fig. 7), of the front and rear G in the DS. The actual vehicle evaluation using these

results indicates that the feeling of acceleration was improved, which demonstrates that a parameter study evaluation with the DS is also possible. The "growth" of each element is explained in this section.

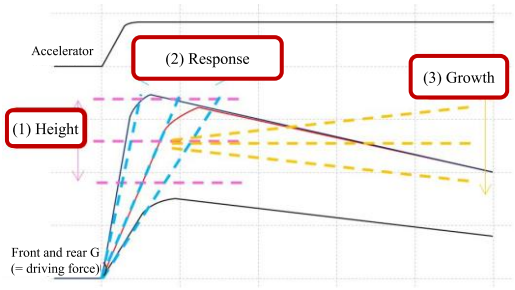

Fig. 7 Elements of acceleration

The decrease in acceleration after peak acceleration in relation to the accelerator opening was investigated to create a feeling of acceleration growth (Fig. 8). The smaller the drop in acceleration after the peak acceleration, the stronger the feeling of acceleration with more growth. However, peak acceleration was difficult to maintain because of the upper limit on the output.

We attempted to reproduce the feeling of acceleration growth by controlling the drop in acceleration. The Y-parallel rails of the DS were used in the test to evaluate front/rear acceleration, which enabled an approximately 3-second evaluation for an acceleration of 0.3 G. The change could be sufficiently felt, although the evaluation was only conducted for a brief time because the actual setup also included a deceleration section. As presented in Fig. 8, the acceleration dropped after the peak acceleration was varied to score the performance in the test. The scores for different drops in acceleration varied at speeds near the start and at medium speed. Acceleration with a feeling of growth could be felt at an acceleration reduction rate of 0.04 G/s or lower for low speeds and at 0.025 G/s or lower for a medium speed range (Fig. 9).

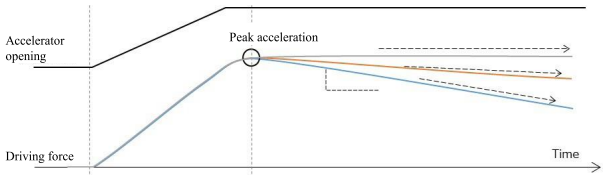

Fig. 8 Method of evaluating feeling of growth

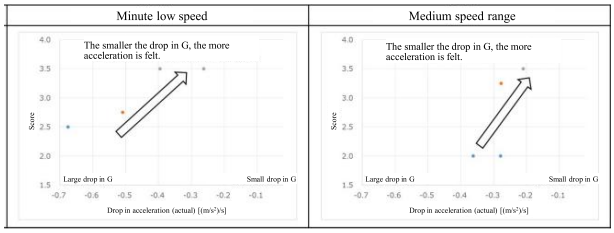

Fig. 9 Sensory evaluation results

AURA NISMO was specially tuned based on these results to provide the "NISMO" mode, which allows drivers to enjoy the feeling of powerful acceleration with growth that is unique to NISMO.

Approximately 130 specifications were evaluated in the three-day test using the DS. This is equivalent to a six-week test for an actual vehicle. The results indicate that analyzing the data in a short time would have been impossible without using the DS, which can perform stable evaluations.

Fig. 10 AURA NISMO

3.2 e-4ORCE acceleration and deceleration control development [1]

The design methodology includes the passenger sensation required for Nissan's automobile development in addition to quantitative performance evaluation. Many laboratories have reported on the prediction of vehicle and system behavior using CAE simulation; however, reports on performance prediction and design that include human subjective evaluation remain limited. The prediction of human senses is required for subjective human evaluations, which leaves a large part of its modeling unknown. Although performance design can be evaluated based on past data and experience, completely new behavior and performance can only be evaluated by testing an actual vehicle. However, building a large number of prototype vehicles is difficult.

Human subjective evaluation is added to predict not only the design and performance in CAE simulations, but also the sensory experience of passengers, which is difficult to include in the development of e-4ORCE control. Comprehensive tests, which include sensory tests, were efficiently developed using a DS without prototype vehicles. A performance design methodology incorporating subjective human evaluation and the influence of passengers is presented.

The performance design methodology using a DS, human body simulation, and vehicle motion simulation is presented in Fig. 11. Using the DS, the vehicle state quantities that can be changed by this new electric AWD were studied to perform a subjective sensitivity analysis for each state quantity. The parameters that most affect human senses were determined based on subjective sensitivity analysis results for clarifying the mechanism and incorporating them into quantitative index values

using a human body simulation. The control logic and vehicle parameters for achieving the performance targets were examined using a vehicle simulation based on the incorporated target quantitative values. The validation prior to an actual vehicle test was conducted on a driving simulator using the final vehicle specifications and control logic, followed by a final checking process in an actual vehicle test.

The prediction of performance, which includes subjective human evaluation, is made possible by following the above procedure, which enables efficient development in actual vehicles.

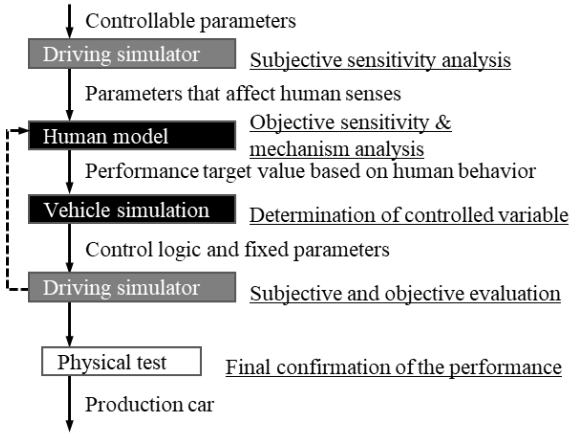

Fig. 11 Performance design process

The details of how a DS is utilized are described in this paper. Fig. 12 presents the steady-state front/rear acceleration magnitudes and front/rear jerk magnitudes, which are derivatives of the front/rear accelerations, for the front/rear motion obtained from the vehicle motion simulation. It also depicts the pitch angle and its derivative, the pitch rate, simulated as arbitrary values and input to the driving simulator to analyze the sensitivity to each influencing factor in the DS.

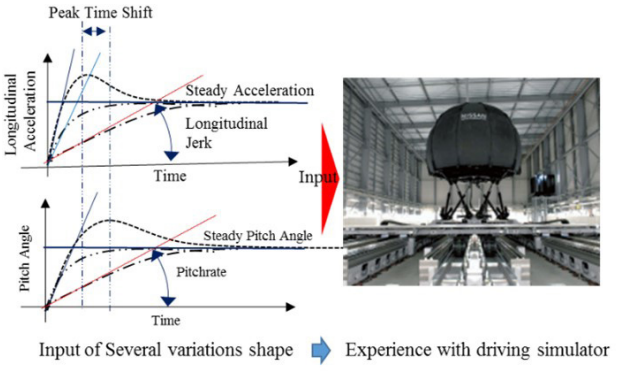

Fig. 12 Sensitivity analysis using the driving simulator

The results of the sensitivity analysis are presented in Fig. 13. With the upper direction of the graph indicating a better subjective score, which is differently colored for each score. The scores for feelings of comfort and acceleration are illustrated in Figs. 13a and 13b, respectively. The lower the pitch rate and front/rear jerk, the higher the passenger comfort level, as indicated in Fig. 13a. By contrast, the greater the front/rear jerk, the higher the score for acceleration; lower scores are observed when the pitch rate is too high. Consequently, both the feeling of acceleration and comfort can be increased by lowering the pitch rate, and a high subjective evaluation can be obtained in the acceleration/deceleration motion by setting the front/rear jerk to a value appropriate for the driver's situation.

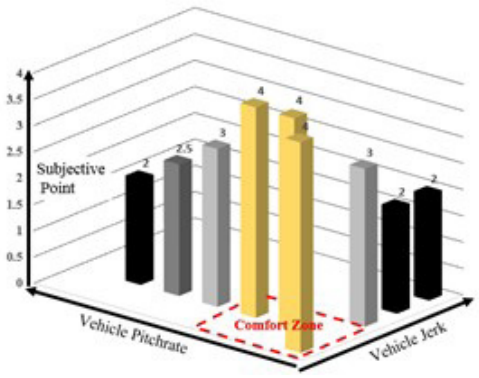

(a) Feeling of comfort

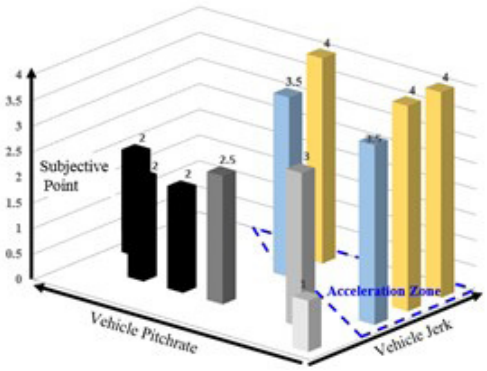

(b) Feeling of acceleration

Fig. 13 Subjective evaluation of driving simulator

Based on the results of the above tests on the driving simulator and the simulation results of the passenger behavior prediction model, performance targets for the front/rear jerk and pitch rate are established to improve passenger comfort.

The effectiveness is verified on an actual prototype vehicle using the aforementioned target settings. Figs. 14a and 14b reveal the results for cases without reducing the load on passengers and with control to reduce the load on passengers when the vehicle accelerates at the same rate from a standstill to a specific vehicle speed, respectively. The front and rear jerks and pitch rates are presented on the second axis. The difference between the acceleration on the human head and that on the vehicle decreases by lowering the front/rear jerk and pitch rate. This implies that the shaking of the passenger's head could be reduced. Similarly, the passenger's feeling of

comfort improved in the subjective evaluation. The results suggest that a smooth feeling of acceleration can be effectively realized using the target values determined by the driving simulator

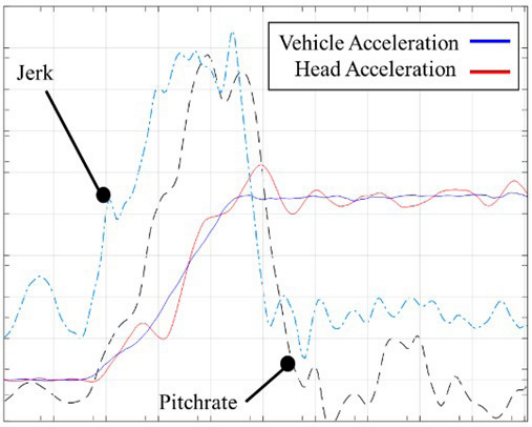

(a) Control OFF

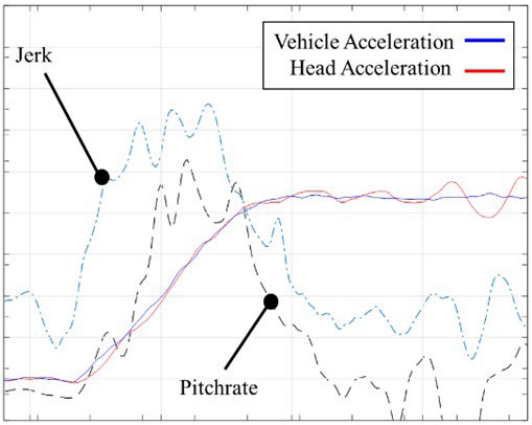

(b) Control ON

Fig. 14 Acceleration and pitch rate by driving force control

4. Summary

Targets for new values associated with electrification and better compliance with achievement levels were made possible through the development of the DS technology, which can reproduce the way people feel with high precision. The development of vehicles with new driving experiences and improved safety, along with electrification and intelligence, will be promoted by continually improving the reproducibility of the driving experience and meeting environmental requirements, such as various road surface unevenness and wind effects worldwide.

References

(1) 町田 直也:ドライビングシミュレータとCAEを用いた電動AWD車加減速挙動設計手法の開発、日産自動車(2022)

Authors


Hiromi Fujita


Youichi Isono

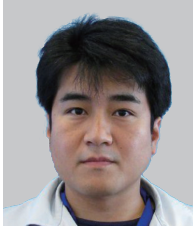
Masayuki Imamura


Naoya Machida


Yutaka Hayashi

3. Virtual Reality Test Technologies for Evaluating Quality of New Mechanical Parts Without Prototyping

Osamu Maruse* Yasunori Nakazono* Noriharu Kubo* Erina Ueno*

1. Introduction

In recent years, the competition to ensure greater cruising distances has intensified, and it has become one of the most important areas in the development of electric vehicles. A retractable door handle, which can retract while the vehicle is in motion, is being studied as a measure for improving cruising distance by reducing aerodynamic drag. Retractable door handles are expected to provide not only improved aerodynamic drag but also added emotional value, such as a sleek appearance when retracted and a sense of hospitality as they automatically unfold when boarding a vehicle. Based on the examples of mass-produced vehicles, door handles protrude in different styles (such as parallel and cantilevered types; Fig. 1). Creating an impression of the automatic door handle movement of protruding and retracting can provide emotional value.

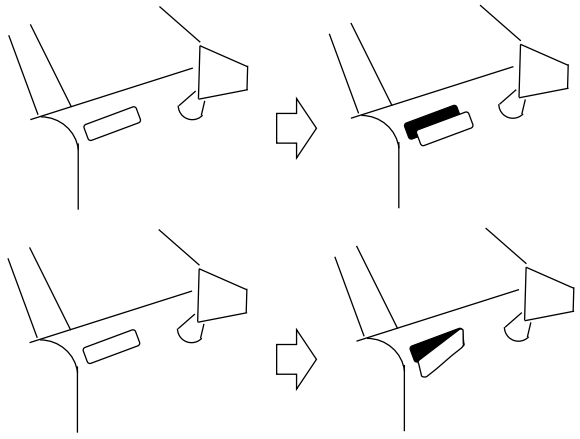

Fig. 1 Examples of retractable door handles

To develop emotional value, how people feel about using a target function must be evaluated, specifically the impression that people receive from the function. Virtual reality (VR) technology is used to reproduce the experience of using a function and to subjectively evaluate the impressions, in line with the idea of the proof of concept at Nissan Motors.

This paper presents the VR evaluation environment developed in-house for evaluating the impression of the experience when using a function. The application of this evaluation method to a feasibility study of a retractable door handle during the development of automobile functions is presented to demonstrate its effectiveness in the providing emotional value.

2. Evaluation methods for emotional value

The impression received from using the target function of a vehicle is used to evaluate the emotional value of the function. A method that measures subjective impressions (psychological scale construction) is often used in product development at Nissan Motors, regardless of the corresponding physical quantity, because the method corresponding to the measurement of the psychological aspect of how people feel must be selected for evaluating the impressions. The reproduction accuracy of the experience of using the target function has a significant effect on the evaluation results as it is based on the direct observation of subjective impressions. Until now, reproducing experience in automobile development has frequently involved the use of physical mockups that replicate the body and interior of a vehicle in its actual size. However, evaluating functions that accompany the movement of parts (which have gradually increased in number in recent years) is difficult within the given development timeline because reproducing the movement with a physical mockup takes time. Thus, a VR evaluation environment that provides a short experience of use is developed by reproducing the body and interior of a vehicle with CAD data and the movement of functions with a program in a virtual space.

3. VR evaluation environment construction

An example of the application of a retractable door handle in a feasibility study is presented in this section. The general functions assumed for retractable door handles are as follows: the door handle automatically protrudes when the door is unlocked with a remote key before the vehicle is boarded; it automatically retracts after the vehicle starts moving; and it automatically

*Customer and Vehicle Performance Engineering Division Customer Performance and Vehicle Test Engineering Department No.2

protrudes after the door is opened while exiting. The door handle then automatically retracts when the door is closed and locked (Fig. 2).

The user approaches the door of the driver's seat.

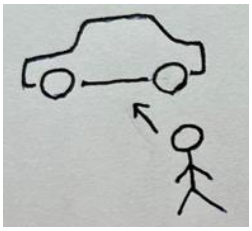

⬇

The door handle automatically protrudes from its retracted position when the door is unlocked by the user using a remote key.

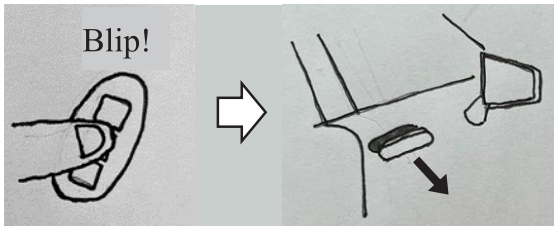

⬇

The user grasps the protruding door handle, opens the door, and enters the driver's seat.

⬇

The door handle automatically retracts from its protruding position when the user starts driving.

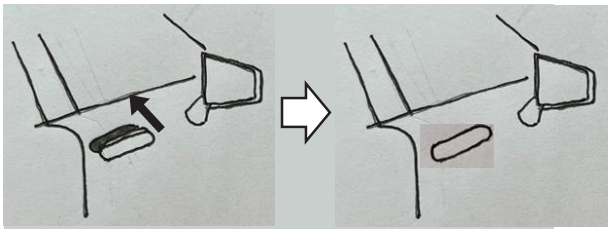

Fig. 2 Functions assumed for a retractable door handle (example)

The impression people receive from the automatic movement of a door handle is examined to determine whether it can provide customers with emotional values such as a sense of hospitality and quality. The following example illustrates how variations in the automatic movement of a door handle can affect the sense of quality.

The timing of automatic protrusion or retraction may be inconsistent between the front and rear ends because actual parts have certain structural design tolerances. The time-series change in the amount of protrusion during automatic protrusion and retraction varies depending on the design tolerance of the parts, as indicated in Fig. 3. The extent to which the variation in the time series changes during protrusion is considered to avoid losing the impression of high quality from the deviation.

Deviation of time-series change in the amount of protrusion during automatic protrusion and retraction: front and rear ends of a door handle.

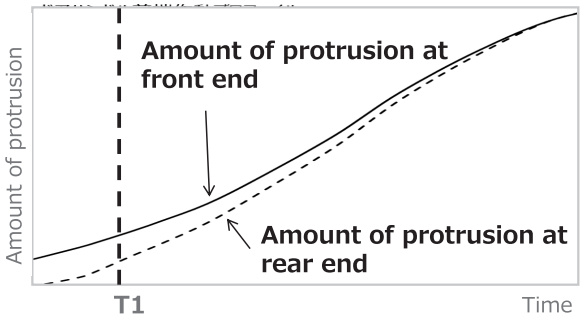

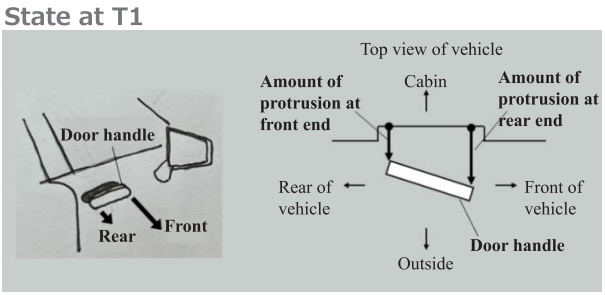

Fig. 3 Variation in the automatic movement of a door handle (example)

The impression received from the movement of the door handle is evaluated for several specifications with different amounts of variation in its automatic movement to determine the relationship between the variation in its automatic movement (Fig. 3) and the impression of high quality.

The environment for evaluating impressions from variations in the automatic movement of a door handle requires (1) the reproduction of slight variations in its automatic movement; and (2) the reproduction of the timing and appearance (viewpoint, field of view, and size of the object to be viewed) when viewing its movement during use.

(1) A mechanism dedicated to the evaluation is required when evaluating multiple specifications that reproduce combinations of deviations in the door handle protrusion timing (combinations of the amount of deviation between the front and rear ends of the door handle). Such a mechanism is required when using a physical mockup because of the design tolerances presented in Fig. 3. This makes completing the evaluation within the development timeline difficult. By contrast, the difference in the movement of different design parameters can be displayed in three-dimensional images in a short time with a VR evaluation environment that reproduces a virtual space.

(2) The impression of the movement of parts, as in the real world, cannot be evaluated without reproducing

the field of view from the viewpoint that matches the posture and physique of the evaluator, changes in the appearance of the object to be viewed synchronously with the behavior of the evaluator, and size of the object during use.

A VR evaluation environment with the potential to satisfy these requirements is selected from a variety of evaluation environments (Fig. 4).

	Evaluation environment		
	Movie	Mockup	VR
(1) Reproduction of slight variations in the automatic movement of a door handle	Poor Slight movements cannot be reproduced in actual size	Poor Long prototyping time make evaluations within the development timeline difficult	Good A virtual model of the door handle movement is required
(2) Changes in the appearance of a door handle synchronized with the behavior of the evaluator during use	Poor Movements of the evaluator are not synchronized with the viewpoints and fields of view	Good	Fair - Good Accurate reproduction of the movement of the viewpoint in response to a behavior is required

Fig. 4 Evaluation environment for the impression of automatic door handle movement

The VR evaluation environment, which reproduces the experience of use in a virtual space, includes three elements: an input section that receives the behavior of the evaluator; an environment reproduction section that reproduces changes in the surrounding environment resulting from the behavior; and an information presentation section that reproduces sensations (visual and audio) based on changes in the surrounding environment (Fig. 5).

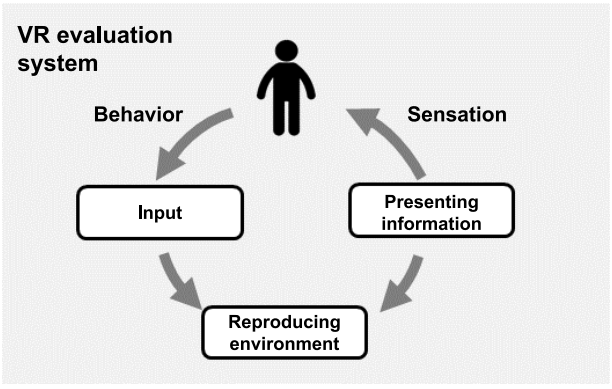

Fig. 5 Elements constituting a VR evaluation environment

The process of establishing a VR evaluation environment for retractable door handles is as follows:

(1) Use cases describing the experience of using retractable door handles in chronological order, as well as the perceptions and behaviors of the user for each use case, are summarized (Fig. 6).

Use case	Perceptions and behaviors of the user
The user approaches the door of the driver's seat.	The user views the vehicle from outside, while focusing on the driver's seat. The user walks up to the driver's seat of the vehicle.
The door handle automatically protrudes from its retracted position when the door is unlocked by the user with a remote key.	The user unlocks the door with a remote key. The user watches the process of the door handle protruding from the retracted position.
The user grabs the protruding door handle and opens the door.	The user sees the door handle. The user grabs the door handle and opens the door

Fig. 6 Use cases and perceptions and behaviors of the user (example)

(2) The reproduction elements necessary to allow users to experience perceptions and behaviors linked to use cases in a virtual space are determined (Fig. 7).

Perceptions and behaviors of user	Reproduction elements
The user views the vehicle from outside, while focusing on the driver's seat.	Omitted
The user walks up to the driver's seat of the vehicle.	Omitted
The user unlocks the door with a remote key.	Omitted
The user watches the process of the door handle protruding from the retracted position.	[Input] • Detection of the actual eye positions and visual line of the evaluator. [Reproduction of environment] • Calculation of the field of view in response to the actual eye positions and visual line of the evaluator. • Calculation of the movement of the door handle protruding from the retracted position. [Presentation of information] • Presentation of the field of view of the evaluator, as well as the movement of the vehicle body and door handle within the field of view. • Reproduction of changes in the field of view in response to changes in the eye positions and visual line of the evaluator.
The user sees the door handle.	Omitted
The user grabs the door handle and opens the door.	Omitted

Fig. 7 Reproduction elements of a virtual space (example)

The determined reproduction elements are structured in a virtual space using a head-mounted display. The software to construct the "field of view in response to the actual eye positions and visual line of the evaluator" among the reproduction elements presented in Fig. 7 in a virtual space was developed in-house. This software allows matching the behavior of the evaluator and the approach to viewing the object with that of reality, and it thus helps realize an accurate evaluation of the impression of the automatic movement of the retractable door handles. Further, a software for the reproduction element "movement of the door handle protruding from the retracted position" was developed in-house. This software allows the direct input of design values for the time-series change in the variation, considering the amount of protrusion presented in Fig. 3. This allows for easy switching between different variation characteristics in the virtual space. Thus, the threshold value for impairing the sense of quality can be evaluated while changing the variation in the amount of protrusion (Fig. 8).

A general-purpose VR system cannot realize a virtual space suitable for evaluating impressions, and therefore, a VR evaluation environment was developed in-house by the test engineering division for automobile development. The developed VR evaluation environment considers the key points of evaluation.

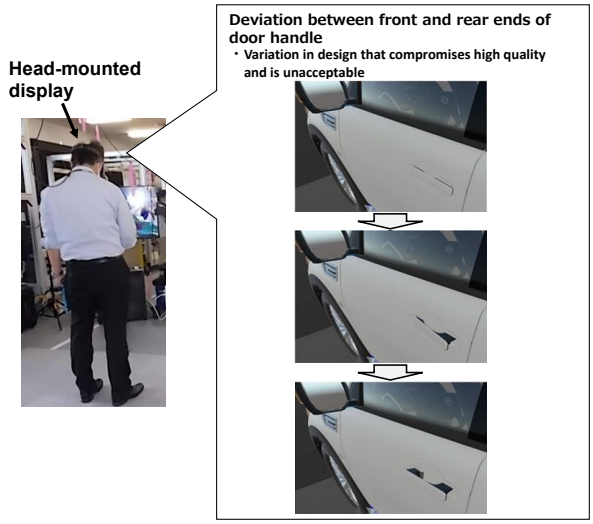

Fig. 8 Evaluation of the sense of quality using VR evaluation environment (example)

4. Technological features

The reproduction of the "field of view" in response to the actual eye positions and visual line of the evaluator contributes to evaluating the impression of appearance in the virtual space. The eye position, visual line, and field of view change in response to the behavior of the driver in real time in actual scenes when using a vehicle. In other words, the appearance of the object when viewed by the user and how it affects the impression are determined by the behaviors of the driver, such as while riding a car. Therefore, it is important to reproduce the field of view in response to the actual eye positions and visual line of the evaluator and to any changes in response to the evaluator's behavior. The position of a viewpoint in a general-purpose VR system is determined by defining a specific position in the virtual space. This implies that it does not reflect the absolute position of the viewpoint in real space relative to a specific reference point. The distance from the contact point between the evaluator's feet and the ground to the head-mounted display is calculated using the general-purpose VR function for detecting the relative position of the reference point and head-mounted display. This distance is used to correct the deviation between the sensor position of the head-mounted display and positions of the eyes to reproduce the position of the viewpoint in the VR evaluation environment.

5. Summary

To evaluate the impression received from the visual sense an in-house VR evaluation environment was developed that includes a digital mockup in which the field of view linked to the evaluator's behaviors and the movement of an object due to design tolerances can be reproduced and viewed in actual size. As a result, it was made possible to set goals for emotional value. The reproduction elements of the VR evaluation environment will be expanded to deal with emotional values of various functions in the future, contributing to maximizing the value of ever-increasing electrified and intelligent parts.

References

(1) D. Zeltzer : "Autonomy, interaction and presence". Presence, 1, 1, pp.127-132(1992) MITPress
(2) 舘 暲: バーチャルリアリティ, 3D映像, Vol.20, No.4, pp.91-98 (2006.11)
(3) 廣瀬　通孝:トコトンやさしいVRの本、日刊工業新聞社 (2019/3/1)

Authors


Osamu Maruse


Yasunori Nakazono

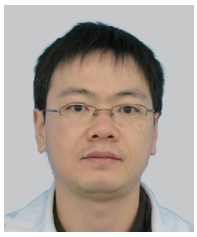
Noriharu Kubo

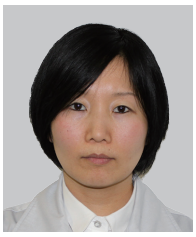
Erina Ueno

Test Technologies Contributing to Electrification

4. Virtual–Real, Simulator–Test Technology for Optimizing Electric Powertrain Performance Without Using an Actual Vehicle

Hidenobu Nakamoto* Koji Hiraya* Hiroyuki Taniai**

1. Introduction

There is a need to reduce carbon dioxide emissions from automobiles to respond to global environmental issues and prevent global warming. To this end, automobile companies have been rushing to develop and commercialize electrified power sources. These developments include hybrid vehicles that combine a conventional engine and a motor for driving and battery electric vehicles (BEV) that run with only a motor for driving. Unlike conventional vehicles that operate with only an engine, the development of vehicles with electrified powertrains is still in the nascent stage. Therefore, there is room to improve the efficiency of different processes and evaluation items. One such example is development of electric powertrains using prototype vehicles in a downstream process; the evaluation can be performed in an upstream process using a test bench equipped with a powertrain system. An upstream test can allow short-period feedback to contribute significantly to shortening the development period.

Nissan has developed a unique electrified powertrain system called the e-POWER system. In the upstream process, the tests are conducted on a test bench, wherein a real powertrain system and virtual vehicle system are combined to comply with various performance calibrations. In this section, we introduce the test technology, which is referred to as the powertrain virtual real simulator (VRS) system; this system reproduces the driving-vehicle conditions. We describe how front-loading powertrain development improves the quality and shortens the development period.

2. Development process and test system

2.1 Development process

Vehicle development involves many steps that can be expressed by a V-shaped diagram. Fig. 1 shows a schematic of the powertrain development process. In the upper-left bank, vehicle targets are initially set based on market requirements. Subsequently, the performance of the systems and components is defined, and the components are designed and evaluated. Finally, as shown in the right side of the V-shaped diagram, the systems and components are evaluated, followed by the vehicle. If a defect occurs during vehicle evaluation (a downstream development process), the entire development process is considerably delayed. During powertrain development, the entire vehicle development process becomes more efficient as it can help prevent defects during the vehicle evaluation process. Thus, it is important to conduct test bench with a powertrain system for simulating a vehicle driving.

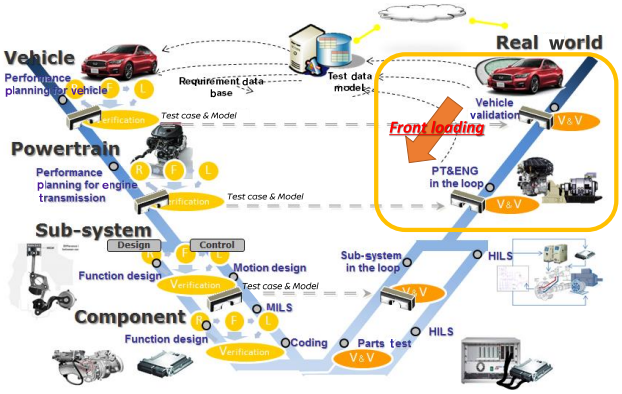

Fig. 1: Schematic of powertrain development process (V-shaped process)

2.2 Overview of VRS test system

Fig. 2 shows the schematic of the VRS test system. The e-POWER system includes an engine and motor for power generation, a motor for driving, an inverter, and a battery. The real powertrain system, which excludes the battery, is installed on a test bench in the laboratory; the power output from the running motor is absorbed by a dynamometer. A model simulating a vehicle is used in the dynamometer control system. The system follows a defined driving mode and simulates the driver, vehicle's travel resistance, and the load that the vehicle receives from the road. Upon receiving the instructions, the powertrain controller controls the running motor to match the required load. In the battery model, the engine is instructed to generate power when the battery capacity

*Powertrain Test Engineering Department **Powertrain and EV Advanced Engineering Department

falls below a certain predetermined value, and the motor for power generation starts the engine. Conversely, the engine is instructed to stop when the battery capacity exceeds a predetermined value, and the motor for power generation stops the engine.

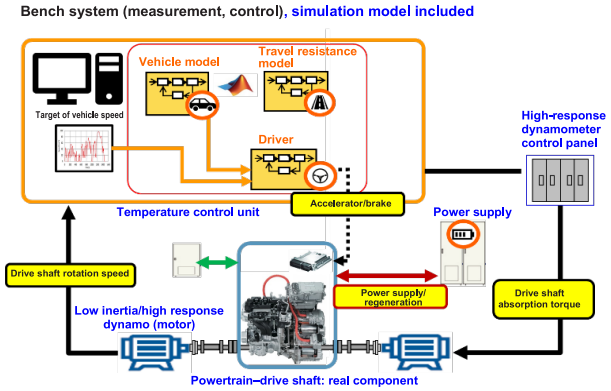

Fig. 2: Overview of VRS test system

Fig. 3 shows a comparison between the PT-VRS test system, in which an entire powertrain (PT) system is mounted on a test bench, and the ENG-VRS test system, in which only an engine (ENG) is mounted. In the PT-VRS used for the evaluation of the e-POWER system, the engine and motor for power generation, motor for driving, inverter, and decelerator are installed on the test bench. In the ENG-VRS system, the engine for power generation is installed on the test bench, but the motor for power generation, motor for driving, and inverter are replaced by a model.

	ENG-VRS	PT-VRS
		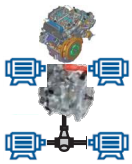
Road	Virtual	Virtual
Driver	Virtual	Virtual
Vehicle body	Virtual	Virtual
Battery	Virtual	Virtual
Motor for driving	Virtual	Real
Motor for power generation	Virtual	Real
Inverter	Virtual	Real
Decelerator	Virtual	Real
Engine	Real	Real
Control unit	Real	Real
Primary applications	Emission performance compliance, and OBD compliance	Electric system evaluation, driving performance, and driving performance/NVH evaluation

Fig. 3 Comparison between PT-VRS and ENG-VRS systems

2.3 Overview of thermal management test

In the VRS tests, it is very important to reproduce the temperature condition of the powertrain for simulating the vehicle driving conditions. Fig 4 shows a system that reproduces the temperature around the exhaust treatment catalyst of a vehicle running on the ENG-VRS test bench. A fan with a variable flow rate is installed to change the airflow rate, which is adjusted to the vehicle speed during the vehicle driving simulation test. This causes the ambient flow volume around the exhaust aftertreatment catalyst to be equivalent to that of the actual vehicle. Consequently, the temperature distribution around the exhaust aftertreatment catalyst becomes equivalent to that of the actual vehicle.

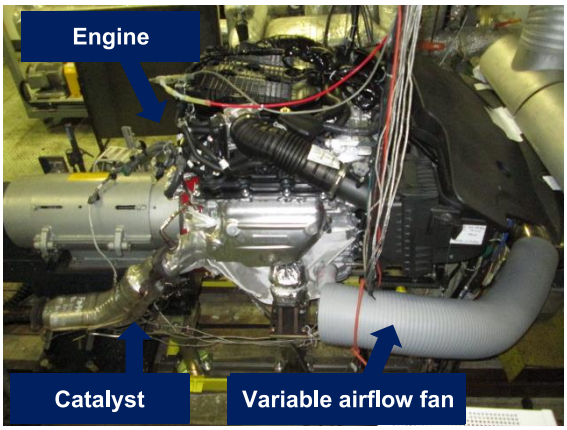

Fig. 4 Exhaust catalyst temperature distribution control system

A test system was constructed to actively control the oil and water temperatures of the engine in the bench test system such that the temperature condition in the test system approached that of the actual vehicle. Fig. 5 shows the test thermal management system. The system includes a controller (2) that controls the oil and water temperatures and model analysis systems (3) and (4) that reproduce the oil and water temperatures of a running vehicle.

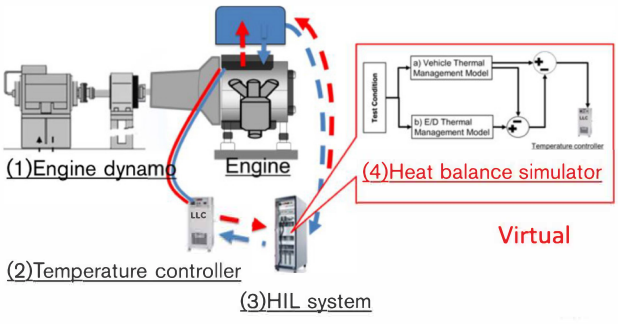

Fig. 5 Overview of thermal management test system

2.4 Overview of NVH evaluation test using FDV-R

Noise, vibration, and harshness (NVH) were evaluated in addition to the driving performance using the PT-VRS test system for the powertrain. The test system was linked to FDV-R, which runs a vehicle model called a functional digital vehicle (FDV) in real time. Fig. 6 illustrates the concept of the FDV. The FDV is a full-vehicle behavior analysis model that comprises all mechanical elements of an actual vehicle to reproduce its characteristics. Coupled plant and control models predict the behavior of the vehicle running in transient and steady states. However, the FDV is not suitable for use with actual components on the bench because the FDV simulation consumes more time than the real one. Therefore, we developed an FDV-R that performs computations in real time. With FDV-R, we evaluated the driving performance and NVH on the PT-VRS test system.

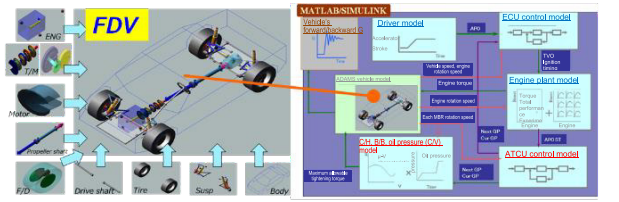

Fig. 6 Concept of FDV

3. Results of vehicle driving simulation test

3.1 Results of real-time test using models

The vehicle simulation model must be computed in real time in a VRS test system. Fig. 7 shows the results of a chassis dynamometer (C/D) test run in NEDC mode driving and a VRS test simulating the NEDC mode. The VRS test demonstrated the feasibility of the test model. The system shown in Section 2.1 shows the same vehicle and engine speeds as those of the actual vehicle running with C/D.

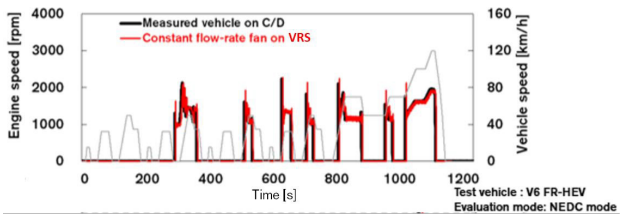

Fig. 7 Result of the real-time accuracy validation of the model

3.2 Results of temperature distribution obtained by vehicle driving simulation

The measurements in the test with C/D must be reproduced in the VRS test to develop powertrains with engine exhaust emissions below the regulatory limits. The test system shown in Section 2.3 is used to compare the internal engine and ambient temperatures with those obtained in the test with C/D. Fig. 8 shows a comparison of the exhaust after-treatment catalyst temperature. In the initial VRS test, the measurements were performed with a constant-rate wind blowing around the aftertreatment catalyst (red line). In this method, the temperature of the aftertreatment catalyst did not reproduce that obtained by the test with C/D, which resulted in a discrepancy in the amount of hydrocarbons (HC) emitted. The temperature of the aftertreatment catalyst became close to that obtained in the test with C/D when a fan with variable air volume was used to match the airflow around the aftertreatment catalyst with that used in the test with C/D (blue line). Therefore, the HC emissions matched well with those observed in the C/D test.

The ENG-VRS test system shown in Figs. 2 and 3 is used along with the techniques used in the tests, as shown in Fig. 8; the amount of modal emissions is measured using a test bench. Fig. 9 shows the unburned HC emissions obtained for the entire test mode. In Fig. 8, the colored lines represent the results obtained by these tests Similar to the behavior of HC emissions shown in Fig. 8, the unburned HC emissions observed over the entire mode reproduced the behavior observed in the test with C/D. The VRS benchtop test system enabled emission compliance tests.

Fig. 10 shows the effect of work-hour reduction in the compliance evaluation of the control constants related to exhaust emissions, and it compares the results obtained by the VRS and vehicle bench-top tests. The VRS test saves 65% workhours by reducing the time required to prepare vehicles and conduct tests.

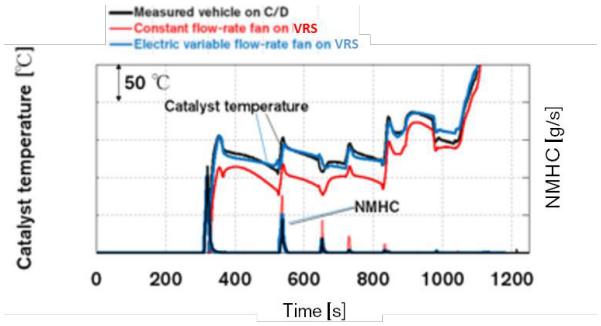

Fig. 8 Temperature comparison between actual vehicle and VRS

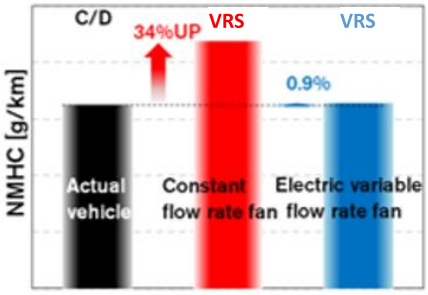

Fig. 9 HC comparison between actual vehicle and VRS

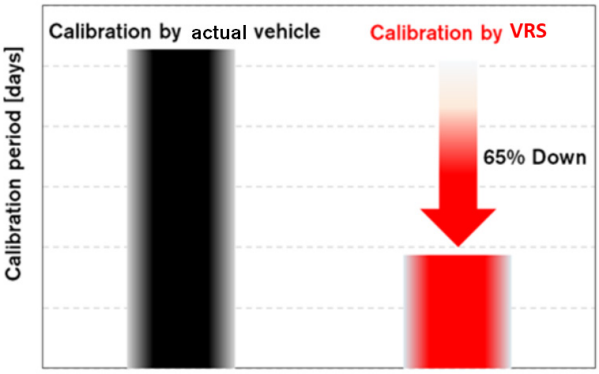

Fig. 10 Effect of workhour reduction achieved by VRS test for emission compliance

3.3 Overview of NVH evaluation test using FDV

A model of the e-POWER system in the PT-VRS test system was used to verify whether the FDV could reproduce the vibrations observed in an actual vehicle. Fig. 11 shows the vertical vibration measured at the engine mount on the rear side of the engine near the center of gravity of the PT system. The figure shows a comparison between the measurement results obtained by the driving vehicle test and the results reproduced by the FDV using the VRS test system. The solid lines represent the results log-fitted to the measurement data, as shown by the dashed line; the difference between the solid lines is less than 3 dB. In the same type of test, the same level of accuracy was obtained at other measurement points and in other vibration directions. These tests demonstrate that the vehicle vibration measured in the test with C/D can be reproduced by the PT-VRS bench-top test. The PT vibration of new vehicles can now be analyzed and evaluated before the prototype vehicle is constructed.

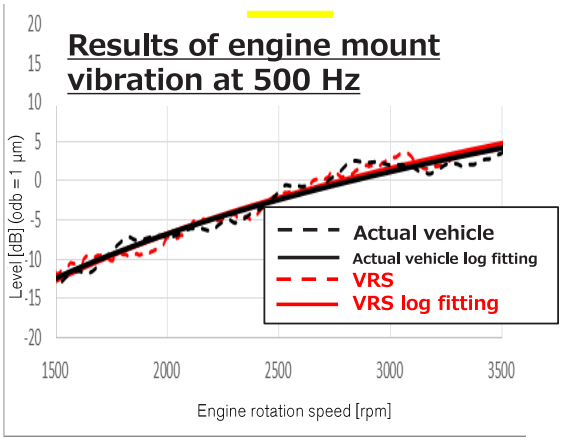

Fig. 11 Result of tests using FDV for validating the reproduced actual vehicle states

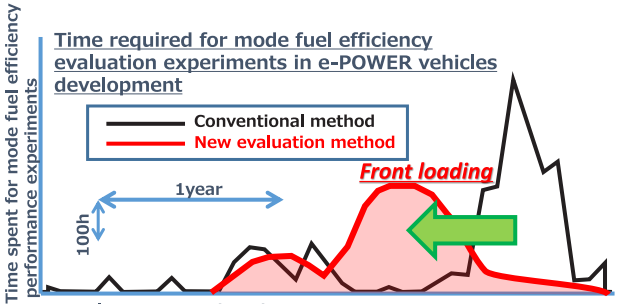

Fig. 12 Development front-loading achieved by applying new method

4. Summary

A VRS test system was developed for powertrain development. The temperature environment was set close to that of the actual vehicle to simulate the driving conditions of an actual vehicle with good real-time performance and model accuracy. With this system, the exhaust emissions and driving performance were evaluated using test bench. This development has made it possible to satisfy the increasingly stricter fuel consumption and exhaust emissions regulations. In addition, the development period was not lengthened, and rework caused by defects occurring in later processes was reduced, even as the electrification of vehicles made the systems more complex. Fig 12 shows the effects of the proposed method.

The conventional development method requires a large number of workhours during the later stages of development. In contrast, the application of the new method realizes not only the front-loading of development but also the prevention of rework. We will continue to develop this method and promote its use as a standard to further streamline the development process.

Authors


Hidenobu Nakamoto


Koji Hiraya


Hiroyuki Taniai

5. Test Technology for Thermal Management System Achieving Both Low Electricity Cost and High Comfort

Masayoshi Tajiri*

1. Introduction

Electrification is achieved by a powertrain comprising a motor, inverter, and high-energy battery, which do not exist in conventional vehicles running with internal combustion engines (ICEs) (Figs. 1 and 2, respectively).

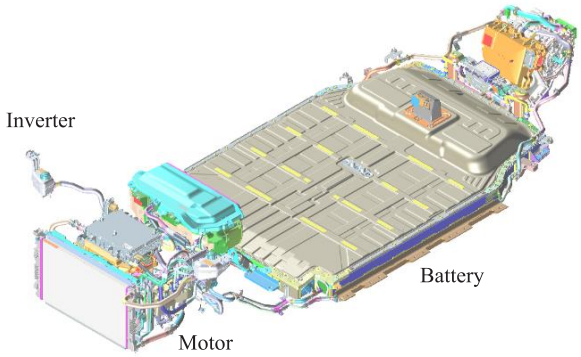

Fig. 1 Components targeted in EV thermal management

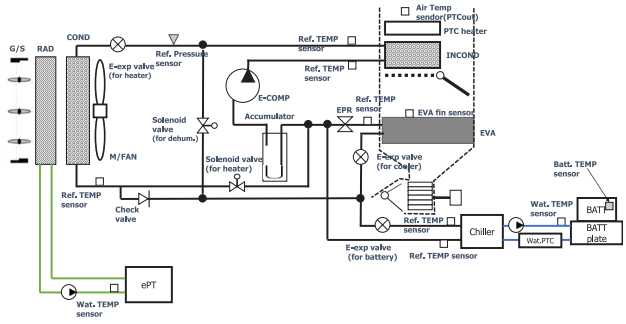

Fig. 2 Schematic of cooling system

EVs have reduced heat emission compared to that of ICEs. However, the temperature of these components must be properly controlled to ensure their efficiency and reliability, and thus, thermal management is important.

In ICEs, the amount of exhaust heat emitted from the engine is so large that it is used as the primary heat source to warm the room. In contrast, electric vehicles must use battery power to produce heat. Therefore, the inefficient use of power can lead to less power being available for driving. Furthermore, the battery generates heat originating from internal resistance, and its performance and life can be reduced depending on the thermal environment. Therefore, the battery temperature must be controlled properly. The thermal environments of the battery and e-PT must be controlled to achieve a good balance between electricity cost and interior comfort.

2. Challenges in tests for EV thermal management

2.1 Increase in test conditions

In ICE tests, operating conditions such as the on/off state of the air conditioner and the amount of heat emitted from the heat-generating engine can be evaluated independently. However, EVs use the cooling energy provided by the air conditioner to regulate the temperatures of the motor, battery, and inverter. Therefore, the electric compressor used by the air conditioner operates not only to switch the air conditioner on and off, but also to respond to the cooling demands of the battery. Furthermore, only the compressor battery cooling operation must be stopped to maintain the battery temperature environment. The combination of these conditions increase the number of driving modes. Further, it is necessary to process a large amount of time-series data obtained from the test because the driving modes change transiently.

2.2 Additional requirements for EV cooling system

Unlike an ICE vehicle, an EV cannot use the waste heat for interior heating, and therefore, battery power is used to produce heat. This increases the battery power consumption, which affects the cruising distance. Heat pump systems that use heat from outdoor air have become the norm for indoor heating in EVs to minimize this negative effect. The compressor must be operated at a high rotation speed to sustain cooling by removing heat from outside, not only when high-temperature outside air is present but also when low-temperature outside air is present. An electric compressor can be operated at any desired rotational speed; however, the noise of the compressor and other cooling components must be maintained at a low value to ensure a low-noise

*Customer and Vehicle Performance Engineering Division Customer Performance and Vehicle Test Engineering Department No.2

environment, which is an attractive feature of EVs.

The EV cooling system operates not only while driving, but also during charging, which is essential for EVs. The battery temperature varies with the charge output and driving conditions applied prior to charging, and this can affect battery performance. Therefore, it is necessary to reproduce not only the outside air temperature and driving conditions but also the temperature environment of the systems associated with the battery.

3. Solutions

3.1 Development of data processing system

The refrigerant used as cooling energy transforms into gas, liquid, and gas–liquid mixtures. The temperature and pressure are measured at multiple points to determine the physical properties of the refrigerant in the corresponding state to monitor whether the refrigerant is in the proper condition. The coupled temperature and flow rate of the cooling water are acquired at multiple points to determine whether the desired cooling is achieved.

Based on the data obtained from these measurement points, further data are obtained through tests in which the number of conditions is defined as the number of temperature levels multiplied by the number of driving modes. A large amount of data processing is required, and such data cannot be analyzed using conventional post-test processing. Therefore, we developed a real-time processing system that can perform these time-consuming evaluations.

Real-time measurements of temperature and pressure are not sufficient for determining the state of the refrigerant that provides cooling energy. The presence of an appropriate gas or liquid state must be confirmed by referring to the physical properties of the refrigerant that corresponds to temperature and pressure. Therefore, it is necessary to draw a pressure–enthalpy (p–h) diagram (see Fig. 3).

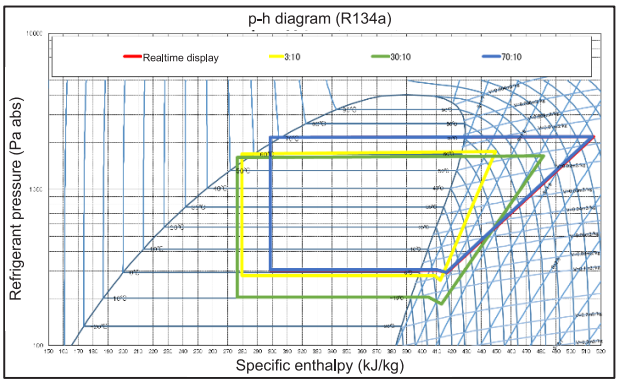

Fig. 3 p–h diagram

Thus, we developed a system to calculate the physical properties in real time based on the data measured in a time series. In this system, the measurement data are captured in real time and listed as time-series data. p–h diagrams were also drawn in real time to visually grasp the state of the refrigerant. This system reduces the data-processing time, as indicated in Fig. 4.

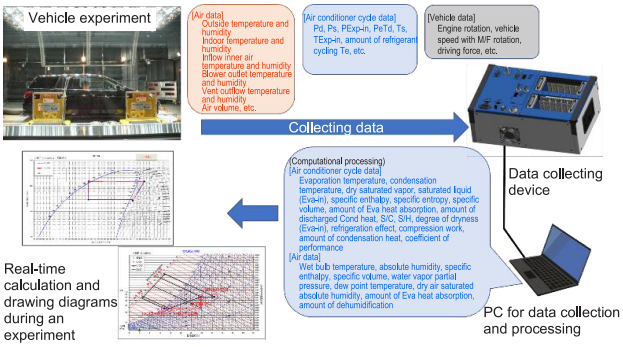

Fig. 4 Real-time data processing system

3.2 Test facilities reproducing temperature environment

The test facilities used to investigate the cooling circuits and interior comfort are equipped with an air-conditioner cycle bench tester and an actual vehicle, which are measured with a chassis dynamometer placed in an all-weather environment. The environment reproduces weather conditions ranging from low and high temperatures to rainfall and snowfall.

The air-conditioner cycle bench test equipment is used to evaluate the system performance prior to building a prototype vehicle. The equipment evaluates the characteristics of the components related to the cooling circuit, from air-conditioner-related components to cooling components (Fig. 5).

Fig. 5 Air-conditioner cycle bench test equipment

The test equipment reproduces the expected temperature environment in an actual vehicle from low to high temperature. It is possible to verify whether the heat balance with the HVAC, compressor, and other cooling circuits is on target. Tests can be performed by modifying the component characteristics and control conditions as required.

An all-weather environmental chassis dynamometer is used in the tests with actual vehicles (Figs. 6 and 7). The

temperature environment of the vehicle is determined by external factors, such as ambient air temperature, humidity, and solar radiation, as well as internal factors derived from driving self-heating sources, such as the powertrain and the battery. These temperature environments affect one another. For example, the self-heating of a vehicle increases the outside air temperature; this change makes it impossible to conduct tests in a constant-temperature environment. Therefore, an test facility that is not affected by the self-heating of the vehicle is required. An additional facility is required to evaluate the noise from the operating HVAC and cooling components.

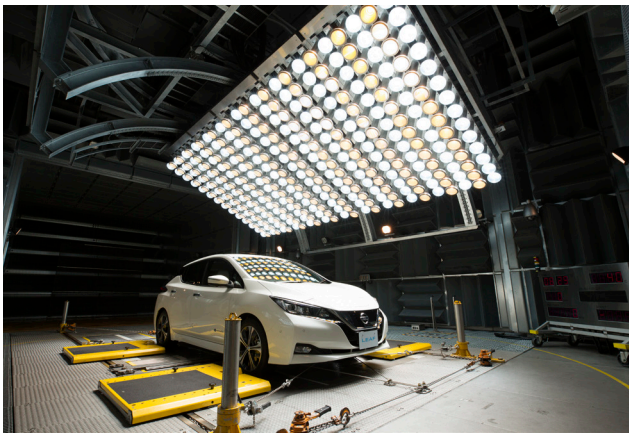

Fig. 6 Low-temperature solar radiation test room with all-weather environmental chassis dynamometer

Fig. 7 Rainfall and snowfall test room with all-weather environmental chassis dynamometer

An all-weather environmental chassis dynamometer responds to four-wheeled vehicles. This system can reproduce not only cold-to-hot temperature environments, humidity, and solar radiation, but also rainfall and snowfall environments. These facilities have sufficient refrigeration capacity to absorb the effects of heat from the vehicles, such as ICE vehicles. Furthermore, the noise from the chassis dynamometer and wind tunnel equipment is reduced to enable noise evaluation (Fig. 8).

Fig. 8 Rainfall and snowfall test room with all-weather environmental chassis dynamometer

The environmental test room is equipped with a rapid charger. With this charger, it is possible to measure the charging behavior immediately after driving in cold and hot environments, the accompanying effects on interior comfort, and even electricity costs.

The environmental chassis dynamometer can accurately reproduce a temperature environment. EV-specific thermal management tests with complex transitions over driving modes are conducted at both low and high temperatures to investigate the performance limit.

4. Summary

EVs are spreading rapidly and expanding their markets. However, the thermal environment of EVs can significantly affect their performance, reliability, and battery life. Therefore, thermal management technology and its supporting test technologies were created to optimize the thermal environments using electrical energy without wasting it.

The comfortable and reliable EVs produced are expected to contribute to improved product appeal and market expansion.

Authors

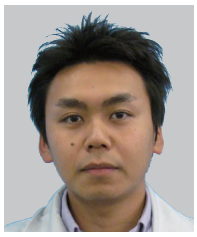

Masayoshi Tajiri

6. X-ray CT Nondestructive Measurement Technology Supporting Vehicle Body Weight Reduction Technology

Yasuhiro Kanda* Yoshitaka Usui*

1.Introduction

Considering the accelerating global competition to develop electric vehicles, product competitiveness is enhanced by increasing the cruising distance. Motor efficiency and battery power density are also increased, and the vehicle weight is reduced to further improve the performance of the electric powertrains, which requires streamlining part structures. Nondestructive measurement technology using X-ray computed tomography (CT) can be used in the research and development phase to analyze fine internal structures whose performances and conditions can change from those of the original when disassembled as three-dimensional profile data. The findings of this analysis can contribute significantly toward improving the performance of electric vehicles.

This study focuses on the use of X-ray CT for vehicle body weight reduction, which is gaining popularity given the advancements in electrification. Structural design technology that optimally combines materials with different physical properties is necessary to realize vehicle body weight reduction. The multi-materialization of vehicle body parts has evolved from using conventional steel sheets to using high-tensile steel sheets, aluminum alloy sheets, resins, carbon fiber-reinforced plastics (CFRP), and other materials, as presented in Fig. 1, in addition to structural streamlining.[1]

In this chapter, materials indispensable for multi-materialization and examples of applications to enhance the technological development of bonding dissimilar materials are presented, followed by the prospects for this measurement technology.

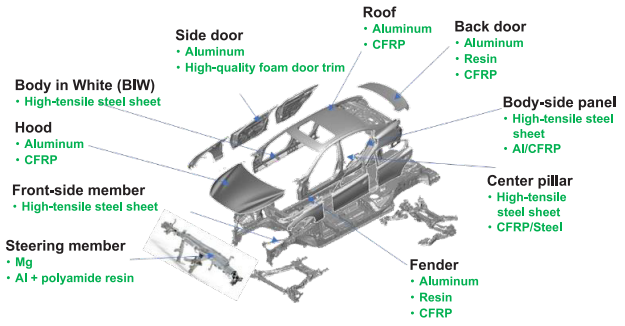

Fig. 1 Examples of lightweight material applications

2. Challenges in vehicle body weight reduction

2.1 Background

The supply chain for materials and parts in the automotive industry has become globalized, and this has prompted the expansion of local development and manufacturing bases. When developing lightweight vehicle bodies that combine individual part materials to achieve the performance goals by combining various materials, facility requirements of a manufacturing base must be considered. For example, the internal structure of joints for dissimilar material bonding and fiber orientation inside the material responsible for ensuring the strength and stiffness of carbon fiber-reinforced plastics (CFRP) must be evaluated. The design optimization of material processing based on the evaluation of several prototypes is necessary to achieve these performance goals.

2.2 Efficiency improvement of materials processing development

Bonding technologies for dissimilar materials (mechanical, solid phase, and adhesive bonding) depend on the application and material characteristics. For example, self-piercing riveting (SPR), used in mechanical bonding technology, is a joining method wherein the leg of a rivet piercing the upper plate is spread without piercing the lower plate.

Recently, the application of CFRP has expanded from the aerospace to automotive fields owing to improvements in material technology. Resin injection molding, press molding, injection molding, and other methods have been used based on application requirements. Resin injection molding is a process where carbon fiber is formed into a part shape in a mold and injected with resin to impregnate itself with the resin and harden it.

Performance indicators that indicate processing results such as strength, stiffness, and durability, and the internal structure, which represents factors associated with the processing parameters, are analyzed during the development of the material processing processes. The internal structure of prototyped parts

*CP and Test Engineering Methodology Innovation Department

must be analyzed and evaluated under different conditions to understand the mechanism of the phenomena and identify factors that affect the processing results. However, conventional analysis and evaluation techniques for internal structures rely on the observation of fractured cross-sections obtained after mechanical processing. Moreover, acquiring information about a specific cross-section is time-consuming.

Fatigue strength under repeated loading must be considered when designing vehicle body parts. Identifying internal structural changes over time using the same sample is an effective approach to understanding the fatigue mechanism. Therefore, a technology to efficiently analyze the internal structure in a nondestructive manner is expected to help realize competitive advantages in the development of vehicle body weight reduction technology. A technology for imaging three-dimensional internal structures developed in-house using X-ray CT is described in this special feature.

3. Internal structure visualization technology using X-ray CT

3.1 Overview of X-ray CT

X-rays can be generated using the following procedure: An electric current is passed through a filament inside the source, which heats the filament to generate thermal electrons. Thermal electrons are then accelerated using a high voltage. These collide with the target to generate X-rays, which are irradiated from all directions (360°) onto an object, and the X-ray transmission intensity is recorded as a transmission image by a detector located on the opposite side. The data from each direction are called projection data, and the three-dimensional image created by reconstructing all projection data from all directions (360°) is called a CT image. The sequence of this process is illustrated in Fig. 2.

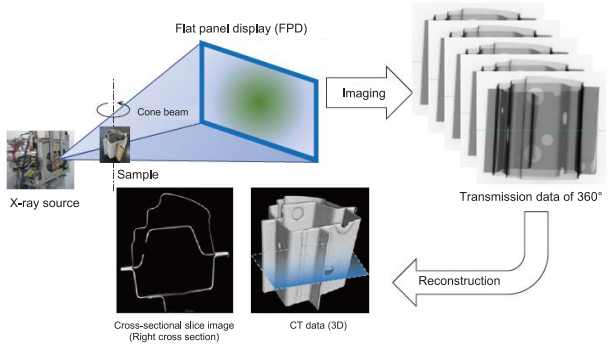

Fig. 2 Reconstruction process of X-ray CT

3.2 Challenges to implementing X-ray CT for vehicle body weight reduction

The energy of X-rays irradiated from commercially available industrial X-ray CT systems indicates a continuous distribution, with a peak on the low-energy side and a gradual decrease toward the high-energy side. X-rays are easily absorbed by parts made of dense iron, and a higher absorption is observed on the low-energy side, which allows only the high-energy X-rays to be transmitted. This is called “hardening” (beam hardening) because the apparent energy distribution shifts to the higher side. The illustrations of X-ray energy transmission and hardening are presented in Figs. 3-1 and 3-2, respectively.

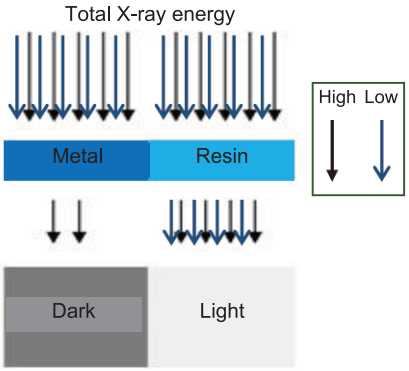

Fig. 3-1 Illustration of X-ray energy transmission

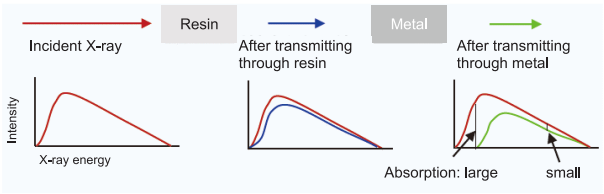

Fig. 3-2 Illustration of hardening

Hardening causes the relationship between the transmission length and transmission rate (irradiation intensity/transmission intensity) to deviate from the Lambert–Beer law, as indicated in Fig. 4. This deviation creates noise (metal artifacts) in the CT image that is not actually present as a structure during the reconstruction process.

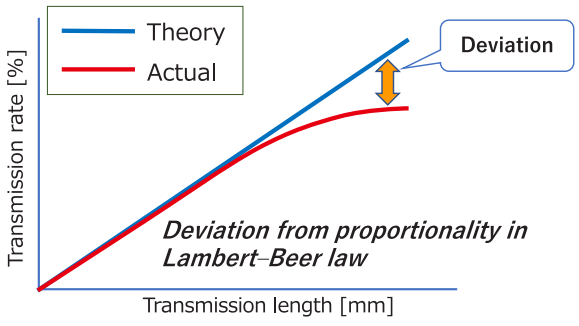

Fig. 4 Deviation of transmission rate as a function of transmission length

In general, metallic filters can be used to suppress hardening. Noise can be reduced by placing a metal plate as a filter in the X-ray irradiation section. The following steps are required to obtain CT images with reduced noise: the installation of a metal filter, trial imaging, and

verification of the noise reduction effect. This process relies on the expertise and intuition of the operator, and therefore, it requires a long time to determine the imaging conditions each time the measurement target is changed. Metal artifact noise is more likely to be generated in X-ray CT imaging of multimaterial parts made of steel or resin-based materials such as CFRP. The challenge is establishing an engineering technique that can efficiently determine the specifications of the metal filter for obtaining accurate information on the internal structure.[2]

3.3 Noise reduction effect using metal filters

An example of the noise-reduction effect achieved by applying a metal filter is illustrated in Fig. 5, which depicts that the metal artifact noise from iron is reduced.

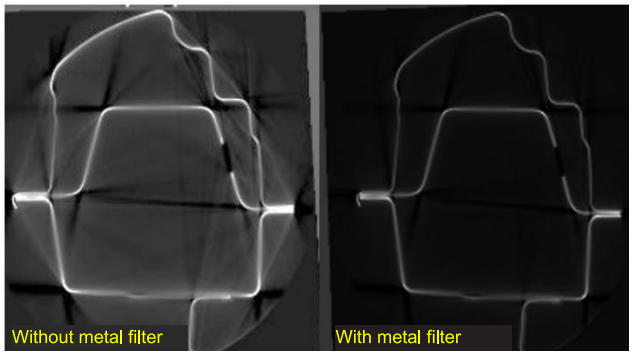

Fig. 5 X-ray CT image (cross section) of the side sill of an iron vehicle body

Fig. 5 illustrates that metal artifact noise is generated in a complex manner in response to the part profile. The noise reduction effect of the metal filter for a simple iron bolt, as indicated in Fig. 6, is evaluated to reduce the noise effect caused by the part profile.

One-mm-thick copper and aluminum plates were prepared as metal filters. A general filtered back projection (FBP) algorithm was used for reconstructing the CT images, and the brightness was corrected to visually emphasize the metal artifact noise, as presented in Fig. 6.

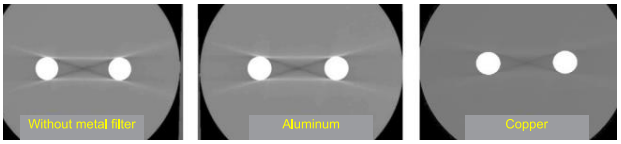

Fig. 6 Metal artifacts at the cylindrical section of iron bolts

The metal artifact noise is generated as white line-shaped false images arising from tangent lines between the two bolts in the CT images of the bolts (Fig. 6). The noise reduction effect increases in the order of copper filter > aluminum filter > no filter.[4]

The relative artifact index (AIr)[3], which is used in the medical field, was selected as the index for the quantitative evaluation of the noise reduction effect. The closer AIr is to 1, the better the noise reduction. The results of the calculation of AIr(*) in the area near the bolts presented in Fig. 6 are listed in Table 1. The AIr is 2.3, 2.0, and 1.3 for no filter, aluminum filter, and copper filter, respectively. These results indicate that the noise reduction effect depends on the metal filter material; the noise reduction effect of the copper filter is greater than that of the aluminum filter.

Table 1 Noise reduction effect by metal filter materials

Material/Thickness	None	1.0 mm
Aluminum	2.3	2.0
Copper		1.3

$$* \quad AIr = \frac{\sqrt{(\sigma^2_A - \sigma^2_B)}}{\sigma_B}$$

σ_A : Standard deviation in areas with noise
σ_B : Standard deviation in background area

3.4 Discussion and hypothesis formulation on noise reduction

Fig. 5 illustrates that a noise reduction effect was observed when using a metal filter, and this suggests that hardening was weakened. The energy distribution on the low-energy side of the incident X-rays can be changed using a metal filter, which is assumed to weaken the hardening.

The principle that absorption increases significantly at the energy where transitions occur between electron orbitals, called absorption edges (unique to a material), is applied to the X-ray absorption fine structure (XAFS) for analyzing the absorption spectrum obtained by irradiating X-rays with a material. The K-shell electron orbitals, where transitions occur, are called K-absorption edges. These were studied to evaluate the effect of metal filters.

The attenuation coefficient of X-rays, which is a physical quantity affecting absorption, is theoretically estimated to determine the change in X-ray absorption from high to low energies; the results are presented in Fig. 7.

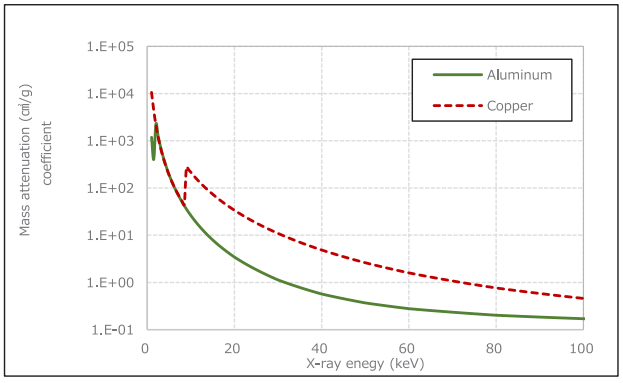

Fig. 7 Mass attenuation coefficient

The larger the attenuation coefficient, the greater the attenuation of the X-rays. Fig. 7 indicates that the attenuation coefficient changes with X-ray energy and becomes larger at lower energies. Moreover, the attenuation coefficient of copper increases sharply at the K-absorption edge of 8 keV, and it is approximately eight times higher than that of aluminum. The results lead to the hypothesis that the change in the energy distribution of the incident X-rays is significantly different at lower energies and affects hardening reduction.

3.5 Verification of the hypothesis

The X-ray spectra obtained to testly verify the above hypothesis for the aluminum and copper filters are presented in Fig. 8. The thickness of each filter is 1 mm.

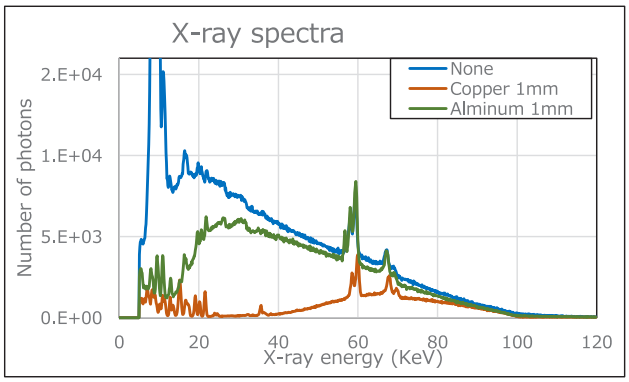

Fig. 8 X-ray spectra

In Fig. 8, The number of X-ray photons was qualitatively reduced on the low-energy side for both copper and aluminum filters. A comparison of the X-ray spectra for both filters indicates that the number of photons for the copper filter was significantly lower than that for the aluminum filter in the 20–40 keV energy band. The reduced number of photons calculated from the partial over-all (POA) in the 20–40 keV and 80–100 keV energy bands is illustrated in Fig. 9 and is used to quantitatively evaluate the difference in the X-ray spectra.

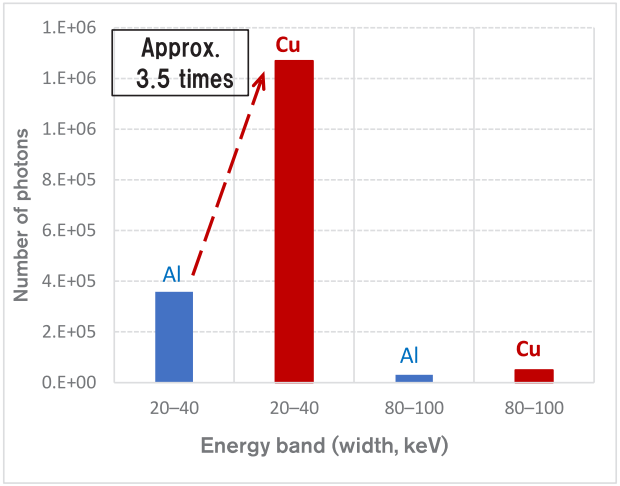

Fig. 9 Value of POA

The reduced number of photons for the copper filter in the 20–40 keV energy band is approximately 3.5 times higher than that for the aluminum filter. By contrast, the number of photons for both filters in the 80–100 keV energy band is 0.1 times less than that for the aluminum filter in the 20–40 keV energy band; this indicates a significant difference in attenuation between copper and aluminum in the 20–40 keV energy band. This result verifies the hypothesis that a change in the energy distribution of incident X-rays in the low-energy band caused by metal filters affects hardening reduction.

4. Results of application to weight-reduced parts

The relationship between the X-ray energy distribution and CT imaging results was determined to develop a method for selecting an optimal metallic filter. Reliable imaging was realized through an engineering approach that does not rely on the expertise and intuition of the operator. High effectiveness was achieved with new materials that had not been used in the past. Examples of clear visualization of internal structures that were previously difficult to visualize because of image noise are listed and illustrated below.

Example 1: The appearance and imaging results of a test piece consisting of aluminum plates bonded with an iron SPR and adhesive are illustrated in Fig. 10. The state (shape) of the adhesive application and the SPR bonding requirements, i.e., the piercing of the upper plate by a rivet, spreading of the rivet leg within the lower plate, and absence of cracks in the lower plate, were evaluated in the three-dimensional structure.

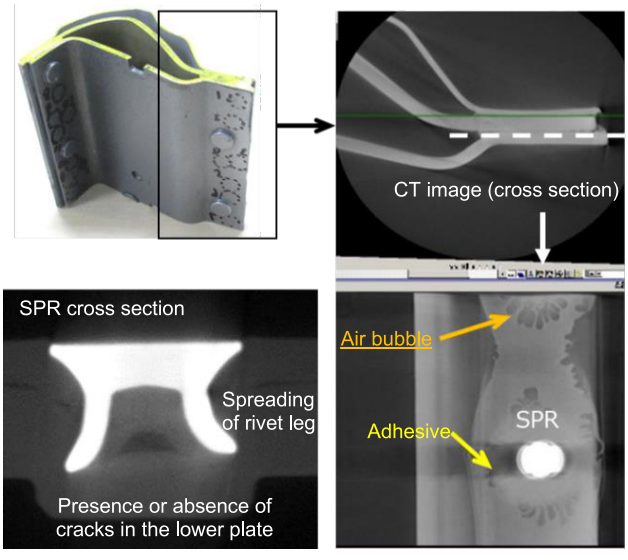

Fig. 10 CT images of a test piece of aluminum plates bonded together

Example 2: The imaging results of the multimaterial composite of iron and CFRP are illustrated in Fig. 11. The fiber orientation of the CFRP was observed in iron-mixed materials even when a metal filter was inserted.

Thus, a correlation with the tensile strength was obtained, which provides feedback on the molding conditions.

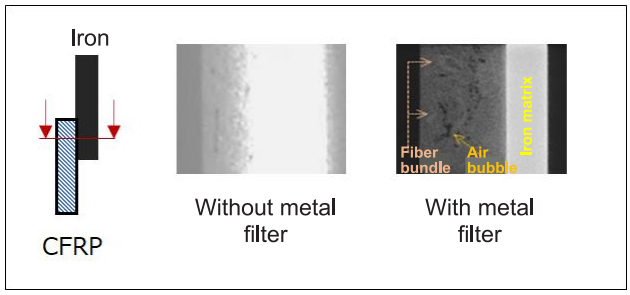

Fig. 11 CT images of a test piece of iron and CFRP bonded together

5. Summary

There is an urgent need to understand the mechanisms linking performance and structure to efficiently realize new structures in this era of innovation in vehicle manufacturing. The effect of using metal filters to reduce metal artifact noise in X-ray CT is not limited to vehicle body weight reduction. High effectiveness was also demonstrated in the visualization of complex structures such as motors and batteries consisting of a variety of materials.

As a powerful measurement technology in electric vehicle development, this technique is expected to help solve the trade-off between high quality and low cost and to contribute toward the development of attractive products.

6. Prospects of measurement technology using X-ray CT

Industrial X-ray CT is utilized globally and is expected to develop into a measurement technology that guarantees the uncertainty of the profile and dimensions. This technique is expected to enhance manufacturing competitiveness, which will play a significant role in the metrological traceability system through digital twin development used in digital engineering such as computer aided engineering and data-driven development such as materials informatics. By extension, this will lead to highly efficient development in the automotive industry, which requires a large labor force and energy in an era of a declining working population.

References

(1) NEDO　材料・ナノテクノロジー部：革新的新構造材料等研究開発」（中間評価）（2014年度～2022年度9年間）
(2) 公益社団法人自動車技術会2020年秋季大会学術講演会：マルチマテリアル部品における欠陥評価の高精度化に向けたX線CT画像のノイズ低減手法（濱名雅之、臼井徳貴；日産自動車）
(3) 日本放射線技術学会雑誌Vol.74　No.4　Apr2018：相対artifact indexによるノイズ特性に依存しないストリークアーチファクト定量評価法の提案（高田賢、坂野信也、乙部克彦；大垣市民病院医療技術部診療検査科、市川勝弘；金沢大学医療保険学域保険学類）
(4) 東京都立産業技術研究センター研究報告, 第7号, 2012年：X線CT画像計測技術による上流技術支援システムの構築（紋川亮、中川朋恵、金城康人、桜井昇、永川栄泰、藤井恭子；バイオ応用技術グループ、横山幸雄；システムデザインセクター）

Authors


Yasuhiro Kanda


Yoshitaka Usui

Paper published in Journal

SAE International Journal of Advances and Current Practices in Mobility

Stainless Steel Thermal Spray Coating of Cylinder Bores for VC-TURBO Engine

Introduction

Hayato Hirayama

Specialized field : Metal material, Tribology
Academic degree : Master of Engineering
Affiliated academic society : Society of Automotive Engineers of Japan

Hiroaki Hoshikawa

Specialized field : Structural Strength, Part/Element Design
Academic degree : Master of Engineering
Affiliated academic society : Society of Automotive Engineers of Japan

Yoshitsugu Noshi

Specialized field : Joining/Processing
Academic degree : Master of Engineering

Daisuke Terada

Specialized field : Joining/Processing
Academic degree : Bachelor of Engineering

Paper published in SAE Journal

SAE International Journal of Advances and Current Practices in Mobility

Stainless Steel Thermal Spray Coating of Cylinder Bores for VC-TURBO Engine

Hayato Hirayama* Hiroaki Hoshikawa**
Yoshitsugu Noshi*** Daisuke Terada***

Abstract The technical paper "Stainless Steel Thermal Spray Coating of Cylinder Bores for VC-TURBO Engine" was presented and highly appreciated at the World Congress Experience Digital Summit (WCX™ Digital Summit) of the Society of Automotive Engineers (SAE), which was held on April 13 through 15, 2021. This study was published in the "SAE International Journal of Advances and Current Practices in Mobility (SAE Journal)."

This study can be summarized as follows:
SAE Mobilus
https://saemobilus.sae.org/content/2021-01-0343/

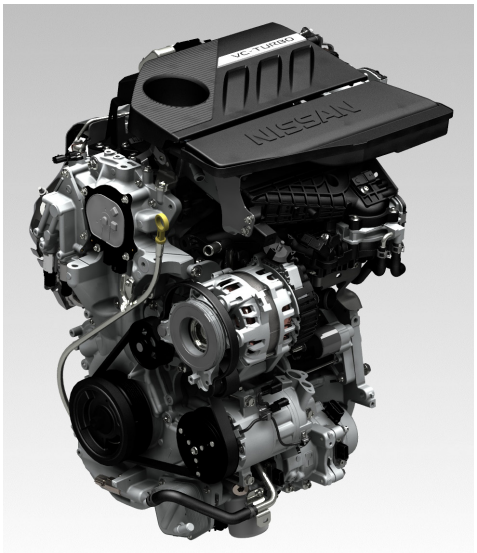

VC-TURBO Engine

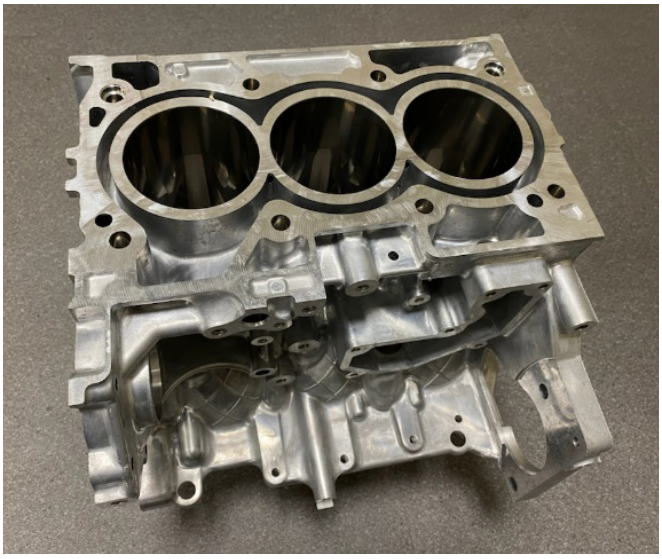

3-cylinder block with Stainless Steel Thermal Spray Coating bores

*Metal materials Group **Powertrain and EV Mechanical system Technology Department
***Powertrain Production Engineering Department

2021 JSAE Award The Outstanding Technical Paper Award

An Approach to Exploring Vehicle Motion to Enhance Ride Quality of Passenger

Introduction

Mitsuhiro Makita

Specialized field : Vehicle Dynamic Performance, Ergonomics
Academic degree : Doctor of Engineering
Affiliated academic society : Society of Automotive Engineers of Japan
The Japan Society of Mechanical Engineers

Akihiro Matsushita

Specialized field : Ergonomics, AD/ADAS
Academic degree : Master of Engineering
Affiliated academic society : Society of Automotive Engineers of Japan

Yoshinori Kusayanagi

Specialized field : Ergonomics
Academic degree : Bachelor of Engineering

Masahiro Miura

Specialized field : Dynamics and Control、AD/ADAS
Academic degree : Bachelor（intelligent mechanical engineering）
Affiliated academic society : Society of Automotive Engineers of Japan

2021 JSAE Award The Outstanding Technical Paper Award

An Approach to Exploring Vehicle Motion to Enhance Ride Quality of Passenger

Mitsuhiro Makita* Akihiro Matsushita**
Yoshinori Kusayanagi*** Masahiro Miura***

Abstract A passenger's passive motion, as a result of the vehicle's motion, impacts ride quality. So, we built the methodology to explore desirable passenger body motion, under a fixed driving task, by employing inverse dynamics analysis based on optimal control. First, we embedded a passenger body model in a vehicle model using a set formula. Next, we developed a soft sensor model so that acceleration and jerk could be integrated into the cost function for minimizing by optimal control. Then, inverse dynamics simulation was becoming executable to derive vehicle motion meets to the aiming passenger's passive motion. Designing passenger motion will lead to the understanding of human perception on vehicle.

1. Introduction

This study aimed to establish a method for analyzing the effects of vehicle dynamics on non-driving passengers from the perspective of ride quality. With regard to ride quality, ride comfort is normally considered, which is affected by the vehicle motion in the direction perpendicular to the road surface. In the future, when autonomous driving becomes common, driving tasks will be conducted independently from that of humans. Therefore, to create a comfortable moving space, the vehicle dynamics in the direction parallel to the road surface will also be an important research subject.

The body of a passenger is moved by an inertial force that is generated by the acceleration of the vehicle. Therefore, the passenger may experience some discomfort due to the body movement. Although the application of an inertial force to the body of the driver, which is the result of his or her own driving style, might be a positive experience for some drivers, this force is usually a cause of discomfort for passengers. Hence, body movement must be restrained by the seat and a restraint device if high-acceleration motion, such as emergency evasion, is necessary. However, within the range of normal driving, it is desirable to enhance ride quality by devising the vehicle motion such that the effect of the inertia force on the passengers is reduced.

In this regard, it is important to determine how vehicle dynamics should be perceived to enhance the ride quality of passengers. The main factors related to vehicle acceleration are <path> and <speed>. Therefore, it is possible to mitigate the inertial load acting on the passenger by driving the vehicle along an appropriate path. As autonomous driving technology is becoming increasingly advanced, setting the travel path is important for controlling vehicle dynamics. Research has focused on generating travel paths while considering the motion perception of the driver[1] and also on setting travel paths that can reduce the occurrence of car sickness among passengers, which can degrade the ride quality.[2]

As a research approach that focuses on passenger behavior, the use of a model that represents the behaviors of the bodies of passengers can be considered. In cases where the vehicle motion is known, a method for analyzing the behavior of passengers has been proposed,[3] and the impacts of the travel path have been investigated.[4]

Previous value-creating research includes analyses of the timing of the inertial force application to the bodies of passengers and its effects on the autonomous posture control of passengers;[5] the creation of the vehicle acceleration that stimulates the motion perception of passengers, enables passengers to recognize vehicle motion, and assists passengers in preparing their posture for motion has also been evaluated.[6] The approach of focusing on the senses and body movement mechanisms, including car sickness, is gaining importance as the understanding of humans has become increasingly advanced.

Considering the aforementioned preceding research, the establishment of a method for exploring vehicle behaviors that suppress the body behavior of passengers and the amount of accompanying motion perception under an assumed travel scene can be expected. Therefore, to respond to such expectations in this study, the research that the authors have been conducting ———the exploration of vehicle motion that optimizes the evaluation values set by applying optimal control ———was designated as an inverse vehicle dynamics analysis method,[7] and the scope of this method was

*Nissan Research Center Mobility & AI Laboratory **Customer Performance and Test Engineering Methodology Innovation Department
***AD/ADAS and Chassis Control System Engineering Department

expanded to include passengers.

If optimal control is employed, it is possible to "derive the desired vehicle motion and the control inputs for its realization by converting the matter into deriving the minimum value of the evaluation function." In other words, "the characteristics of vehicle motion that can enhance ride quality can be extracted using the evaluation function by using various values that are considered to have impact on ride quality."

The following section of this paper describes the case where inverse vehicle dynamics analysis is performed using optimal control and indicates that the analysis method is limited when applied for analyzing the behavior of passengers. Subsequently, technical solutions for overcoming these limitations are described. Lastly, the method for exploring the ride quality of a passenger is presented using transient motion as a case example and by describing the calculations, actual vehicle testing, and evaluations.

2. Ride quality analysis using inverse vehicle dynamics

If the forward vehicle dynamics analysis is considered as "set the control inputs and derive the corresponding vehicle motion," inverse vehicle dynamics analysis[7] can be considered as "reverse the cause-and-effect relationship, specify the desired vehicle motion, and derive the control inputs and vehicle motion that satisfy the specified motion." For the inverse direction, the calculation method will differ depending on what is specified for the desired vehicle motion. In this study, the travel scene was specified as the precondition, the motion comfort of the passengers was explored, and inverse vehicle dynamics analysis was performed using optimal control (the schematic flow of the inverse vehicle dynamics methodology is shown in Fig. 1, and the variable names are provided in Table 1).

Optimal control uses the stage cost function $L(\mathbf{x}(t),\mathbf{u}(t))$, which is described using variables such as the input variables $\mathbf{u}(t)$ and state variables that represent the state of the subject of motion $\mathbf{x}(t)$. The objective is to derive the vehicle motion that yields the minimum value of the function. From a different perspective, the vehicle motion is designed using the stage cost function. The forms of functions that can actually be used for description are limited, such as the quadratic forms of the variables. However, vehicle motion can be designed at least using this function.

The travel scene is specified by setting the initial and terminal values of the state variables and control inputs in the vehicle motion task. In other words, the state of the vehicle motion is fixed at both ends (the analysis becomes a boundary value problem). Therefore, it is possible to derive the control inputs $\mathbf{u}(t)$ that minimize the stage cost function value.

Table.1 Variables and functions for optimal control

Notation	Description
$\mathbf{u}(t)$	Input Variables (1,..., p)
$\mathbf{x}(t)$	State Variables (1,..., m)
t_0 / t_f	Initial / Terminal Time
$\mathbf{u}_0$ / $\mathbf{u}_f$	Initial / Terminal value of Input Variables (1,..., p)
$\mathbf{x}_0$ / $\mathbf{x}_f$	Initial / Terminal value of State Variables (1,..., m)
$\mathbf{f}(\mathbf{x},\mathbf{u})$	State Equation of motion (1,..., m)
$\boldsymbol{\lambda}(t)$	Adjoint Variables (Lagrangian) (1,..., m)
$L(\mathbf{x},\mathbf{u})$	Stage Cost
$J(\mathbf{u})$	Cost Function

p: Number of Inputs
m: Number of State Variables

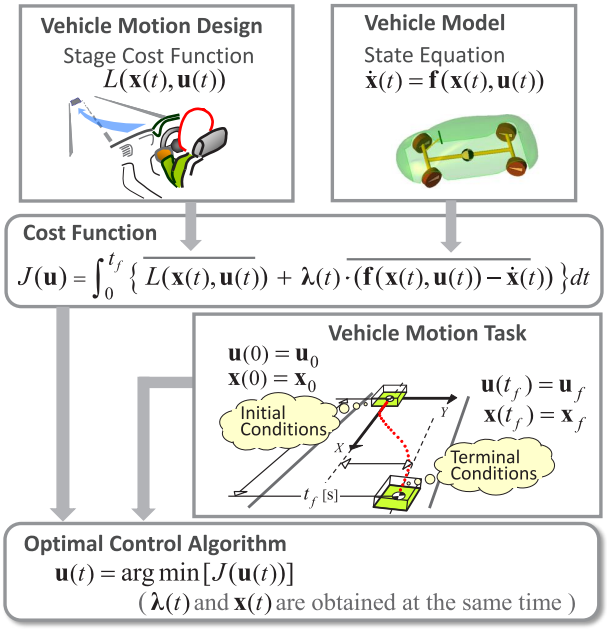

Fig.1 Schematic flow of the inverse vehicle dynamics methodology by optimal control: Ride quality is reflected to stage cost to describe motion design.

To evaluate the ride quality of passengers, in the vehicle model, reproducing the three-dimensional movements of the vehicle body in which the passengers ride is necessary. In addition, when formulating the optimal control using the ordinary variational principle, the vehicle model (in the form of a state equation) is added to the stage cost function using the adjoint variables. However, there are limitations in the model description for the evaluation function, which are related to the time integration of the added values. Specifically, in the description of the state equation, the differential quantities $\dot{\mathbf{x}}(t)$ of the state variable $\mathbf{x}(t)$ needs to be described <Explicitly> using the state variable, as shown in equation (2), and not in the form of equation (1):

$$\dot{\mathbf{x}}(t)=\mathbf{f}(\dot{\mathbf{x}}(t),\ \mathbf{x}(t),\mathbf{u}(t))\ . \tag{1}$$

$$\dot{\mathbf{x}}(t)=\mathbf{f}(\mathbf{x}(t),\mathbf{u}(t))\ . \tag{2}$$

In a previous study,[7] the authors developed a vehicle model to express the vehicle dynamics accurately, including the load transfer among the wheels, while observing the restrictions for describing the equation. Table 2 and Fig. 2 present the vehicle model, including

the vehicle dynamics and state variables. The coordinate system is based on the unsprung position. For the tire characteristics, the response characteristics using the relaxation length were added to the simplified Magic Formula. Refer to the previous research of the authors[7] for details regarding the vehicle model using equation (2).

Table.2 Variables and input functions of vehicle model

Notation		Description
State Variables $\mathbf{X}(t)$	$X_G(t)$, $Y_G(t)$, $Z_G(t)$	C.G. Position (Ground Coordinate)
	$V_\xi(t)$, $V_\eta(t)$, $V_Z(t)$	C.G. Velocity (Vehicle Coordinate)
	$\Omega(t)$, $\omega(t)$	Yaw Angle, Yaw Rate
	$\Phi(t)$, $\phi(t)$	Roll Angle, Roll Rate
	$\Theta(t)$, $\theta(t)$	Pitch Angle, Pitch Rate
	$\alpha_i(t)$	Tire Slip Angle
Inputs $\mathbf{u}(t)$	$\delta(t)$	Front Tire Toe Angle
	$Acc(t)$	Longitudinal(ξ) Acceleration

Subscript i: Wheel Position [Front → FR, FL ; Rear → RR, RL]

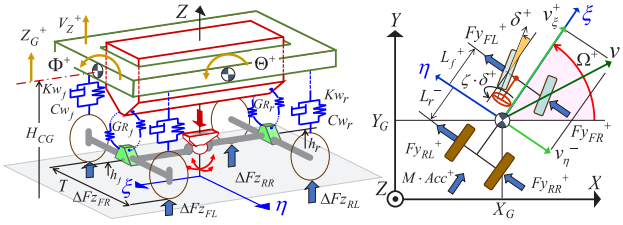

Fig.2 Two track and body motion vehicle model conforms to equation (2): Refer to author's previous research[7]

Using the inverse vehicle dynamics analysis described thus far, passenger ride quality enhancement is discussed. First, the passenger body model must be placed inside the vehicle body model. When doing so, passenger modeling is conducted using the form of equation (2), as in the case of the vehicle model.

Next, to deal with the ride quality in motion design, a value related to the passenger perception of the vehicle motion needs to be provided as a state variable $\mathbf{x}(t)$. For example, the vestibular organ recognizes the translational acceleration and angular velocity. Because, as shown in equation (1), acceleration is not a state variable but is rather the differential $\dot{\mathbf{x}}(t)$ of the state variable, acceleration cannot be incorporated into the stage cost function when creating the motion design policy. Thus, a method of converting acceleration into a state variable is required.

The abovementioned considerations suggest that two issues need to be addressed to apply the inverse vehicle dynamics analysis to passenger ride quality. The resolution of these issues is discussed in the subsequent section.

3. Expansion to passenger ride quality evaluation

3.1 Passenger body behavior modeling

The passenger body motion model was created while observing the restriction of <explicitly> expressing the state variables, as shown in equation (2). If the inertia force of the passenger motion acts on the vehicle, it will not be possible to make <explicit> expressions using the state variables of the vehicle and passenger. Therefore, only the passive motion due to the inertia force of the vehicle motion is considered, and a model for the motion of the upper body in the lateral direction (roll), without separating the head portion, is proposed.

Table.3 Variables and parameters of passenger model

Notation		Unit	Description
State Variables	$\Phi_B(t)$, $(\dot{\Phi}_B(t))$	[rad], [rad/s]	Upper Body Roll Angle (Angular Velocity) (Vehicle Body-Fixed Coordinate)
Temporal Variables	$X_S(t)$, $Y_S(t)$, $Z_S(t)$	[m]	Seating Pivot Point (Ground Coordinate)
	$Fy_B(t)$, $Fz_B(t)$	[N]	Applied Force at Upper Body C.G.
Model Parameters	ξ_S, η_S, ζ_S	[m]	Seating Pivot Point (Vehicle Body-Fixed Coordinate)
	h_{BCG}	[m]	Height of Upper Body C.G. from Pivot
	I_B / m_B	[kg-m^2] / [m]	Upper Body Mass / Inertia
	K_B / C_B	[Nm/rad] / [Nm/(rad/s)]	Upper Body Roll Stiffness / Damping

$\Phi(t)$, $\phi(t)$, $\theta(t)$, $\dot{\omega}(t)$, $V_\xi(t)$, $V_\eta(t)$, $V_\zeta(t)$ are the state valiables of vehicle model[7]

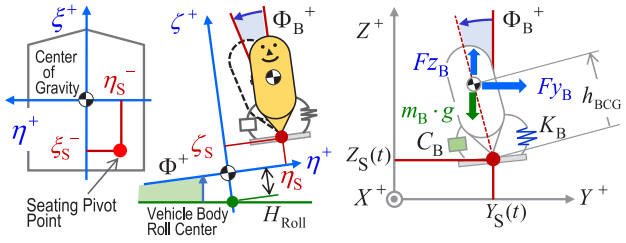

Fig.3 Passenger seating point configuration: Passenger upper body (including head) is simplified to a single inverted pendulum, then affected with vehicle motion.

As the first step, the inertia force of the vehicle motion, which is applied to the passenger, is expressed. The passenger seating point in the fixed coordinate system of the vehicle body as well as the rigid upper body model that has a pivot at that point are presented at the left and center of Fig. 3; the variables and constants that are related to the passenger model described below are listed in Table 3. Owing to the vehicle motion, the three-axis translational acceleration shown in equation (3) is applied to this pivot (terms that have little effect are omitted):

$$\begin{cases} \ddot{X}_S(t) = -V_\eta(t)\cdot\omega(t) + \dot{V}_\xi(t) - \eta_S\cdot\dot{\omega}(t), \\ \ddot{Y}_S(t) = V_\xi(t)\cdot\omega(t) + \dot{V}_\eta(t) + \xi_S\cdot\dot{\omega}(t) - \left(\zeta_S + H_{\mathrm{Roll}}\right)\cdot\dot{\phi}(t), \\ \ddot{Z}_S(t) = \dot{V}\ (t) + \eta\ \cdot\dot{\phi}(t) - \xi\ \cdot\dot{\theta}(t). \end{cases} \quad (3)$$

In the next step, the force acting on the center of gravity (CG) of the upper body is expressed. To this end, it is necessary to derive the acceleration at the CG of the upper body. Here, the acceleration is given by the second-order differentiation of the upper body CG position (pivot point + effect of upper body roll posture angle), which is expressed using the coordinate system based on the ground. The force acting in the lateral and vertical directions, as shown on the right side of Fig. 3, are approximated as the acceleration by multiplying the

mass of the upper body and are expressed in equation (4):

$$\begin{cases} Fy_{\mathrm{B}}(t) = m_{\mathrm{B}} \cdot \dfrac{d^2}{dt^2}\left(Y_{\mathrm{S}}(t) - h_{\mathrm{BCG}} \cdot \mathrm{Sin}\left(\Phi_{\mathrm{B}}(t) + \Phi(t)\right)\right), \\ Fz_{\mathrm{B}}(t) = m_{\mathrm{B}} \cdot \dfrac{d^2}{dt^2}\left(Z_{\mathrm{S}}(t) + h_{\mathrm{BCG}} \cdot \mathrm{Cos}\left(\Phi_{\mathrm{B}}(t) + \Phi(t)\right)\right) \\ \qquad + m_{\mathrm{B}} \cdot g\,. \end{cases} \tag{4}$$

The equation of motion of the upper body about the pivot in the roll direction, caused by the forces Fy_B and Fz_B acting on the upper body CG, is expressed as equation (5). For the roll stiffness and damping, the effects of the supporting force acting between the passenger and the seat surface, friction, etc. are included as approximate values:

$$\begin{aligned} I_{\mathrm{B}} \cdot \ddot{\Phi}_{\mathrm{B}}(t) + C_{\mathrm{B}} \cdot \dot{\Phi}_{\mathrm{B}}(t) + K_{\mathrm{B}} \cdot \Phi_{\mathrm{B}}(t) = \\ Fy_{\mathrm{B}}(t) \cdot h_{\mathrm{BCG}} \cdot \mathrm{Cos}\left(\Phi_{\mathrm{B}}(t) + \Phi(t)\right) \\ + Fz_{\mathrm{B}}(t) \cdot h_{\mathrm{BCG}} \cdot \mathrm{Sin}\left(\Phi_{\mathrm{B}}(t) + \Phi(t)\right). \end{aligned} \tag{5}$$

In the last step, equations (3) and (4) are substituted into the equation of motion of the upper body (equation (5)) to determine the roll angle acceleration of the upper body $\ddot{\Phi}_{\mathrm{B}}$ <explicitly>, as shown in equation (6):

$$\begin{aligned} \ddot{\Phi}_{\mathrm{B}}(t) = \frac{1}{I_{\mathrm{B}} + h_{\mathrm{BCG}}^2 \cdot m_{\mathrm{B}}} \cdot \\ \left(g \cdot \mathrm{Sin}\left(\Phi_{\mathrm{B}}(t) + \Phi(t)\right) \cdot h_{\mathrm{BCG}} \cdot m_{\mathrm{B}} \right. \\ - K_{\mathrm{B}} \cdot \Phi_{\mathrm{B}}(t) - C_{\mathrm{B}} \cdot \dot{\Phi}_{\mathrm{B}}(t) \\ + \mathrm{Sin}\left(\Phi_{\mathrm{B}}(t) + \Phi(t)\right) \cdot h_{\mathrm{BCG}} \cdot m_{\mathrm{B}} \cdot \\ \left(\dot{V}_{\zeta}(t) + \eta_{\mathrm{S}} \cdot \dot{\phi}(t) - \xi_{\mathrm{S}} \cdot \dot{\theta}(t)\right) \\ + \mathrm{Cos}\left(\Phi_{\mathrm{B}}(t) + \Phi(t)\right) \cdot h_{\mathrm{BCG}} \cdot m_{\mathrm{B}} \cdot \\ \left(V_{\xi}(t) \cdot \omega(t) + \dot{V}_{\eta}(t) + \xi_{\mathrm{S}} \cdot \dot{\omega}(t) - \left(\zeta_{\mathrm{S}} + H_{\mathrm{Roll}}\right) \cdot \dot{\phi}(t)\right) \\ \left. - h_{\mathrm{BCG}}^2 \cdot m_{\mathrm{B}} \cdot \dot{\phi}(t) \right). \end{aligned} \tag{6}$$

The differential quantities of the state variables of the vehicle model, $\dot{V}_{\eta}, \dot{V}_{\zeta}, \dot{\phi}, \dot{\theta}$, and $\dot{\omega}$, are included in the derived passenger model, as shown in equation (6). However, if equation (6) is converted from the equation of motion to the equation of state and if the converted equation and the vehicle model are considered as a set of simultaneous equations, replacement with the state variables can be performed such that the equation will converge to the form of equation (2). In this manner, the formulation of the optimal control used for the inverse vehicle dynamics analysis was realized.

3.2 Converting motion perceived by passengers into state variables

The physical quantities that can be expected to be related to the ride quality may include the translational and angular accelerations applied to the passenger body. However, as mentioned in the previous section, quantities other than the state and input variables cannot be incorporated into the evaluation function.

The acceleration can be converted into a state variable by differentiating the equation of motion, which is expressed as a second-order differential equation, once more to a third-order differential equation (and to the fourth order for conversion to the jerk state variable). However, this increases the number of equations that need to be solved, leading to a calculation burden and making this approach unsuitable for inverse vehicle dynamics calculations. To address this problem, a state observer is used to derive the approximate state variables that can be incorporated in the evaluation function.

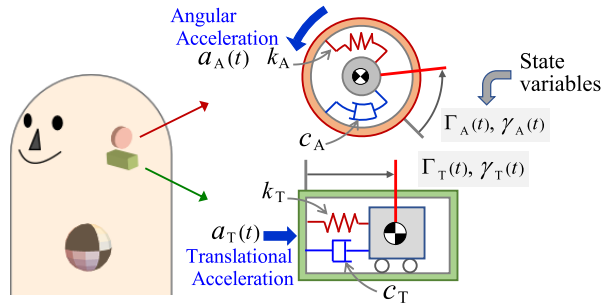

Fig.4 Acceleration and jerk detection with soft sensor (physical image of state observer) : Acceleration and jerk at the attached body are approximated to state variables.

To formulate optimal control by combining the vehicle and passenger models, the state observer is used as a soft sensor, as shown in Fig. 4. Specifically, the state equation described in equation (7) is employed, and the acceleration at the passenger body or at the measurement target position of the vehicle body is used as input $a(t)$. Utilizing this method, the translational acceleration, roll acceleration, and jerk at the mounting position can be observed as approximate state variables $\Gamma(t)$, $\gamma(t)$:

$$\begin{cases} \dot{\gamma}(t) = c \cdot \gamma(t) + k \cdot \Gamma(t) - a(t)\,, \\ \dot{\Gamma}(t) = \gamma(t)\,. \end{cases} \tag{7}$$

The approximation accuracy of the state variables is determined by setting the c and k values in equation (7). Fig. 5 shows the characteristics corresponding to different natural frequencies when the set values are altered. The set values are selected such that the gain, which represents the degree of approximation, is close to 1; this implies that the characteristics will be flat.

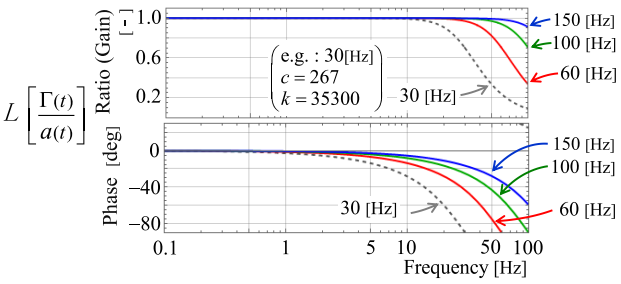

Fig.5 Frequency response characteristic of state observer: Four cases of translational and angular accelerations.

At this point, the effect of the approximation accuracy of the state observer in the inverse vehicle dynamics analysis is reviewed. In the lane change behavior analysis, discussed in the next section, the state observer was mounted at the vehicle body CG position, and calculations were performed such that the lateral acceleration at the vehicle CG was minimized. The calculation results are presented in Fig. 6. With regard to the stage cost function values, it is evident that there exists an appropriate value range within which the approximation accuracy can be increased by increasing the response frequency. In other words, if the response frequency is excessively high, the differential equation of the state observer stiffens the overall system to be solved. Thus, when calculating the values, it is necessary to consider the trade-off between accuracy and the accumulation of calculation errors.

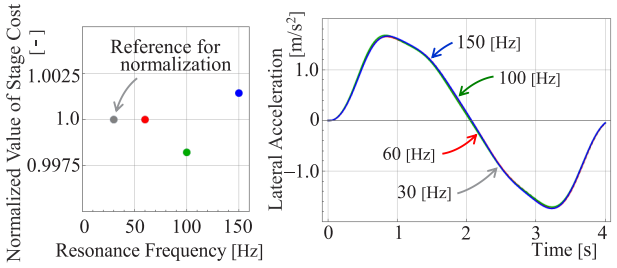

Fig.6 The degree of approximation of state observer (stage cost is quadratic value of lateral acceleration): There is an appropriate value for the resonance frequency of state observer.

Using the state observer described above, it was possible to approximate the values of the acceleration and jerk (which are related to the motion perceived by passengers) and to design the evaluation function by incorporating the approximated values in the evaluation function as state variables.

4. Exploring ride quality factors by designing passive motion of passengers

4.1 Designing motion for ride quality evaluation

Here, the method of exploring the vehicle motion to enhance the ride quality is specified. In this method, it is necessary to consider how to use the inverse vehicle dynamics to derive the minimum value of the evaluation functions, which include the amount of motion perception that occurs due to the body motion of the passengers.

An important aspect in the vehicle evaluation is to maintain identity, that is, "the condition that should be kept the same when making comparisons." The logic of this matter has been presented in previous reports.[7] When solving the functions in the inverse vehicle dynamics analysis, identity is ensured by setting the state variables and input variables for the initial and terminal motion conditions for the vehicle motion task shown in Fig. 1. Using this method, a motion design based on the evaluation functions is established.

The design flow can be classified into the following three phases:

(i) Set the travel scene to be evaluated (vehicle motion task).
(ii) Set the ride quality factors in the evaluation function and calculate the optimal solution.
(iii) Reproduce the optimal solution as the vehicle motion and conduct tests and evaluations.

The characteristics that can be obtained as the optimal solution are the control inputs and motion of the target vehicle. Therefore, when reproducing the vehicle motion in the last phase, the control inputs are provided to the actual vehicle, or the motion is applied to the passenger using equipment that can reproduce the acceleration space (as shown in Fig. 7).

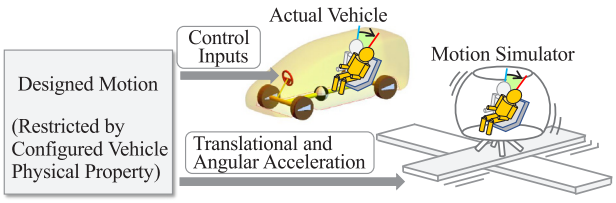

Fig.7 Methodology to construct acceleration space

In the first phase, i.e., setting the travel scene for ride quality evaluation, there will be no significant difference in the results of the evaluation function related to motion perception if the travel scene is the steady driving mode; however, the results may depend on the types of control inputs (such as steering only and the addition of active acceleration/deceleration using the brake/accelerator). Therefore, in this work, transient motion is utilized as the travel scene example because it is easier to obtain the difference in motion perception under this case than in the other situations (Fig. 8).

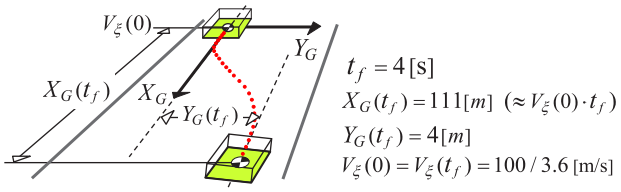

Fig.8 Example of vehicle motion task: Lane change as a typical transient vehicle motion scene.

Next, the design specifications for the vehicle motion in this example are presented in Table 4. In the vehicle motion task, a lane change scene was set, in which the following terminal conditions were returned to straight-line travel (=0): the control inputs and the track angle and yaw angle velocity, which are the state variables for plane motion on the road. Assuming passenger ride quality enhancement, the following specifications were set for the evaluation functions: the steering control input minimizing specification V0, assuming the ride quality of the driver, and the body roll angle acceleration minimizing specification R1. For comparison, specification R2 was also set; R2 represents the body roll angle

acceleration minimization specification added with the conditions for returning the roll angle acceleration and angle velocity to zero at the terminal.

Table.4 Vehicle and passenger motion design specification: Three condition to exemplify design methodology.

Stage Cost *		Terminal Condition (Motion Task)			Symbol
		Vehicle		Passenger	
Subject	Roll Angular Acceleration	Control Input	Plane Motion	Body Roll Motion	
Driver (Vehicle)	Vehicle Body	Steering Angle & Angular Velocity return to 0	Track Angle & Yaw Rate return to 0	Arbitrary State	V0
Passenger	Passenger's Body	Same Speed as initial condition	Lateral Velocity of C.G. return to 0	Angular Acceleration &Velocity back to 0	R1
			Set C.G. Position		R2

* Applied quadratic form of state and/or input variables

4.2 Calculating passenger acceleration space based on design

The calculations were performed in accordance with the motion design specifications. Here, the characteristics of the passenger body model need to be determined (the settings of the vehicle characteristics are the same as those mentioned in a previous report by the authors[7]). Because the passenger model is simple, the accuracy improvement effect will be small, even if the thoroughness of the model characteristics definition is improved. Therefore, for the characteristic values of the shape and mass, values close to those of the actual vehicle test evaluator, as mentioned in subsection 4.3, are used. The body stiffness, K_B , near a lateral acceleration of 2 m/s² was set by referring to the distribution results of the measurements of the test subjects (n = 15). Examples of the stiffness measurements are presented in the box-and-whisker plot in Fig. 9. The value when the passenger was facing down and reading text was used for the calculations, and the passenger was considered to be seated on the left side of the rear seat.

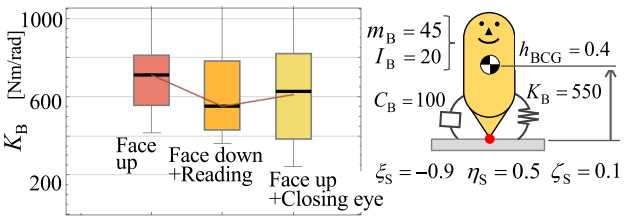

Fig.9 Passenger body roll stiffness (box-and-whisker plot) and other characteristics: Passenger model parameters were fixed from subject measurement (n=15) and estimation.

The settings necessary for the calculation were implemented. Thereafter, inverse vehicle dynamics analysis was performed to calculate the control inputs and vehicle motion (Fig. 10 shows the path of the vehicle CG) that minimizes the evaluation functions while satisfying the terminal conditions.

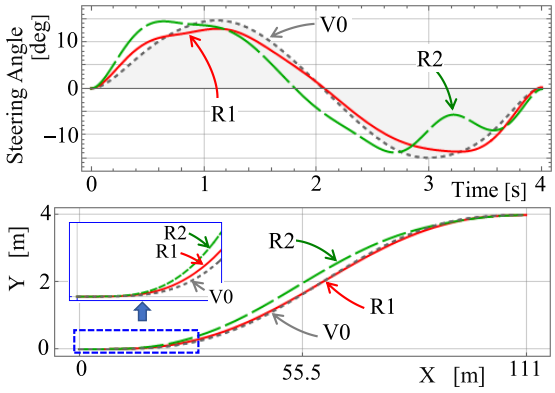

Fig.10 Steering pattern and vehicle C.G. path (with enlarged view) to satisfy design specification of vehicle and passenger motion: Inverse vehicle dynamics analysis fixes both input and state variables simultaneously.

The calculated optimal vehicle motion, lateral acceleration of the vehicle CG, and roll posture angle of the passenger body Φ_B are depicted in Fig. 11. According to the calculation results, the transition of V0 appears as a sine function. Compared to V0, the peak value of the passenger behavior is suppressed for R1 (in which case the passenger behavior is optimized). In R2 (in which case additional terminal constraints are implemented), the posture angle converges to a certain value at the end of the calculation.

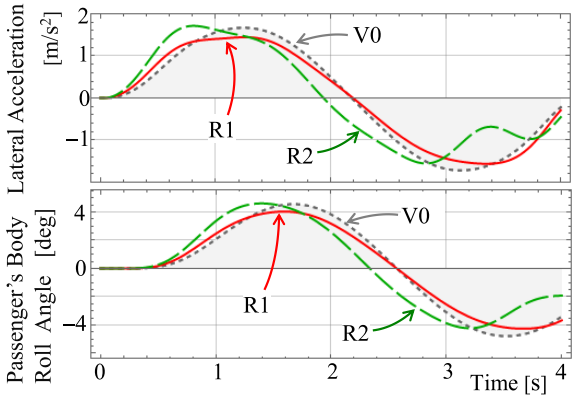

Fig.11 Vehicle and passenger motion to satisfy the design specification: Calculated results.

4.3 Evaluation using the acceleration (vehicle) space

In the test method, a steering robot was mounted on a vehicle to reproduce the calculated steering waveform such that acceleration was applied to the passenger seated on the rear seat. To correspond to the actual environment, a term that represents the effects of slopes was included in the vehicle model when performing the calculations. The test values were compared with the calculated values for the last 4 seconds.

The passenger has a body build close to the average of the measurement results of the passenger characteristics and is an expert in vehicle dynamics evaluation. The passenger can recognize the start of the vehicle motion based on the inevitable driving noise of the steering robot. However, it should not be easy for the passenger to

predict the vehicle motion because the passenger can only view the external environment through the surrounding view. Therefore, the test environment should be similar to that in the passive motion evaluation. The transitions in the passenger posture were estimated using the movement detected by the displacement sensor attached to the rear of the neck.

The test results are presented in Fig. 12 in a manner that corresponds to the calculation examples (Fig. 11). It can be considered that the reproducibility of the acceleration space was ensured. The deviation between the passenger posture transition and the calculated value (the results in the figure were multiplied with a coefficient of 2.0) is attributed to the differences between individual evaluators, as the passenger model characteristic values in Fig. 9 were used for the calculation (the values differ by a factor of approximately 2 for some data within the quartile range). It is judged that the relative relationship between the specifications is in-line with the predictions based on the calculations.

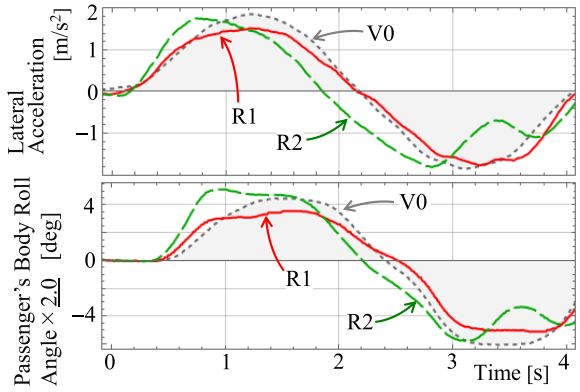

Fig.12 Vehicle and passenger motion of actual vehicle test: Every data curve was averaged (n=5).

In the subjective evaluation, it "seems that the motion is smooth while the body posture transition is large" with specification V0, whereas it "seems that the body roll posture transition is small" with specification R1 (in which the body roll angle acceleration is suppressed). In other words, the result that "the body seems to have moved along with the vehicle motion" was obtained. However, in the case of specification R2 (in which additional terminal constraints for the roll posture are implemented), the evaluation "movement at the early stage of the motion was large compared to V0" was obtained. In addition, the evaluation that "while the high-frequency motion was somewhat noticeable, it was possible to feel the load reduction due to the suppressed body motion" was obtained for the "body roll suppression" terminal condition, with the objective of maintaining body posture. In summary, it was possible to parameterize the ride quality in terms of both the measurements and subjective evaluations using the passenger passive motion design.

5. Considerations for exploring ride quality

In the passenger body model, increasing the degree of freedom (such as by separately defining the head portion) is possible. However, this will make it difficult to determine the appropriate model characteristic values, such as the stiffness at the neck portion, even if the scope of the model is limited to passive motion. It is assumed that passengers will perform various activities and be in various states in the vehicle. Therefore, in addition to addressing the complexity of the passenger model, determining the settings of the characteristic values of the model needs to be resolved in future research.

However, the motion perceived by the passenger cannot be mechanically calculated based on the body model. Thus, it may be important to add a model that represents the human inner sensory characteristics such that the evaluation function is configured using the actual perception values. Fig. 13 shows the body behavior (calculated values) under the specifications, where the body roll angle acceleration is used as the evaluation function. R1 does not include terminal constraints, whereas R2 has terminal constraints. Compared to specification R1, specification R2 causes more lateral movements during the intermediate test time. It is clear that the body roll movement must occur early to control the body behavior at the terminal. Although the roll motion is suppressed, the translational acceleration is increased. Therefore, the mechanism of the perceptual recognition of translational and rotational motions must be considered.

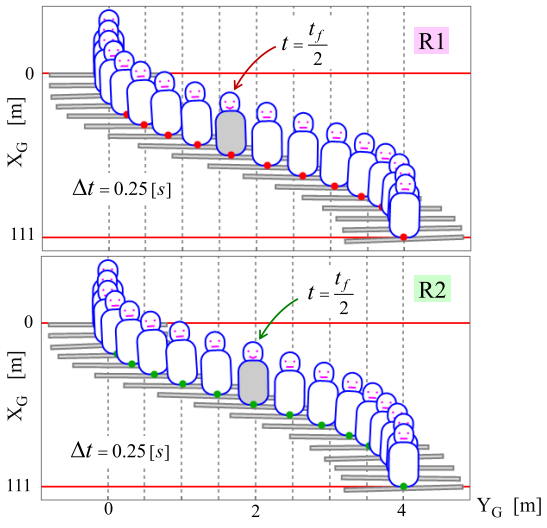

Fig.13 Passenger upper body posture transition: Earlier motion generation is required for terminal posture control, then needs quick initial motion, too.

The degree of freedom of the motion design depends on the limitations in the form of the evaluation function. The variables that can be incorporated are typically limited to a combination of quadratic forms. In addition, in the travel scene expanded to multiple control inputs,

the terms corresponding to each control input must be set in the evaluation functions. Otherwise, simultaneous optimization is not possible (ensuring orthogonality of the terms). To advance research on ride quality, the flexibility of expressing the evaluation functions needs to be improved.

6. Conclusion

In this study, the effects of vehicle dynamics on passengers were considered from the perspective of ride quality, and a <methodology for testing/evaluation> for improving ride quality was presented herein. Passenger ride quality can be improved by determining the vehicle motion if it is assumed that the ride quality depends on the passive motion load applied to the body and on the perception caused by the vehicle motion within the acceleration space.

Therefore, the desirable motion was set as the evaluation function, and motion design was attempted using inverse vehicle dynamics analysis, where the vehicle motion was derived from the optimal control. An observer was established to incorporate a passenger body model which estimate the load, and acceleration which used to estimate the motion perceived by passengers into the evaluation function. In this manner, an inverse dynamics analysis that combines the passenger and the vehicle was realized.

It is necessary to subjectively evaluate whether the form of the evaluation function successfully indicates the improvements in the ride quality of the designed vehicle motion and to also investigate the passengers' perception of vehicle motion. For these purposes, this paper presents an evaluation flow using a specific example. In the first phase, a travel scene is assumed. In the next phase, the vehicle dynamics are designed using a candidate evaluation function setting. In the last phase, evaluation is performed by placing a passenger in the designed acceleration space (the actual vehicle in this study).

This research will be extended such that the "vehicle motion gentle to the passenger" can be incorporated into the technological developments in autonomous driving via control logics and artificial intelligence, among others.

(Addendum): The tests conducted in this study were examined and approved by the Experimentation Ethics Committee of Nissan Motor Co., Ltd. The tests were conducted after obtaining informed consent from the participants.

References

(1) Tatsuya Yoshimoto, Takanori Fukao, Yasuyoshi Yokokohji, Hiroshi Inou: Path Generation of Lane Change in Dynamic Environments Considering Characteristics of Driver's Operation, Transactions of the JSAE, Vol.47, No.2, p.633-638 (2016)

(2) Takahiro Wada: On Motion Sickness in Highly Automated Vehicles, Proceedings of the JSAE Annual Congress (2016), 20165263

(3) Katsunori Yamada, Harutoshi Motojima, Yuichi Kitagawa, Tsuyoshi Yasuki: Investigation of Relations between Occupant Kinematics and Supporting by the Seat in Lane Change Maneuvers, Proceedings of the JSAE Annual Congress (2016), 20165176

(4) Makoto Yamamoto, Tadashi Yamamoto, Shuji Nishiyama: Proposal for a Transition Curve with Smoothly Changing Curvature Using Multiple Clothoid Curve, Transactions of the JSME, Vol.83, No.852 (2017)

(5) Tohru Yoshioka, Masato Abe, Makoto Yamakado, Yoshio Kano, Yusaku Takeda, Kazuhiro Takemura, Takatoshi Tsukano, Fuminori Kato, Daisuke Umetsu: Analyses on Vehicle Dynamics Improvements from Human Aspects with G-Vectoring Control, Proceedings of the JSAE Annual Congress (2016), 20165250

(6) Alexander Lange, Martin Albert, Karl-Heinz Siedersberger, Klaus Bengler: Ergonomic Design of the Vehicle Motion in an Automated Driving Car, 6th International Conference on Applied Human Factors and Ergonomics (AHFE) (2015)

(7) Mitsuhiro Makita: A Solution to Apply Load-Transfer Including Vehicle Model to Optimal Control Formulation, Transactions of the JSME, Vol.81, No.826 (2015)

Source

公益社団法人自動車技術会
自動車技術会論文集
Vol.50, No.5 文献番号：20194687

2022 JSAE Award The Outstanding Technical Paper Award

Surrogate Model Development for Prediction of Car Aerodynamics Using Machine Learning

Introduction

Kei Akasaka

Specialized field : CFD(Computational Fluid Dynamics), Machine Learning
Academic degree : Doctor of Engineering
Affiliated academic society : Society of Automotive Engineers of Japan
The Japan DataScientist Society

Fangge Chen

Specialized field : Machine Learning
Academic degree : Master of Engineering

Takehito Teraguchi

Specialized field : Dialogue system, Machine Learning、UX
Academic degree : Doctor of Philosophy in the field of Information Science and Technology

2022 JSAE Award The Outstanding Technical Paper Award

Surrogate Model Development for Prediction of Car Aerodynamics Using Machine Learning

Kei Akasaka* Fangge Chen** Takehito Teraguchi**

Abstract In the evaluation of car aerodynamics, Computational Fluid Dynamics (CFD) are frequently used as well as a wind-tunnel. However, the CFD simulations consume a lot of resources and time. In this study, a surrogate model using machine learning was developed to reduce the amount of resource and time needed for CFD. In the proposed model, the relation between car shapes and CFD results was learned for rapid prediction of pressure, velocity, and coefficient of drag for aerodynamics. In this paper, we introduce the proposed model, the training dataset, the accuracy, and the computational time.

1. Introduction

In recent years, it has become necessary to further reduce aerodynamic drag in order to improve the fuel efficiency competitiveness of cars and comply with new environmental regulations. Computational fluid dynamics (CFD) is often used as well as wind tunnel experiments to evaluate the aerodynamic performance of cars [1,2]. However, CFD requires a significant amount of time and resources. In particular, the resources required to perform CFD computations are increasing every year owing to the necessity of pre-calculations prior to experiments, the increase in the number of evaluation specifications, and the demand for improved calculation accuracies. Therefore, this study attempted to develop a surrogate model that estimates the CFD results (flow velocity, pressure, and drag coefficient C_D) using machine learning method, by learning the relationships between the car shape and the quantities evaluated using CFD. Using this approach, aerodynamic analyses can be replaced with the surrogate model, such that the amount of CFD computations and time consumption, as well as the corresponding costs, can be reduced. This paper outlines the proposed method, the dataset, and the validation results.*Received on November 10, 2020. Presented at the Technical Sessions of the Autumn Congress of the Society of Automotive Engineers of Japan on October 23, 2020.

2. Machine learning model

2.1 Previous Studies & Related Studies

Several studies similar to the present investigation have been reported. For instance, Umetani et al. [3] constructed a machine learning model to learn and estimate the quantified features and characteristics evaluated via CFD (flow velocity, pressure, and C_D) for the car shape by using the Gaussian process to estimate the C_D values and flow fields of the cars. They trained the model with approximately 800 examples of car shapes and CFD results. They reported that the C_D and flow field estimation results matched the CFD calculation results, which served as reference information for our research. However, it is difficult to learn complex shapes of actual cars using their method. Specifically, this method uses a polyhedron called "PolyCube" and projects the constituent points of the PolyCube onto a car shape within a range in which the topology does not vary. The coordinates and heights of each projected constituent point are used as features. It is necessary to prepare a PolyCube with a topology similar to the shape of the car to be learned. However, it is difficult to use the same PolyCube for all car shapes because actual shapes have different topologies; for instance, minivans, hatchbacks, and sedans have 1-, 2-, and 3-BOX topologies, respectively. Hence, a PolyCube suitable for each car model needs to be prepared for individual learning, which requires time and effort. In addition, the actual cars have complicated shapes such as engine room parts, tires, floor components, and door mirrors, and it is difficult to prepare a PolyCube with a topology that can express such complicated shape elements. Therefore, the results obtained by Umetani et al. can only be applied to relatively simple car shapes.

By contrast, Guo et al. [4] used a distance function that represents the distance from an object as input data and constructed a machine learning model that estimates two- and three-dimensional flow fields (corresponding to the flow velocity vector and pressure) based on a convolutional neural network (CNN) [5]. Because the

*Integrated CAE・PLM Department **Nissan Research Center Mobility & AI Laboratory

distance function can be applied to complicated shapes and can also be extended to three dimensions relatively easily, the model structure proposed by Guo et al. was adopted for the flow field (i.e., flow velocity and pressure) estimation.

However, because C_D cannot be estimated using the model of Guo et al., a separate surrogate model for estimating C_D is required. Therefore, we proposed a surrogate model that estimates C_D [6] based on the input of voxel data. Because the estimation accuracy of C_D is satisfactory, the surrogate model structure of C_D was adopted in this study as well.

In related studies, a single model that can learn both the flow field and C_D has not been proposed thus far. Therefore, in this research, two different machine learning models based on related studies were developed to estimate the flow field and C_D.

2.2 Outline of estimation model for estimating flow field

The basic configuration of the flow field estimation model adopts the network structure proposed by Guo et al., as shown in Fig. 1. This model consists of an encoder and a decoder connected by a fully connected layer. When applying the model practically, such as in this study, it is necessary to increase the size of the distance function to be input according to the degree of complexity of the shape. In addition, the intermediate layers between the encoder and decoder need to be multilayered to improve the estimation performance. However, the use of multilayered intermediate layers easily causes gradient disappearance or gradient explosion problems during training, making it difficult to proceed with training. Therefore, to solve the gradient disappearance and explosion problems, in this study, residual blocks [7] were used instead of the fully connected layer in the model structure of Guo et al. The model proposed herein is illustrated in Figs. 2 and 3. This model inputs a distance function and outputs (a) the three components of the flow velocity vector and (b) the pressure. For the encoder and decoder, batch normalization [8] and instance normalization [9] are used to suppress the disappearance of the gradient.

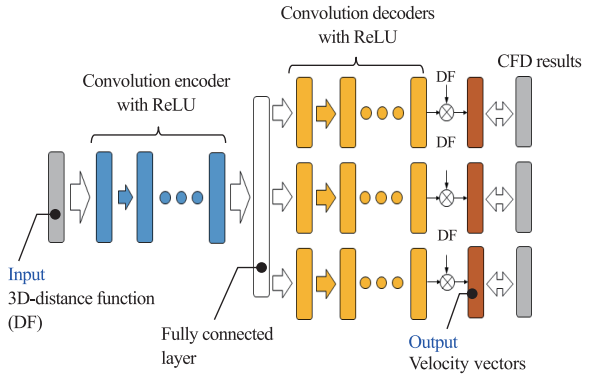

Fig.1 CNN structure of prediction model for flow filed proposed by Guo [4]

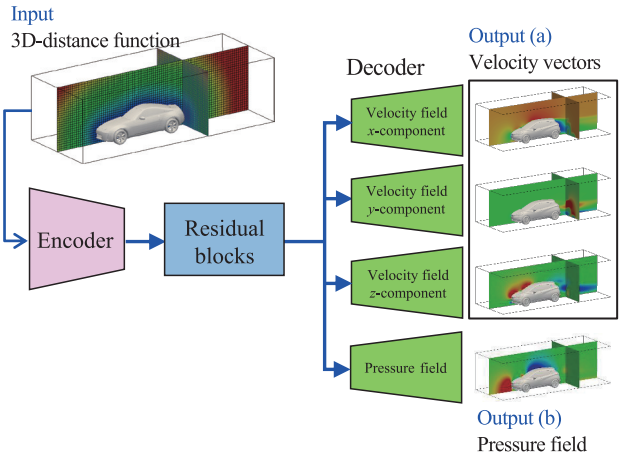

Fig.2 Structure of proposed model for flow field estimation

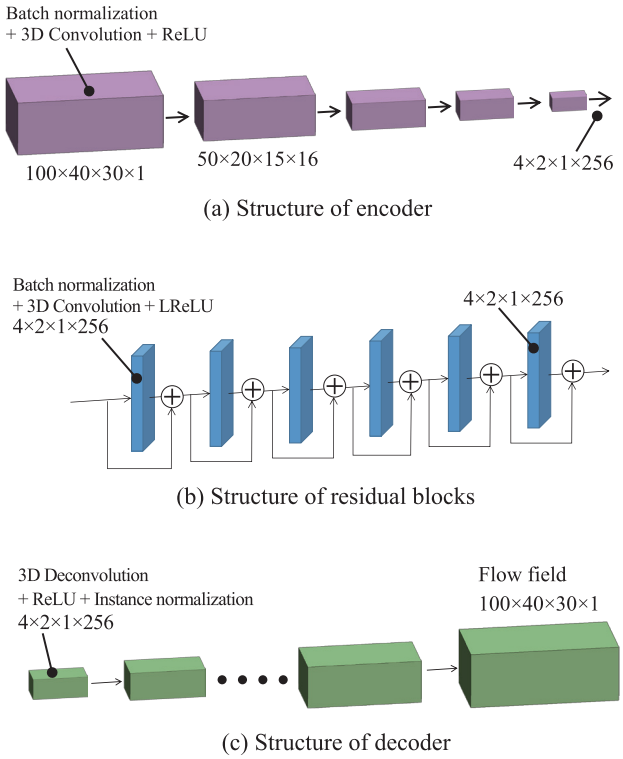

Fig.3 Details of encoder, residual blocks and decoder of proposed model for flow field estimation

2.3 Outline of estimation model for estimating C_D

The estimation model for estimating C_D is described in this section. We previously proposed an estimation model that estimates C_D based on the input of voxel data [6]. Although the model is based on Voxnet, proposed by Maturana [10], global average pooling, instead of a fully connected layer, is used according to the research of Lin et al. [11] to reduce the amount of calculation when converting the intermediate layer into one dimension. Because the estimation accuracy of C_D is satisfactory, the estimation model structure based on our previous study was adopted in this study as well.

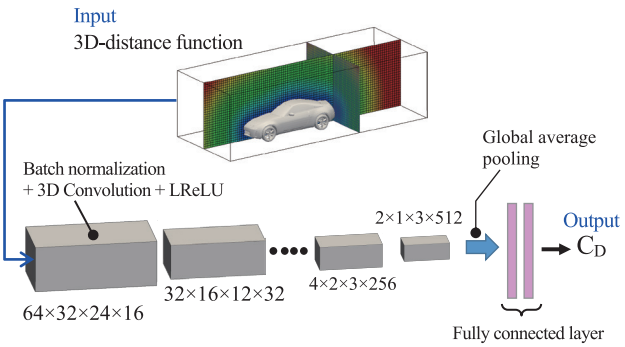

Fig.4 Structure of proposed model for coefficient of aerodynamic drag (C_D) estimation

However, in terms of convenience, it is desirable to avoid the use of different input data when estimating the flow field and C_D. Therefore, the input data for the C_D estimation model are converted from the voxel into the distance function to unify the flow field and C_D estimation model input data into the distance function. The network structure in which the input data are unified into a distance function is show in Fig. 4.

2.4 Distance function and hyper-parameters

First, the distance function to be input into the estimation model can be described as follows. The distance field of the three-dimensional distance function used in this study is illustrated in Fig. 5. The colors indicate the distances from the car shape at each grid point. The distance function was created as follows. A bounding box was set around the car shape, and orthogonal equal-interval grid points were arranged in the bounding box. The shortest distance from the car shape was calculated for each grid point to create the relevant distance field. The sizes of the bounding boxes, grid pitches, and numbers of grids are provided in Table 1. For the distance function used to predict C_D, a smaller grid pitch is employed to ensure that even a slight shape change can be captured.

The optimizers, loss functions, and hyper-parameters used in this study are listed in Table 2.

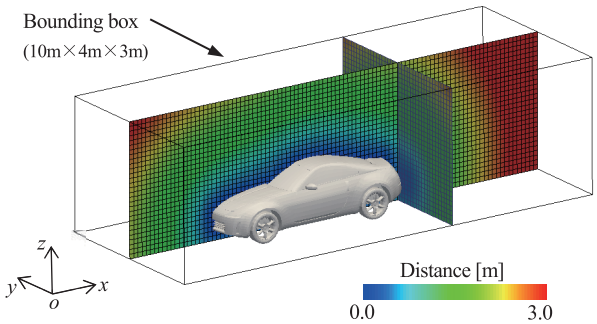

Fig.5 3-dimensional distance function around car shape

Table 1 Parameter of distance function

	Flow field prediction	C_D prediction
Bounding box	10.0m×4.0m×3.0m	6.4m×3.2m×2.4m
Grid pitch	0.10m	0.05m
Num. of grids	100×40×30	128×64×48
	120,000	393,216

Table 2 Optimizer, loss function and hyper-parameters

	Flow field prediction	C_D prediction
Optimizer	Adam	Adam
Loss function	Mean absolute error	Mean absolute error
Learning rate	10^{-3}	10^{-4}
Epoch	5,000	2,000
Batch size	16	16

3. Dataset and validation results

3.1 Dataset

The dataset is shown in Fig. 6. One case includes six pieces of information: the distance function, three components of the flow velocity vector, pressure, and C_D value. Only the distance function is input into the estimation models, and the flow fields and C_D value are the outputs of the models respectively. Training was performed such that these outputs matched the flow velocity, pressure, and C_D value of the training case. For this study, 1,123 cases were prepared and divided in a ratio of 10:1 into training and testing datasets. The datasets included six types of cars: sedans, coupes, SUVs, hatchbacks, pickup trucks, and light cars. The proportions of car types included in the training and test datasets were approximately the same. The flow velocity vectors, pressures, and C_D values used for training and test were calculated using commercial CFD software. The calculations were performed under straight running conditions at a car speed of 33.3 m/s and Reynolds number of 1.0×10^7. Because a grid unrelated to the distance function was used in the CFD calculations, the CFD calculation results were mapped to the grid for the distance function.

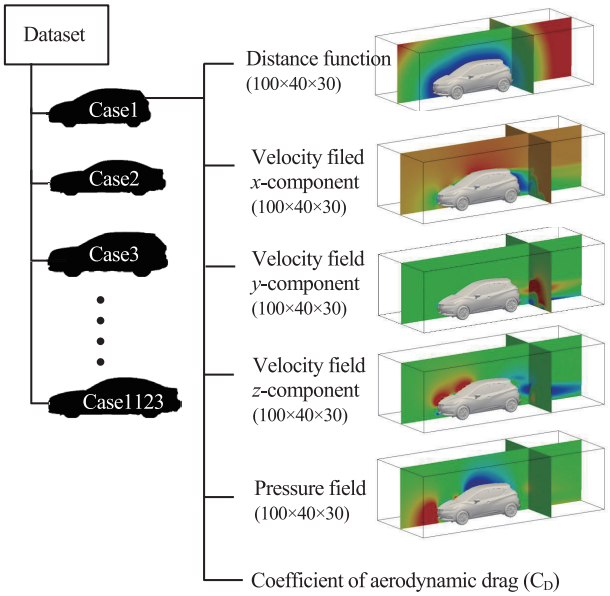

Fig.6 Distance function, flow fields and aerodynamic drag (C_D) in dataset

In addition, because the distance function and CFD results are dimensional information, normalization was performed before using them for learning and testing in this study.

A NVIDIA DGX-1™ (1 GPU) was used as a computational resource for learning, and Tensorflow 2.0 was employed as a library for machine learning. The time required for learning the flow field was approximately 4 days, whereas the time for learning C_D was approximately 0.5 days. In addition, by calculating the number of epochs shown in Table 2, it was confirmed that the values of the final loss function of the three components of the velocity vector, pressure, and C_D value are reduced to the extent shown in Table 3.

Table 3 Errors of loss functions in velocity vectors, pressure and C_D at last epoch of proposed model

Velocity vectors	Pressure	C_D
0.003～0.005	0.002	0.001

3.2 Flow field validation results

Next, the flow field estimated by this method was considered as follows. Each test case had a flow velocity vector of 120,000 points (100 × 40 × 30). The mean error of those 120,000 points was considered using the mean absolute error (MAE) shown in equation (1):

$$MAE = \frac{1}{n}\sum_{i=1}^{n}|a_i - y_i| \qquad (1)$$

where ai and yi represent the CFD results and the estimation results of the proposed model, respectively. In addition, n represents the number of grid points, which was 120,000 in this case.

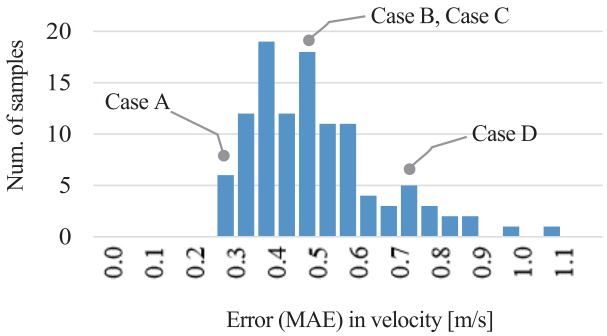

Fig.7 Histogram of mean absolute error in x-component of velocity vector on test cases

The mean absolute error (MAE) of the x-direction component of the velocity vector is presented in Fig. 7. The mean error of the x-component is 0.2–1.1 m/s, which is within the error range of the car speed wind (0.6%–3.3%). In addition, the mean errors of the y- and z-components were smaller than that of the x-component.

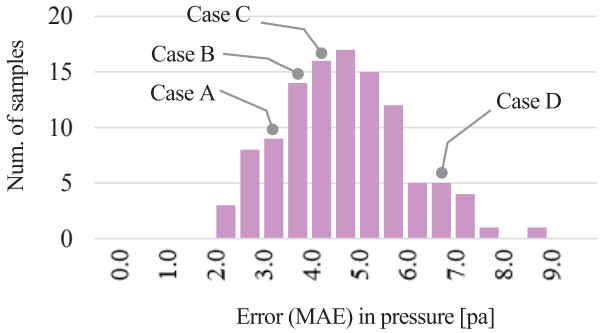

Fig.8 Histogram of mean absolute error in pressure on test cases

The MAE results for the pressure estimated by the proposed model and evaluated at 120,000 points in the same manner as the velocity vector are presented as a histogram in Fig. 8. The MAE of the pressure is 2.0–9.0 Pa, which is within the error range of approximately 0.3%–1.3% of the dynamic pressure based on the car speed wind. There were no significant differences in the error tendencies among the car types in terms of both velocity and pressure.

The pressure and velocity magnitude distributions obtained from the CFD calculations and proposed model are compared in Figs. 9 and 10, respectively. Cases A–D are typical examples of the test cases, and the velocity and pressure errors in each case are shown in Fig. 7 and Fig. 8, respectively. In both Fig. 9 and Fig. 10, the upper rows show the CFD calculation results, whereas the lower rows indicate the estimation results of the proposed model to be compared for each case.

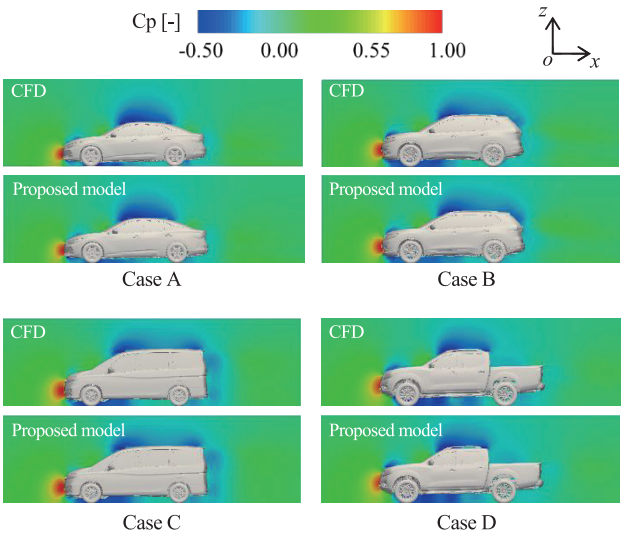

Fig.9 Comparison of pressure between CFD and proposed model in central cross-section

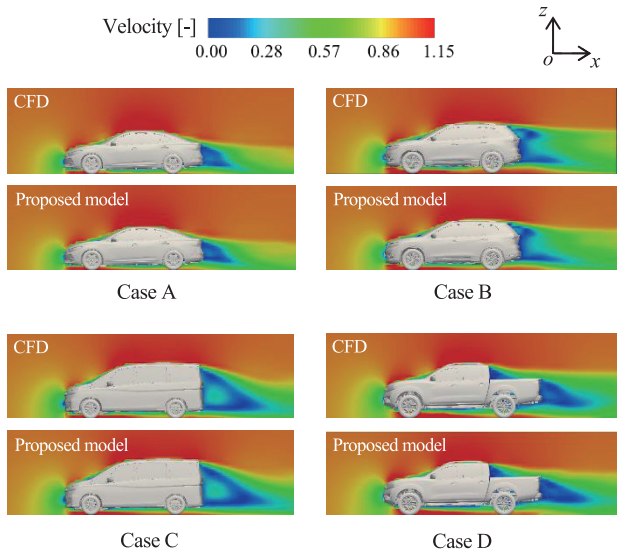

Fig.10 Comparison of velocity magnitude between CFD and proposed model in central cross-section

The pressure distribution at the central cross-section of the car is shown in Fig. 9, where the pressure is converted into a dimensionless value by using the dynamic pressure. In each case, the pressure distribution estimated by the proposed model reproduces the tendency of the CFD results.

The velocity magnitudes in the central cross-section of the car are shown in Fig. 10. The velocity was made dimensionless by using the car speed. The proposed model qualitatively reproduces the CFD results in terms of the size of the rear stream region behind the car and the tendency of the velocity magnitude, which are important, especially in aerodynamic evaluations.

According to the comparison results shown in Fig. 9 and Fig. 10, it was confirmed that the proposed model can reproduce not only the qualitative tendency of the flow field even in case D, in which the error between pressure and velocity is relatively large, but also the characteristics of the flow fields of different car types.

3.3 Effect of the residual blocks

The network structure proposed by Guo et al., in which a fully connected layer was adopted for the connection between the encoder and decoder, and the network structure proposed in this study, in which residual blocks were adopted instead of a fully connected layer, are compared in this section. The velocity magnitudes at the central cross-section of the car are shown in Fig. 11. The results of the CFD calculations and training using the residual blocks are presented in Figs. 11 (a) and (b), respectively. Here, the results of the proposed model are similar to the CFD calculation results. By contrast, in the results of training using the fully connected layer, shown in Fig. 11 (c), the tendency of the velocity magnitude is different from that in the CFD results. Owing to the gradient explosion, the weight optimization failed during training, and the value of the loss function of the velocity vector was 0.1. This value is larger than that of the loss function of the proposed method, as shown in Table 3, and it did not decrease even when the number of epochs was increased. According to these results, the residual blocks were considered to be effective.

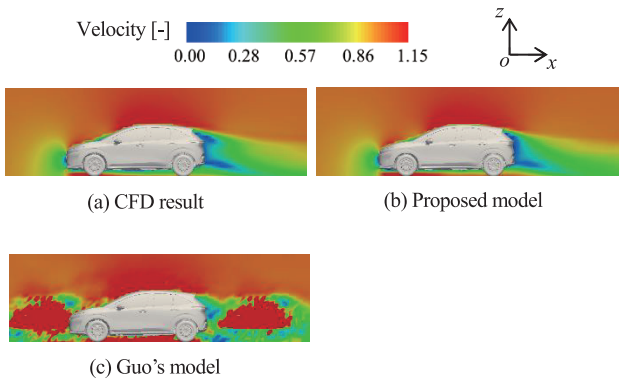

Fig.11 Comparison of velocity magnitude between Guo's model and proposed model in central cross-section

3.4 C_D validation results

The errors in the C_D values estimated using the proposed model are depicted in Fig. 12; the errors obtained in the training and testing cases are shown in (a) and (b), respectively. Table 4 shows the results of evaluating the error using the mean absolute percentage error (MAPE), described in equation (2), and the standard deviation:

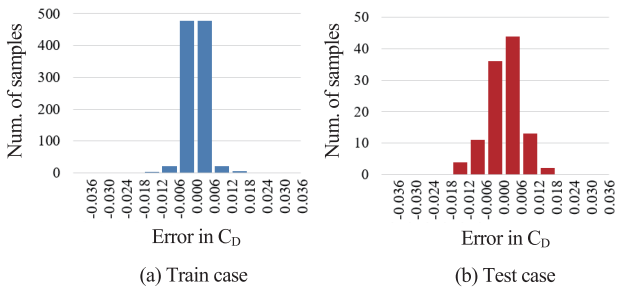

Fig.12 Histograms of error in C_D

Table 4 Error in C_D of train and test

	(a) Train case	(b) Test case
Std. deviation	0.002	0.006
MAPE	0.5%	1.4%

$$MAPE = \frac{100}{n}\sum_{i=1}^{n}\frac{|a_i - y_i|}{a_i} \quad (2)$$

In equation (2), *ai* and *yi* represent the CFD result and the estimation result of the proposed model, respectively, and n represents the number of training cases or the number of testing cases.

Because the standard deviation and MAPE of the training case (a) shown in Fig. 12 and Table 4 are sufficiently small, it is evident that the dataset has been trained appropriately. For the testing case (b), however, the error is larger than that for the training case, and there exists a problem with the generalization performance.

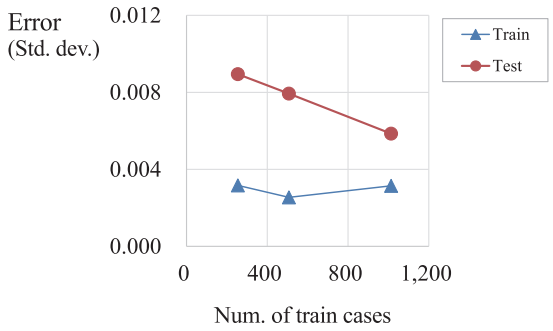

Fig.13 Error history in C_D with increase of train cases

The error trend with an increase in training cases is shown in Fig. 13. The horizontal axis represents the number of training cases, and the vertical axis represents the error (standard deviation). As the number of training cases increases, the error of the testing cases decreases. Therefore, it is considered effective to increase the number of training cases in order to improve the generalization performance.

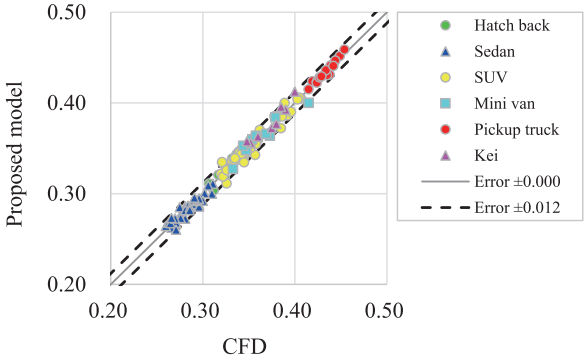

Fig.14 Comparison of coefficient of aerodynamic drag (C_D) between CFD and proposed model

The C_D values and CFD results of the test cases estimated by the proposed model are compared using a scatter plot, as shown in Fig. 14. The vertical axis represents the C_D values estimated by the proposed model, and the horizontal axis represents the values calculated using CFD. The testing case includes six car types, and the C_D values estimated by the proposed model for each car type are generally within ±0.012 of the CFD results.

In the initial phase of car development, aerodynamic evaluation is performed on multiple car design proposals; however, various car shapes have been proposed, and C_D also varies considerably more than the error of the proposed model. Therefore, in the initial phase, the proposed model can be used to evaluate the superiority or inferiority of C_D for each proposed design, and it is expected that the frequency of CFD usage and the amount of calculations can be reduced.

3.5 Estimated time required for machine learning model

The times required to predict the velocity, pressure, and C_D in Case A described above when using the proposed model are shown in Table 5 and compared with the times required when the commercial CFD software is used.

Table 5 Comparison of computational time between CFD and proposed model

Proposed model		CFD	
Distance function	11.4 min.	Mesh generation	4.0 H
Prediction of velocity, pressure and C_D	0.1 min.	Flow calculation	20.0 H
Sum.	11.5 min.	Sum.	24.0 H

In the case of CFD, approximately 24 h was required for mesh preparation and flow calculation [(1)]. This calculation time was recorded when using Intel® Xeon® (approximately 80 million meshes and 256 CPU cores). For the proposed model, a notebook PC (CPU: Intel® Core-i5™) was used to compute the distance function; this required approximately 11 minutes, whereas the predictions of the velocity, pressure, and C_D only required 3 seconds. Therefore, the proposed model is deemed useful for checking the qualitative flow field and C_D for various shape designs within a short period of time.

4. Summary and conclusion

In this study, a practical surrogate model that can predict the flow field and C_D around a car with a complicated three-dimensional shape was developed.

1 We developed a model using residual blocks, instead of the fully connected layers used in the network structure of Guo et al., to effectively avoid gradient explosion and accurately predict the flow field around the car shape.

2 It was confirmed that the flow field estimated by the proposed model could qualitatively reproduce the

CFD results.

3 The error (MAPE) in the C_D value estimated by the proposed model was 1.4%.

4 The proposed model is a useful surrogate model that can replace CFD because the flow fields and C_D values for various shape designs can be estimated within a significantly short period of time. Using the proposed model, it is expected that the resources required for aerodynamic analyses can be reduced considerably.

References

(1) K. Akasaka, et al.: Simultaneous Estimation of Aerodynamic and Thermal Performances Using CFD, Proceedings of SAE Seminar, No.96-05, pp.11–14 (2005).

(2) M. Arai, et al.: Development of the Aerodynamics of the New Nissan Murano, SAE Technical Paper, 2015-01-1542 (2015).

(3) N. Umetani, et al.: Learning Three-Dimensional Flow for Interactive Aerodynamic Design,ACM Trans. Graph., Vol. 37, No. 4, Article 89 (2018).

(4) A. Guo, et al: Convolutional Neural Networks for Steady Flow Approximation, Proceedings of the 22nd ACM SIGKDD International Conference on Knowledge Discovery and Data Mining, pp.481–490 (2016).

(5) Y. LeCun, et al.: Gradient-based learning applied to document recognition, Proceedings of the IEEE, 86(11), pp.2278–2324 (1998).

(6) K. Akasaka, et al.: Development of A Tool for Interactive Prediction of Car Drag Coefficient Using Machine Learning, at The 34th Annual Conference of the Japanese Society for Artificial Intelligence, 2O6-GS-13-02 (2020).

(7) K. He, et al: Deep residual learning for image recognition, Proceedings of the IEEE conference on computer vision and pattern recognition, pp. 770-778 (2016).

(8) Ioffe, et al.: Batch normalization: Accelerating deep network training by reducing internal covariate shift, arXiv preprint arXiv:1502.03167 (2015).

(9) Ulyanov, et al. :Instance normalization: The missing ingredient for fast stylization, arXiv preprint arXiv:1607.08022 (2016).

(10) D. Maturana, et al.: VoxNet: A 3D Convolutional Neural Network for real-time object recognition, IEEE/RSJ International Conference on Intelligent Robots and Systems (IROS), Hamburg, pp. 922-928 (2015).

(11) M. Lin, et al.: Network in network, arXiv:1312.4400 (2013).

Source

公益社団法人自動車技術会
自動車技術会論文集
Vol.52, No.3 文献番号：20214248

2022 JSAE Award The Outstanding Technical Paper Award

A Study on Pitch Characteristic to Reduce Line Trace Deviation in Small Steering Angle

Introduction

Mitsunori Tao

Specialized field : Vehicle Dynamics
Academic degree : Doctor of Informatics
Affiliated academic society : Society of Automotive Engineers of Japan
The Japan Society of Mechanical Engineers
Awards : Society of Automotive Engineers of Japan Award,
Technical Category Contribution Award (2021)

Naoya Machida

Specialized field : Vehicle Dynamics, Simulation Engineering
Academic degree : Master of Mechanical Engineering
Affiliated academic society : Society of Automotive Engineers of Japan

Yutaka Hayashi

Specialized field : Vehicle Dynamics, Simulation Engineering
Academic degree : Bachelor of Electronics
Affiliated academic society : Society of Automotive Engineers of Japan

2022 JSAE Award The Outstanding Technical Paper Award

A Study on Pitch Characteristic to Reduce Line Trace Deviation in Small Steering Angle

Mitsunori Tao* Naoya Machida** Yutaka Hayashi*** Ken Nagasao****

Abstract When driving along a straight roadway, a driver regularly makes minute steering adjustments in order to maintain the vehicle's position within the driving lane. In the research of the previous report, the quantitative relationship of several steering characteristics in this scenario was clarified for accurate line tracing. However, it was found that the deviation of the tracing line by trials was not small at the same time. This paper clarifies one of the factors of the deviation and its improvement by adding minute pitching motion to the vehicle in proportion to the steering angle.

1. Introduction

For the daily driving scenarios encountered by typical drivers, most driving is performed along straight trajectories, including operations performed for fine adjustments in the travel path with small steering angles. According to our survey conducted in Europe and Japan, steering with angles of 5° or less, which is considered as minute steering, accounts for more than half (51.1%) of all steering across all vehicle speed ranges and approximately 80% (79.6%) in zones with higher speed limits of 80 km/h or more, which is supported by some data. The traceability of a target driving line with such small steering angles is an important aspect of performance that is frequently encountered by many drivers; however, its mechanism has not been fully clarified thus far. Therefore, at actual development sites, there are many cases where the development of this ability relies on tuning an actual vehicle.

With regard to this issue, our previous paper [1] clarified the quantitative relationships between the steering force and yaw characteristics with respect to line traceability; this was achieved by quantitatively determining the dead zone of the driver in the minute steering angle range and the dead band of the yaw characteristics of the vehicle and then analyzing the relationship between the evaluated line traceability defined in the study and the two dead zones. However, a new issue was also observed: the line trace deviations of the drivers varied considerably between trials.

In this study, considering that one of the causes of this variation in the line tracing deviations originates from the steering mechanism of the driver within the minute steering angle range, it was hypothesized that the variations can be reduced by adding a certain amount of pitch motion to the steering angle in order to reduce variations. This hypothesis was verified using a driving simulator, and the quantitative effect of the variation reduction was extracted. Following our previous work, which clarified the vehicle characteristics that enable drivers to drive accurately, on average, along a target driving line, this research focused on the vehicle characteristics that enable accurate driving with little variations between trials.

To explain this research, an outline of our previous work and the variation in the line trace deviations, which is the subject of the present study, is first provided. Next, the driver steering mechanism, which is considered to cause variations in the minute steering angle range and also defined as a hypothesis in the previous work, will be described; the reasons for choosing the pitch as the vehicle behavior to be added to reduce variations are also explained. Subsequently, the quantitative pitch characteristics that can reduce the variation in the line trace deviations based on the driver sensitivity characteristics (related to the pitch motion obtained from experiments) are hypothesized, and the results of the experimental verification are reported.

In this study, two experiments were conducted with 25 male drivers in their 20s and 50s who drove their cars on a daily basis. The tests were examined and approved by the Experimentation Ethics Committee of Nissan Motor Co., Ltd., and informed consent was obtained from the test participants.

2. Outline of and issues in our previous study

In our previous study, an evaluation course was established, consisting of an R1200 curve and its

*Nissan Research Center Mobility & AI Laboratory **Powertrain and EV Performance Engineering Department
***Customer Performance and Test Engineering Methodology Innovation Department ****Vehicle Performance Engineering Department

relaxation section; this required a steering input of approximately 5° from a straight line at a constant speed of 80 km/h, as shown in Fig. 1, and the drivers drove along the course with the target line. The actual deviations in the travel trajectories during driving were defined as "line trace deviations," whose mechanism was clarified.

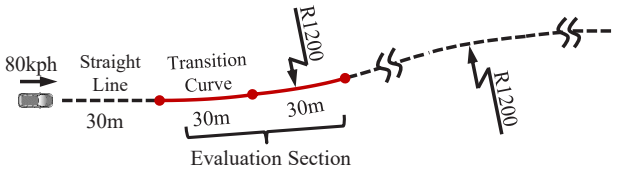

Fig.1 Evaluation Course

As shown in Fig. 2, the line trace deviations can be accurately indicated using two types of characteristics: the steering reaction force characteristics, which are highly sensitive to the minimum steering angle that the driver recognizes as "steering input to the vehicle," and the "yaw-rate dead band" characteristic (shown in Figs. 3 and 4), which is highly sensitive to the steering angle generating the minimum yaw rate of 0.21°/s that enables the driver to sense that "the vehicle has moved." This was clarified through the driver–vehicle model hypothesis and the simulator-based verification conducted by the evaluators. The verification results are shown in Fig. 5. For the specifications at the front of the graph, indicating significant steering forces and large yaw-rate dead bands, the line trace deviation is negative, causing the vehicle to move outward with respect to the target line. Conversely, under the specifications for weak forces and small dead zones, the vehicle moves inward. Therefore, the target line can be traced accurately by setting the steering force and dead band along the thick broken line.

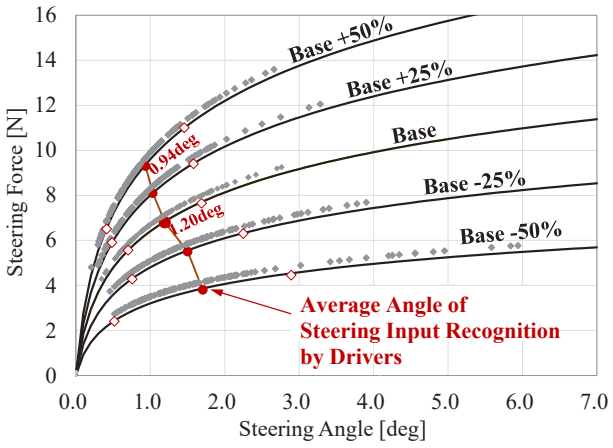

Fig.2 Steering Force & Driver's Input Recognition Angle

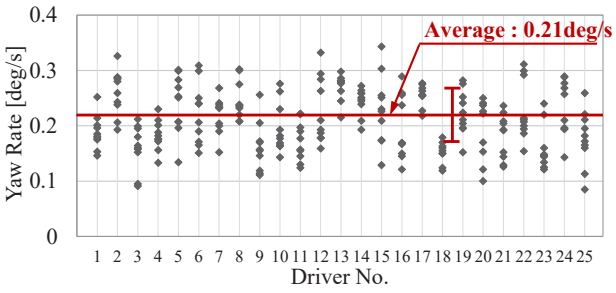

Fig.3 Driver's Yaw-Rate Sensitivity Experimental Result

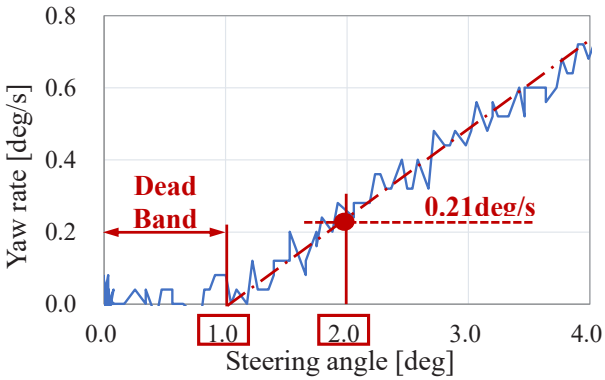

Fig.4 Yaw-Rate Characteristic in Small Steering Angle

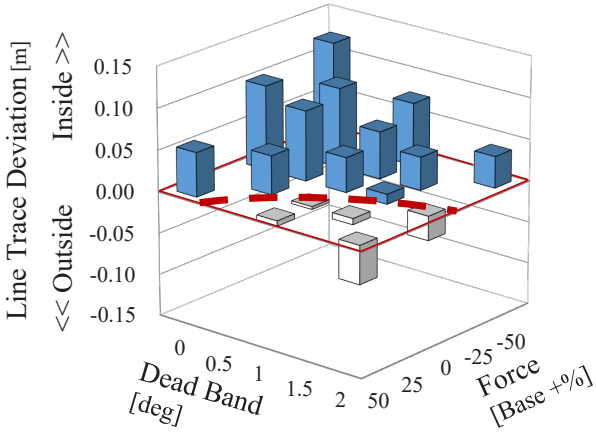

Fig.5 Experimental Result of Line Trace Deviation

However, as a new issue, it was confirmed that the line trace deviations varied considerably between the trials performed by individual drivers. The line trace deviations for a certain driver across six trials under the specifications of a steering reaction force of +25% and a yaw-rate dead band of 1°, which allow the average of the line trace deviations of 25 drivers to be almost zero, are shown in Fig. 6. On average, they appear to coincide with the thick, dashed target line; however, certain variations exist.

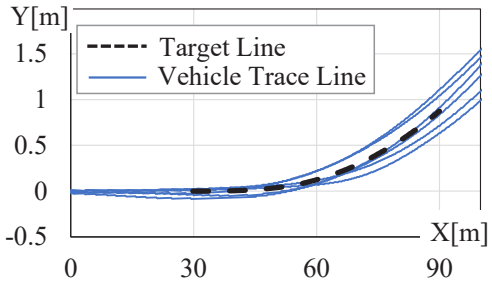

Fig.6 Line Trace Deviation by a Driver

The variations in the line trace deviations of 25 drivers based on their respective standard deviations under the same specifications are depicted in Fig. 7, with the average value of 0.047 m. This average is not sufficiently small, even compared with the fluctuation in the line trace deviations under the different specifications defined for the average value of all the trials by all the drivers, as shown in Fig. 5.

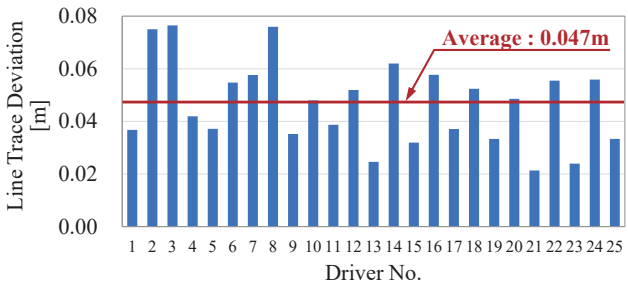

Fig.7 Average of Line Trace Deviation by 25 Drivers

Following our previous work, which clarified the vehicle characteristics that enable drivers to drive accurately, on average, along a target driving line, this research focused on the vehicle characteristics that enable accurate driving with little variations between trials.

3. Causes of variation in line trace deviations and reduction measures

3.1 Steering mechanism for minute steering angles and variation in line trace deviations

Various factors can be considered as the causes of the variation in the line trace deviations for each trial of a driver, such as differences in the line of sight, how the steering wheel is held, or the degree of concentration when driving. This work focused on the steering mechanisms of the drivers with minute steering angles, as hypothesized in the previous work, and conducted a detailed analysis.

As shown in Fig. 8, when steering from straight running toward the target line, the driver first recognizes that the steering input to the vehicle is commenced at a steering angle of approximately 1° based on the steering reaction force information. Therefore, by setting a dead band in the yaw rate such that the vehicle can initiate the yaw movement simultaneously, the vehicle movement that matches the feeling of the driver can be realized. As a result, on an average, the line trace deviations are reduced. However, the driver can only sense the movement due to this yaw rate as visual information when the value exceeds 0.21°/s and the steering angle reaches approximately 2°. In other words, in the section where the steering angle is 1°–2°, it can be considered that the driver is performing blind steering without obtaining feedback regarding vehicle movement in the visual sense and relying solely on the information from the steering reaction force.

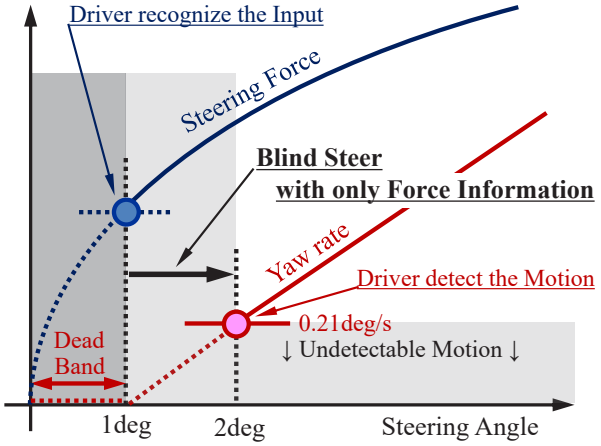

Fig.8 Driver's Steering Process in Small Steering Angle

It is clear that visual feedback is one of the most important types of information for stable and accurate driving, and it is conceivable that even a small steering angle range, such as 1°–2°, has an unexpectedly large influence on stable and accurate driving. In particular, with regard to the line traceability at minute steering angles of less than 5°, as in this case, the effect is considerably large and likely one of the major factors in the variation of the line trace deviations.

Therefore, visual information is fed back to the driver, indicating that the vehicle begins to move in the yaw direction at a steering angle of approximately 1°, which the driver can recognize as a steering input. When movement increases with the steering angle, the driver will be able to steer in a more accurate and stable manner; consequently, variations in the line trace deviations will be reduced.

3.2 Vehicle behaviors for providing visual information to drivers

As mentioned earlier, the yaw movement itself does not enable the driver to sense that the vehicle responds to the steering and begins to move in the yaw direction; this is because a yaw rate of 0.21°/s or higher is required for the driver to detect movement in the yaw direction. By contrast, if a higher yaw rate threshold for the driver to sense vehicle start movement is set, the yaw-direction movement of the vehicle may become excessive and the vehicle will not travel accurately along the originally

targeted driving line.

In this study, based on the vehicle movements in the six translational and rotational motion directions, the movement to convey to the driver as visual information on behalf of the yaw movement of the vehicle that the vehicle is responding immediately after the start of the yaw movement was examined. First, the roll, pitch, and bounce motions were selected as candidates, excluding the plane motions in the front–back and left–right directions, which directly affect the travel trace of the vehicle, such as the yaw-direction motion. Subsequently, referring to previous studies [2] where human sensitivity was investigated, the motion in the pitch direction, to which it was reported that humans have the same high visual sensitivity as the yaw-direction motion, was finally selected.

In previous literature [3), 4)], it was reported that the feeling of steering, or the equivalent characteristics, could be improved by imparting a downward pitch to the vehicle during steering, as compared to the cases where no pitch motion was provided or an upward pitch was provided. Therefore, in this study, downward pitch motion was imparted to the vehicle during steering.

4. Hypothesis for reducing variations in line trace deviations using vehicle pitch motion

4.1 Experiments on driver sensitivity to pitch motion

To determine the minimum pitch motion that a driver can detect, a sensitivity experiment was conducted using a driving simulator. The experimental setup is depicted in Fig. 9. When a constant downward pitch was provided to the vehicle, the drivers were instructed to gaze at the front view of the screen and to press the switch at hand the moment they sensed the pitch movement. A total of eight experiments with different pitch rates, ranging from an extremely low pitch rate of 0.0125°/s to a relatively high pitch rate of 0.3°/s, were conducted five times each, and the pitch angles sensed by the drivers were recorded for each trial.

Fig.9 Pitch Sensitivity Experimental Scene

The measurement results are presented in Fig. 10. The experimentally specified pitch rates (eight specifications) are provided on the horizontal axis, whereas the pitch angles sensed by the driver at each pitch rate are denoted on the vertical axis. The measurement data obtained from the 25 experimental evaluators (drivers) are indicated by the dots, and the average values are connected by the solid line. For the highest pitch rate of 0.3°/s, the results of the push-button switch operation and the evaluation comments confirmed that all the drivers could feel the pitch movement as soon as it was initiated; therefore, the data in Fig. 10 can be considered as the operational time differences of the drivers between the moment at which the pitch rate of 0.3°/s was generated and the time at which the button was pressed by the individual drivers. The average value (0.51 s) of the operation times for all the drivers was subtracted from all the experimental data for correction.

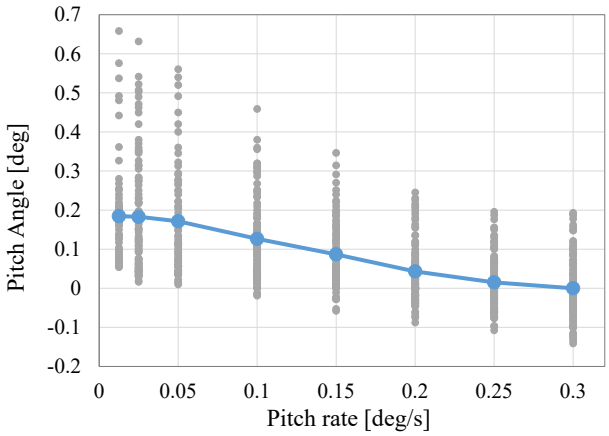

Fig.10 Driver's Sensitivity for Pitch Motion

At low angular velocities with pitch rates of 0.05°/s or less, all the drivers sensed the movement at a pitch angle of 0.15°–0.2° (refer to the left side of the graph); the drivers could not sense pitch rates lower than 0.05°/s and the movement was detected for the first time by the size of the integrated pitch angle. By contrast, at a high pitch rate of 0.3°/s, the drivers sensed the movement with almost no pitch angle (see the right side of the graph), which is likely because the drivers could detect the speed at this pitch rate, as described above. The central region between these two regions is considered as the section where the drivers could sense the pitch rate and the pitch angle as a whole; hence, the sensitivity graph presents a downward-sloping line connecting the two regions. Next, using this sensitivity line, the pitch motion that enables drivers to sense the initiation of yaw motion was hypothesized.

4.2 Hypothesis of pitch characteristics to reduce variation in line trace deviations

The pitch characteristics were hypothesized based on the pitch motion required for drivers to recognize a steering input and sense the vehicle response near a steering angle of 1° (at which the yaw motion commences and increases). Although various generated pitch motion patterns can be considered, such as steering angle proportionality, steering wheel angle rate proportionality, and the addition of non-linearity to each, this study aimed to verify the mechanism in the simplest possible manner and selected the pitch angle (downward) proportional to the steering angle, shown in Fig. 11, to formulate a hypothesis of the required proportionality constant. In addition, the experimental results of our

previous research confirmed that drivers steer at an angular velocity of approximately 3°/s in the target scene; hence, this steering wheel angle rate was added to the prerequisites.

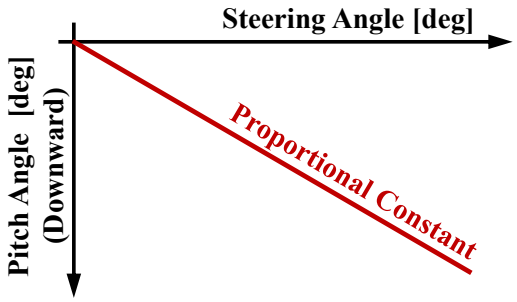

Fig.11 Pitch Characteristics for Driver's Information

$$\theta_{pitch} = K \times \theta_{steer} \qquad (1)$$

$$\dot{\theta}_{pitch} = K \times \dot{\theta}_{steer} = 3K \qquad (2)$$

θ_{pitch} : Pitch Angle (Downward) [deg]
θ_{steer} : Steering Wheel Angle [deg]
K : Proportional Constant
$\dot{\theta}_{pitch}$: Pitch Angle Rate (Downward) [deg/s]
$\dot{\theta}_{steer}$: Steering Wheel Angle Rate [deg/s]

Based on the driver sensitivity line for the pitch motion (Fig. 10), obtained through the experiment, and the pitch characteristics during steering, defined in equations (1) and (2), the proportionality constant K, which enables drivers to sense the pitch motion at a steering angle of 1°, was obtained. A graph of the pitch rates and pitch angles generated at a steering angle of 1° when K was changed from 0 to 0.08 in 0.02 increments, with respect to the driver sensitivity line for the pitch motion, is shown in Fig. 12.

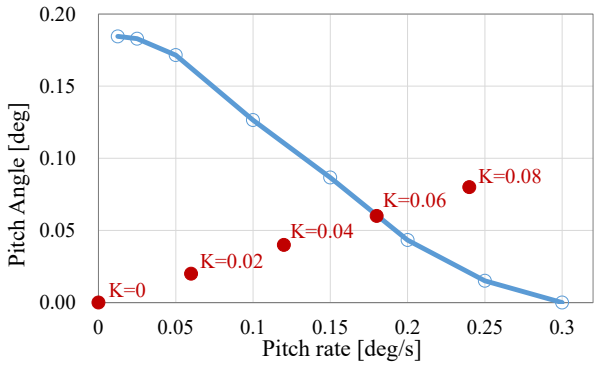

Fig.12 Pitch Motion by each "K" at Steering Angle 1deg

When K is 0.04 or less, the pitch motion generated at the steering angle of 1° does not reach the driver sensitivity line, indicating that this setting does not enable the driver to sense the pitch motion at a steering angle of 1°. However, when K = 0.08, the pitch motion has already considerably exceeded the driver sensitivity line at a steering angle of 1°; thus, it is considered that the driver can sense the motion before the steering angle reaches 1°. When K = 0.06, the pitch motion almost falls on the driver sensitivity line. In other words, this value of K enables the driver to sense the pitch motion at a steering angle of 1°.

$$\theta_{pitch} = 0.06 \times \theta_{steer} \qquad (3)$$

As shown in equation (3), which uses the pitch angle and steering angle, the visual information (pitch motion) enables the driver to recognize a steering input and sense the vehicle response near a steering angle of 1° (at which the yaw motion of the vehicle commences and increases). Therefore, it is assumed that the variation in the steering angles and the line trace deviations can be reduced by adding visual feedback in the minute steering angle range, wherein the drivers were deemed to have performed blind steering. The abovementioned hypothesis was verified as discussed in the following section.

5. Verification of hypothesis

The hypothesis was verified using the model of a certain C-segment vehicle and the driving simulator that reproduced the evaluation course shown in Fig. 1, as in our previous research. The outline, method, and results of the experiment are as follows.

5.1. Overview of vehicle model and simulator used in experiments

The main parameters of the vehicle model used in the experiment are listed in Table 1.

Table 1 Vehicle Model Parameter

Parameter	unit	Value
Vehicle Mass	kg	1670
Vehicle Yaw Inertia	kgm^2	2600
Vehicle Pitch Inertia	kgm^2	2300
Height of C.G.	m	535
Front axle～C.G.	m	1.08
Rear axle～C.G.	m	1.62
Front Cornering Power	kN/rad	62.5
Rear Cornering Power	kN/rad	95.5
Steering Gear Ratio	-	15.0

An external view of the driving simulator used in the experiment is provided in Fig. 13. This simulator is equipped with a cabin with a hexapod mounted on slide rails (motion range of 22 × 6 m) and 64 linear motors that drive the hexapod with high precision; thus, this simulator can reproduce the actual vehicle motions under many scenarios. [5)]

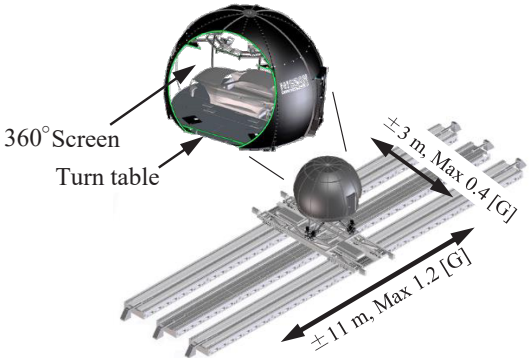

Fig.13 Driving Simulator

Next, the accuracy of this simulator was verified as follows. The actual data measured using the C-segment vehicle and simulator for the dependence of the steering force and yaw rate on the steering angle are presented in Fig. 14; notably, both exhibit high reproducibility.

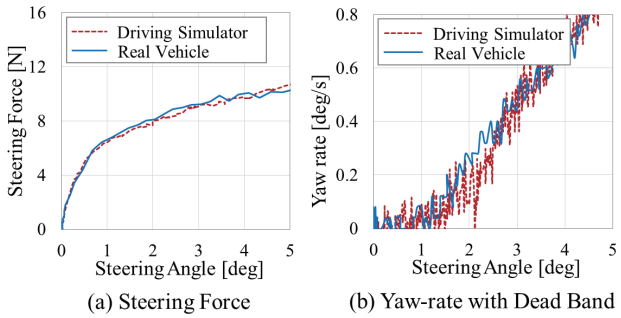

Fig.14 Driving Simulator Accuracy Confirmation

5.2 Experimental method

The experiment was conducted using the same 25 drivers as in the pitch rate sensitivity experiment. The vehicle speed was fixed to 80 km/h, and the drivers were instructed to operate the steering wheel to solely drive the vehicle along the center of the lane. With regard to the experimental specifications, the yaw-rate dead band and steering reaction force were set to 1° and the standard +25%, respectively, which afforded the smallest average value (almost zero) of the line trace deviations for all trials in our previous research. Furthermore, K of the pitch angle to the steering angle was changed five steps from 0 to 0.08 in increments of 0.02. For each step, the experiments were conducted by performing a total of 30 randomly arranged trials, with three right steering and three left steering experiments. The steering angle and the line trace deviations were measured.

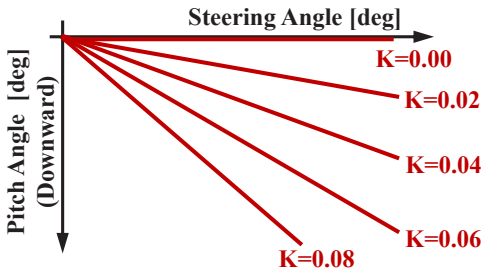

Fig.15 Pitch Characteristics

5.3 Experimental results

The measured line trace deviations for a certain driver with respect to different values of K of the pitch are presented in Fig. 16. The right-turn data were mirror-compensated in the left-turn direction. The variation in the line trace deviation from the target line decreases as K increases. In addition, the numerical values in each graph, which represent the calculated line trace deviations, quantitatively confirm the tendency of the variations.

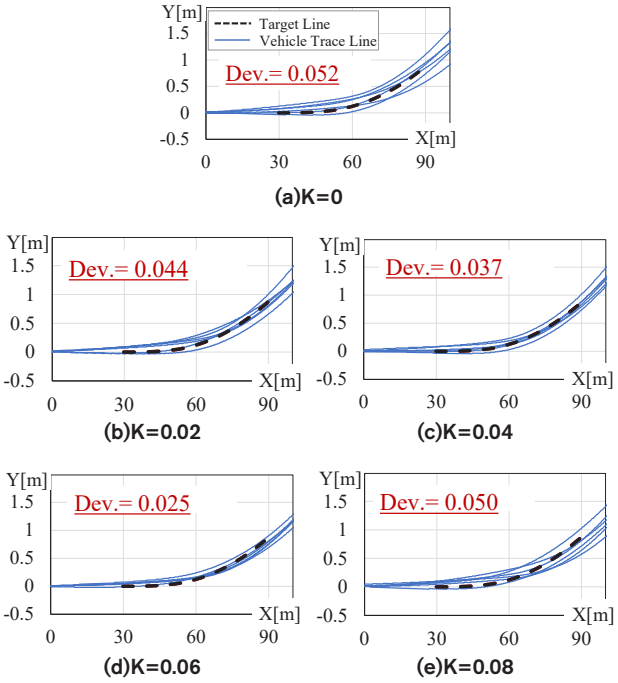

Fig.16 Line Trace Experimental Result

The variations in the line trace deviations under different pitch specifications, calculated from the measurement results of the travel trajectories of 25 drivers, are depicted in Fig. 17, with the horizontal axis representing K. It is evident that the variation in the line trace deviations tends to decrease as K increases. The thick solid line, which connects the average values obtained under the different specifications, indicates that the deviation is the smallest at K = 0.06 and then increases again at K = 0.08. Thus, the hypothesis established in this study was verified. Further, when K =

0.06 was added, the variation in the line trace deviations could be reduced by approximately 33%, as compared to that in the case where no pitch motion was added.

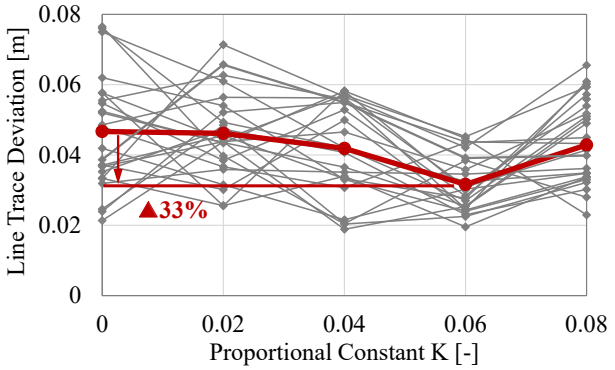

Fig.17 Line Trace Deviation Experimental Result

Subsequently, the change in the line trace deviation with increasing K was evaluated. There was no significant difference between the deviations for K = 0 and K = 0.02, because K = 0 does not generate any pitch motion; furthermore, even when K = 0.02, the driver cannot detect the movement before the steering angle reaches approximately 3° and the yaw movement is near 2°. Hence, it is likely that no visual information was provided within the blind steering section of 1°–2°. Similarly, when K = 0.04, the driver can detect the pitch movement at a steering angle of approximately 1.5°; therefore, even if it is not possible to completely cover the blind section, as in the case of K = 0.06, it is possible to provide visual information to the driver for approximately half of this section, thereby reducing the variation to a certain extent. However, when K = 0.08, it is conceivable that the pitch motion was detected by the driver before the steering angle reached approximately 1°. Generally, when the driver recognized the steering input and the vehicle actually commenced the yaw movement, there was an increase in the variation, as compared to that in the case of K = 0.06; this was attributed to the additional visual information that hindered accurate operation by the driver.

Finally, the effect of pitch motion on the average value of the line trace deviations was studied. In this study, the purpose of adding the pitch motion was to reduce the variation in the line trace deviations by providing drivers with visual information regarding the pitch motion, in addition to the steering reaction force information, on which drivers relied at the start of vehicle movement. Therefore, it is considered that the pitch motion required for this purpose does not affect the average value of the line trace deviations. The average values of the line trace deviations for the 25 drivers who participated in this study are shown in Fig. 18. It is confirmed that the addition of the pitch motion does not significantly alter the values.

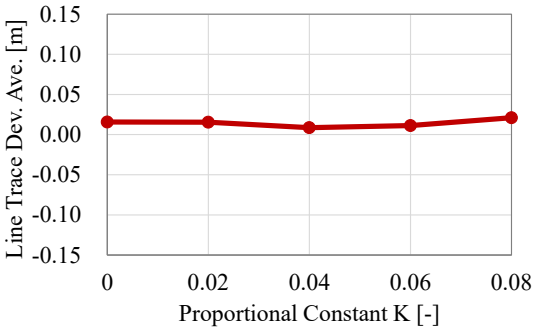

Fig.18 Line Trace Deviation Average Experimental Result

6. Summary and conclusion

Considering that one of the causes of the variation in the line trace deviations originates from the blind steering section in the minute steering angle range, it was confirmed that this variation can be reduced by adding a certain amount of pitch motion as visual information within the blind steering section.

Based on investigations of driver sensitivity to the pitch motion, the appropriate amount of pitch motion to be added was hypothesized and experimentally verified, and the quantitative effect of reducing the variation in the line trace deviations was extracted. In addition to the vehicle characteristics that enable drivers to drive appropriately, on average, in the minute steering angle range, which were clarified in our previous research, the other characteristics necessary for accurate driving were identified.

References

(1) Mitsunori Tao et al., “A Clarification of Relationship of Steering Force and Yaw Characteristics to Line Traceability in Small Steering Angle”, Transactions of the Society of Automotive Engineers of Japan Vol.51 No.3 pp.428-433 (2020)
(2) Katsuhiko Fukui et al., “Technology for Improving Roll Feeling Based on Visual Characteristics”, Transactions of the Society of Automotive Engineers of Japan Vol.40 No.5 pp.1185-1190 (2009)
(3) Hideki Sakai et al., “Damping Force Control That Emphasizes Transient Turning Sensation”, Transactions of the Society of Automotive Engineers of Japan Vol.43 No.3 pp.709-716 (2012)
(4) Makoto Yamakado, “Study on 3-Dimensional Ideal Body Behavior by EV's Precise Braking and Driving Force Control”, Journal of the Japan Society of Precision Engineering Vol.84 No.9 pp.765-768 (2018)
(5) Masayuki Imamura et al., “Development of High-Performance Driving Simulator”, Nissan Technical Review (Dynamic Performance Technology) No.83 pp.60-65 (2018)

Source

公益社団法人自動車技術会
自動車技術会論文集
Vol.52, No.2 文献番号：20214137

The 28th International Display Workshops (IDW) Best Paper Award (2021)

Optically Switchable Transparent Liquid Crystal Display

Introduction

Yoshimi Ohta

Specialized field : Display, Optical Engineering
Academic degree : Master of Engineering
Affiliated academic society : Society of Automotive Engineers of Japan
The Japanese Liquid Crystal Society

Shunta Nabetani

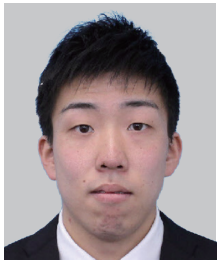

Specialized field : Display, Photochemistry
Academic degree : Master of Engineering
Affiliated academic society : The Japanese Liquid Crystal Society
The Japan Society of Applied Physics

Maki Kamikubo

Specialized field : Organic Photochemistry, Catalytic Chemistry
Academic degree : Bachelor of Science
Affiliated academic society : The Japanese Photochemistry Association
Awards : Japan Institute of Invention and Innovation National Commendation for Invention Invention Award(2006)

Tomoya Ohara

Specialized field : Organic Photochemistry, Heat Transfer Engineering
Academic degree : Master of Engineering
Affiliated academic society : Society of Automotive Engineers of Japan

Ryota Maehashi

Specialized field : Display, Optical Engineering
Academic degree : Master of Engineering

Fuminori Sato

Specialized field : Semiconductor Device, Display, Electrochemistry
Academic degree : Bachelor of Engineering
Affiliated academic society : Society of Automotive Engineers of Japan
The Institute of Electrical Engineers of Japan

Technical Awards : The 28th International Display Workshops(IDW) Best Paper Award (2021)

Optically Switchable Transparent Liquid Crystal Display

Yoshimi Ohta* Shunta Nabetani* Maki Kamikubo*
Tomoya Ohara* Ryota Maehashi* Fuminori Sato*

Abstract We demonstrated a new transparent display consisting of an optically switchable polymer network liquid crystal and light sources. Optical switching between transparent and screen states was achieved through trans-cis photoisomerization of azobenzene. Furthermore, we improved screen reflectance by increasing the helical twisting power difference between the trans and cis states.

1. Introduction

Recently, transparent displays have been actively developed for applications in signage windows of stores and automotive windows. Transparent displays are required to meet demands such as large sizes, good flexibility, high transparency, cost-effectiveness, and high contrast.

Organic light-emitting diode (OLED) displays [1] are a type of transparent display. OLED displays can be large and offer advantages in terms of image quality, such as a large viewing angle, superior color gamut, and high resolution. However, OLED transmittance is low due to the several thin-film transistors (TFTs) and capacitors in each pixel.

Transparent liquid crystal displays (LCDs) are another type of transparent display. Polymer-dispersed liquid crystal (PDLC) displays with TFTs [2, 3] can achieve a high transmittance of > 80% in the transparent state, on account of the high aperture ratio of each pixel. When flexible displays with TFTs, such as OLED displays and LCDs, are mounted on a curved surface, such as automotive windows, they are required to be flexible. Transparent polyimide (PI) films are typically used to fabricate TFTs on the substrate surfaces. To date, the demand for transparent PI films is limited only to high-end optoelectronic products, and they are not economical [4].

However, transparent PDLC and polymer-network liquid crystal (PNLC) displays using affordable polyethylene terephthalate (PET) films coated with indium tin oxide (ITO) are commercially available. A transparent display using the combination of a projector with PDLCs or PNLCs was proposed [5, 6]. However, the area to be controlled from transparent to screen state by applying voltage was limited, depending on the ITO coating. Therefore, when mounted in the entire area of a car windshield, there was an issue of blocking the driver's view in the screen state.

Optical switching of liquid crystals (LCs) doped with chiral azobenzene compounds were proposed as an alternative to electrical switching [7, 8]. It was considered to possess high transparency, flexibility, and screen area control. A compensated and transparent nematic phase LC was formed by mixing a chiral azobenzene with a non-photochromic chiral compound having opposite chirality in the host nematic LC by balancing the helical twisting powers (HTPs) of both chiral compounds. The HTP of the chiral azobenzene compounds was decreased using ultraviolet (UV) irradiation to induce their trans-cis photoisomerization and consequently transform the compensated nematic LC into a cholesteric phase. Resultantly, the optically switching LC film changed from its transparent state to light scattering screen state. The transmittance was restored using visible light (Vis) irradiation. As the difference in HTP (ΔHTP) between the trans and cis states of the chiral azobenzene increased, the specular transmittance changed significantly. However, reflectance has not been investigated.

In this paper, we describe the improvement of the optical performance of optically switchable reverse-mode PNLCs by increasing the ΔHTP of azobenzene and present a front-projection transparent LCD.

2. Principle of optical switching in transparent LCD

2.1 System set-up

Fig. 1 depicts the system layout of the optically switchable transparent LCD. It is composed of an optically switchable reverse-mode PNLC, a Vis projector,

*Advanced Materials and Processing Laboratory

a UV LED, and a blue LED. Typically, a PNLC is transparent; upon irradiation with UV light, its irradiated area converts from the transparent state to the screen state. The Vis projector stops the UV irradiation and projects images on the screen area in front of the viewer. Subsequently, blue light irradiation reverts the PNLC to its initial transparent state.

2.2 Structure of optically switchable reverse-mode PNLC

The optically switchable reverse-mode PNLC is a composite of an LC, polymer network, chiral azobenzene, and non-photochromic chiral compounds. The polymer network consists of reactive mesogen (RM) monomers. It is phase-separated from the LC and has a strong aligning effect on the LC. When the HTP of chiral azobenzene in the trans state without UV irradiation is equal to that of the non-photochromic chiral compound having opposite chirality, the LC is in a compensated and transparent nematic phase. The PNLC composite was sandwiched between two glass substrates covered with ITO and a vertically aligned PI layer. Before the application of UV light, the LC and polymer network are aligned vertically, resulting in the transparent state, as shown in Fig. 2(a).

Upon UV irradiation, the chiral azobenzene transforms from the trans state to cis state by photoisomerization, thus disrupting the balance of the chirality and generating a twisting power in the LC. Consequently, the orientation of the LC is disordered, and it becomes a light-scattering screen, as shown in Fig. 2(b).

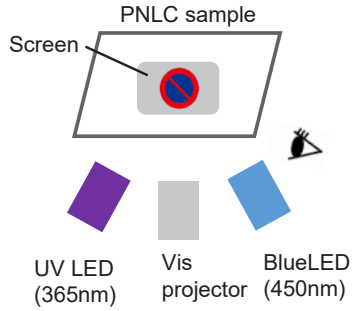

Fig.1 System layout of optically switchable transparent LCD

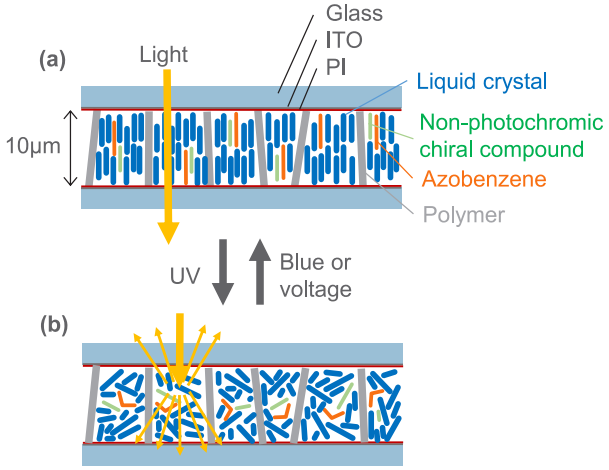

Fig.2 Schematic diagram of optically switchable reverse-mode PNLC in (a) transparent state and (b) screen state

3. Experimental

Fig. 3 presents the materials used in this experiment. Chiral azobenzene (Azo-A and Azo-B) and a non-photochromic chiral compound (Chiral) were synthesized, and their HTPs are presented in Table 1. The ΔHTP of Azo-A with axial chirality of binaphthyl moiety[9] is stronger than that of Azo-B with point chirality. We prepared two LC mixtures using Azo-A and Azo-B to investigate the effects of their ΔHTP. Table 2 lists the composition of each material. In this study, we used a positive nematic LC, Sb-826010 (Shanben. Co., Ltd), which has birefringence of Δn = 0.26 . RM, 4,4'-bis(6-(acryloyloxy)-hexyloxy)biphenyl (Tokyo Chemical Industry Co., Ltd.), and photo-initiator, Iragcure819 (Ciba Specialty Chemicals Inc.). Compensated and transparent samples were prepared by mixing the chiral azobenzene and Chiral, according to the measured HTP values listed in Table 1.

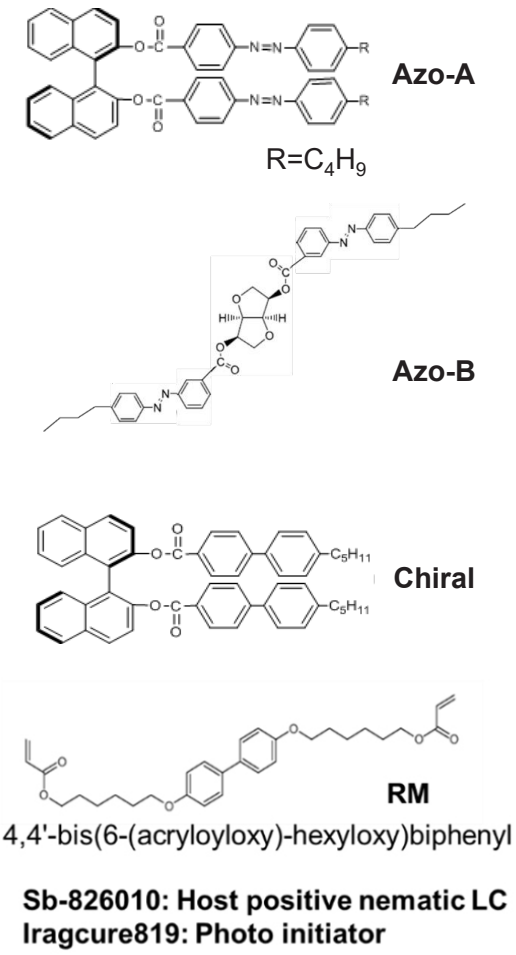

Fig.3 Material structures

Table 1 HTP of chiral materials

	HTP (μm)		ΔHTP (μm)
	trans	cis	
Azo-A	76	37	29
Azo-B	20	3	17
Chiral	60		-

Table 2 Material composition (wt.%)

No	Azobenzene	Chiral	LC	RM	Photo initiator
1	Azo-A: 5.1	2.9	83.75	7.5	0.75
2	Azo-B: 6.2	1.8	83.75	7.5	0.75

Empty glass cells (EHC. Co., Ltd) with a cell gap of 10 μm were prepared by assembling two ITO glass substrates treated with vertically aligned PI layers. Each LC mixture was injected into the empty glass cells using the capillary force on a hot plate at 100°C, which is equal to the LC clearing point. The cells were cured by exposure to blue light from an LED (λmax = 450 nm), under 50 V–50 Hz at room temperature, to align the LC orientation. The power of the blue light was 7 mW/cm^2. After 10 min of curing, the optically switchable reverse-mode PNLC was prepared in the transparent state without the application of voltage.

To investigate the optical properties of the PNLC, its total transmittance spectra in the transparent state and total reflectance spectra in the screen state were measured using a spectrometer with an integrating sphere (U-4000, Hitachi, Ltd). Each haze was measured using a haze meter (HM-65 W, Murakami Color Research Laboratory).

4. Results and discussion

Fig. 4(a) demonstrates the total transmittance of the PNLC samples in the transparent state. Transmittance spectra were as high as approximately 80% over a wide visible range. In the region less than 500 nm, the transmittance decreased due to the absorption of the azobenzene itself. Fig. 4(b) depicts the total reflectance of the PNLC samples in the screen state after sufficient UV irradiation at 20 mW/cm^2 for 60 s at room temperature. The PNLC samples were sufficiently screened using this UV energy until the optical properties stopped fluctuating. The reflectance of No.1 sample with Azo-A was higher than that of No. 2 sample with Azo-B. The optical properties in terms of haze values are summarized in Table 3. From Table 2, it is evident that the ΔHTP of azobenzene influenced the reflectance and haze of the PNLC in the screen state. As ΔHTP increased, the orientation of the LC was disturbed more significantly, resulting in greater reflectance and haze in the screen state.

Fig. 5 depicts the dependence of luminance on the viewing angle. In the screen state of sample No.1 after UV irradiation, a white image was projected using the Vis projector (MW612, BenQ Corporation) under the illuminance of 3350 lx, and we measured the luminance excluding the background light using a luminance meter (LS-110, Minolta Co., Ltd) for different viewing angles. The light scattering effect indicated that images could be seen at a viewing angle of 60°.

The photographs in Fig. 6 present sample No. 1 in each state. The sample was 10 × 10 cm in size. In the transparent state, it was as transparent as the glass. Following UV irradiation, a screen appeared in the irradiated area. After turning off the UV LED, we could see the images projected from the front projector. When the projection was stopped and blue light irradiation was applied, the sample reverted to the transparent state.

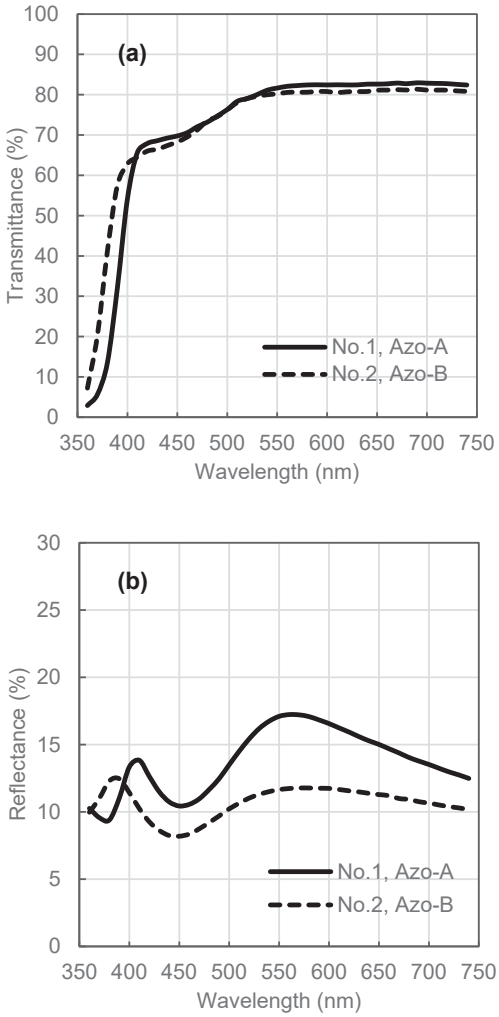

Fig.4 Optical properties of PNLC samples. (a) Total transmittance spectra in the transparent state before UV irradiation, and (b) total reflectance spectra in the screen state after UV irradiation.

Table 3 Optical properties

	Transparent state	Screen state
	Transmittance @550 nm/Haze	Reflectance @550 nm/Haze
No.1	81.6% / 2.3%	17.1% / 94.9%
No.2	80.2% / 2.3%	11.7% / 39.3%

5. Conclusions

We demonstrated a new transparent display consisting of an optically switchable reverse-mode PNLC (of size 10 cm × 10 cm), a Vis projector, a UV LED, and a blue LED. Optical switching between the transparent state and the screen state of the PNLC was achieved through the reversible trans-cis photoisomerization of chiral azobenzene molecules under UV and blue light irradiation. A low-haze transparent state and a higher reflecting screen state of the PNLC were achieved at a high ΔHTP of chiral azobenzene. We confirmed that the projected images on the screen could be seen at a viewing angle of 60° due to the light scattering by the screen. We expect that this PNLC can be made flexible and large in size by utilizing PET films instead of glass substrates. This display can be used not only for signage but also for curved car windows.

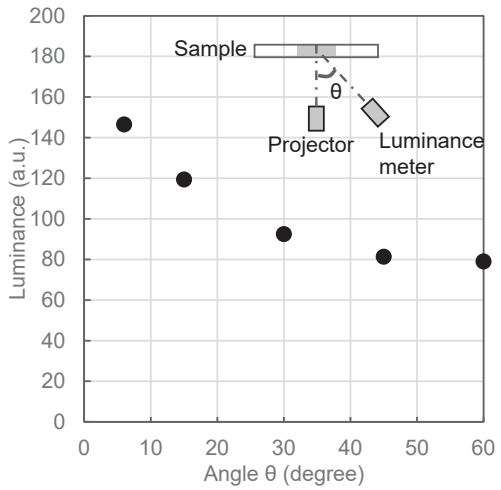

Fig.5 Viewing angle property in the screen state of sample No. 1 with Azo-A under the illuminance of 3350 lx.

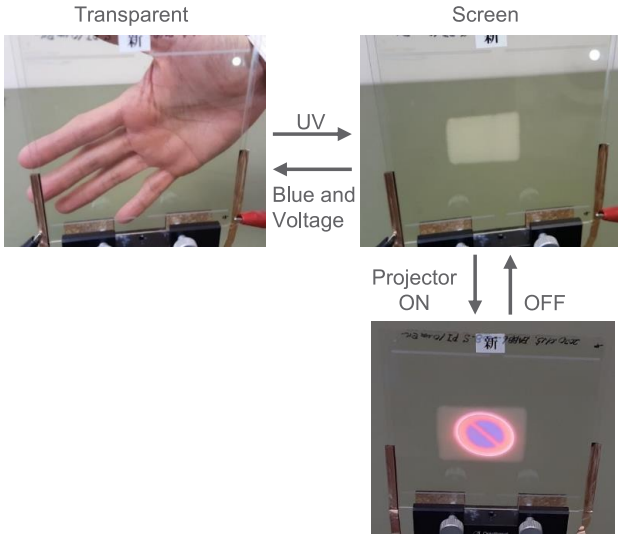

Fig.6 Photographs of optically switchable transparent liquid crystal display of 10 cm x 10 cm sample No. 1. Image is projected from the front projector after UV irradiation.

Acknowledgement

This research was partly supported by the Adaptable and Seamless Technology Transfer Program through Target-driven R&D (A-STEP) from the Japan Science and Technology Agency (JST).

References

[1] C. Park, M. Seong, M. A. Kim, D. Kim, H. Jung, M. Cho, S. H. Lee, H. Lee, S. Min, J. Kim, M. Kim, J. H. Park, S. Kwon, B. Kim, S. J. Kim, W. Park, J. Y. Yang, S. Yoon and I. Kang "54-1: Distinguished Paper: World 1st Large Size 77-inch Transparent Flexible OLED Display." SID. Vol. 49, No. 1, pp. 710-713, (2018).

[2] K. Okuyama, Y. Omori, M. Miyao, K. Kitamura, M. Zako, Y. Maruoka, K. Akutsu, H. Sugiyama, Y. Oue, T. Nakamura, K. Ichihara, H. Irie, S Ito, K Hirama, N Asano, T Imai, D Takano and S. Ishida, "12.3-in Highly Transparent LCD by Scattering Mode with Direct Edge Light and Field-Sequential Color-Driving Method" SID 2021 DIGEST, pp. 519-522 (2021).

[3] M. Honda, K. Murata, K. Nakamura, T. Hasegawa, Y. Haseba, K. Hanaoka, S. Shimada, "Transparent Display with High-Contrast-Ratio Reverse-Mode PDLC," SID 2021 DIGEST, pp. 535-538 (2021).

[4] H. Ni, J. Liu, Z. Wang, S. Yang, "A review on colorless and optically transparent polyimide films: Chemistry, process and engineering applications," Journal of Industrial and Engineering Chemistry, 28, pp16–27, (2015).

[5] T. Higuchi, T. Yoshikawa, K. Hashikawa, M. Akagi, T. Yoshizawa, K. Iwawaki, Y. Ito, H. Kogoma, N. Saegusa, "See-Through Projection System" Proc. IDW '15, pp. 820-821 (2015).

[6] S. Ho, N. Oh, and S. Kwon, "Electro-optical properties of vertically aligned polymer network liquid crystals for normally transparent light shutters." Molecular Crystals and Liquid Crystals 644.1, pp. 130-136 (2017).

[7] S. Kurihara, S. Nomiyama, T. Nonaka, "Photochemical switching between a compensated nematic phase and a twisted nematic phase by photoisomerization of chiral azobenzene molecules," Proc. SPIE Vol. 4107, pp. 69-76 (2000).
[8] M. Z. Alam, T. Yoshioka, T. Ogata, T. Nonaka, and S. Kurihara, "Influence of Helical Twisting Poweron the Photoswitching Behavior of Chiral Azobenzene Compounds: Applications to High-Performance Switching Devices," Chem. Eur. J. 13, pp. 2641-2647 (2007).
[9] X. Chen, L. Wang, Y. Chen, C. Li, G. Hou, X. Liu, X. Zhang, W. He and H. Yang, "Broadband reflection of polymer-stabilized chiral nematic liquid crystals induced by a chiral azobenzene compound," Chem. Commun., 50, pp. 691 (2014).

Editorial Postscript

Thank you for regularly reading the Nissan Technical Review. We highlight two topics as special features of No. 89. The first topic is the new fourth-generation X-TRAIL, and the second is test technologies that support the competitiveness of Nissan's various electric vehicles, including X-TRAIL.

The first topic, the new X-TRAIL, is Nissan's latest genuine SUV launched in July 2022. This model realizes both "TOUGH GEAR" × "High Quality" and is equipped with various advanced technologies in the newly developed powertrain, including the second-generation e-POWER, which combines the VC-Turbo engine and motor, and e-4ORCE, which is the electric drive four-wheel control technology. The confidence features are described in the first topic. The second topic describes test technologies that support the development of new and attractive vehicle models, focusing on new test technologies such as driving simulators and virtual reality. These technologies represent important core fields in the development of EVs.

Experts working in Nissan in the technological development field have contributed to these articles. I would like to take this opportunity to thank all contributors and editors who wish to make Nissan's technologies known widely.

I sincerely hope that the advanced technologies developed in accordance with "Nissan Ambition 2030," the long-term vision announced by Nissan in November 2021, will be accessible to our readers.

Tomohiro Yamamura,
Research Planning Department,
Nissan Research Center

NISSAN TECHINICAL REVIEW 2023 No.89

Published	July,2023
Publishing office	NISSAN MOTOR CO., LTD. Research Division Research Planning Department Address: 1-1, Morinosatoaoyama, Atsugi-shi, Kanagawa 243-0123
Publisher	Research Division Research Planning Department General Manager TOMOHIRO YAMAMURA
Editorial office	NISSAN CREATIVE SERVICES CO., LTD. Office Service Department 560-2 Okatsu.Koku Atsugi Kanagawa 243-0126 C/O Nissan Technical Center

Nissan Motor Co., Ltd.